In-Situ Capacity and Resistance Estimation Algorithm Development for Lithium-Ion Batteries Used in Electrified Vehicles

THESIS

Presented in Partial Fulfillment of the Requirements for the Degree Master of Science in the Graduate School of The Ohio State University

By

Adhyarth Chaitanyabhai Varia

Graduate Program in Mechanical Engineering

The Ohio State University

2014

Master's Examination Committee:

Guezennec, Yann, Advisor

Rizzoni, Giorgio

Abstract

Battery life, cost and weight are some of the most important factors considered while designing battery packs for electrified vehicles. These factors directly affect the appeal of electric vehicles in the market. While, performance, cost and weight can be evaluated at the production and design stage, battery life is a dynamic parameter influenced by a multitude of factors and is hard to accurately predict, often leading to conservative designs with oversized and more expensive battery packs. Expensive batteries and complex, multi-factor aging phenomena ideally would require continuous tracking of the battery state of health. Battery capacity and internal resistance are commonly used to quantify battery state of health, as these metrics translate directly into range and power at the user level. While resistance growth is relatively easy to estimate in a vehicle, capacity fade requires measurements typically done at the laboratory level and conditions never encountered in a vehicle. This thesis aims to develop an algorithm capable of tracking *in situ* these two parameters throughout the life of battery.

By far the most challenging aspects of battery state of health estimation is to only use information available in the vehicle during its normal use, and furthermore, suitable with available on-board computing resources for real-time implementation. To that effect, the 'needs and wants' of an ideal *in situ* capacity estimator were clearly defined at the beginning of this work and algorithms that satisfy all the constraints were developed, tested

and validated. This work leverages the experimental results of an aging campaign conducted in out laboratories on a total of 17 cells aged under a variety of realistic operating conditions. A sensitivity analysis of the output of the algorithm was then carried out to assess accuracy of the algorithms in the presence of parameter variations and sensor errors. Next, the separate capacity and resistance estimation algorithms were integrated into a single framework to estimate both parameters simultaneously and hence tracking both metrics required to assess the state of health. Finally, tools for post-processing the raw capacity and resistance estimation results were developed to deal with data drops and other issues.

In summary, a computationally inexpensive algorithm that could be imbedded on a micro-processor on board an electric or hybrid vehicle was developed to accurately track capacity and internal resistance during normal vehicle operations. This algorithm produces a data rich stream of estimates (1 per charge depleting driving event) which can then be fed into a state of health estimator to make remaining useful life predictions. Having such an *in situ* tool provides feedback to continuously refine life prediction in light of possibly changing usage conditions in actual vehicles in operation.

The capabilities of the novel algorithms developed and validated in this thesis led to the filing of a provisional US patent (Application Number: 62/010, 671) in June 2014 to protect the intellectual property resulting from work done in this project.

This document is dedicated to my family.

Acknowledgments

Thank you to Professor Giorgio Rizzoni and his entourage for creating a wonderful learning platform for students at OSU Center for Automotive Research. I would like to thank Professor Guezennec for giving me an opportunity to be part of this research and providing me with constant guidance, Dr. Simona Onori for her contribution towards the project and all the people associated with battery aging activities at OSU CAR. I would also like to thank the members of CAR Industrial Consortium for providing funding to carry out experimental activities at CAR Battery Aging Laboratory.

Vita

May 2007 .....St. Paul's Sr. Secondary School

June 2012 .....B.E. Mechanical Engineering, Visvesvaraya Technological University

2013 to present.....Graduate Research Associate, Department of Mechanical and Aerospace Engineering, The Ohio State University

Fields of Study

Major Field: Mechanical Engineering

Table of Contents

List of Tables

List of Figures

List of Symbols

Variable	(Units)	Description
k	-	Event number
I_{meas}	[A]	Measured current ($I > 0 \Rightarrow$ battery discharging and $I < 0 \Rightarrow$ battery charging)
V_{meas}	[V]	Measured voltage at the output terminals of battery
V_{est}	[V]	Estimated voltage at the output terminals of battery
V_{dyn}	[V]	Dynamic voltage estimated by the battery model
OCV_{exp}	[V]	Experimentally determined battery open circuit voltage
OCV_{est}	[V]	Estimated battery open circuit voltage
SoC	-	Battery state of charge
$SoC_{0,k}$	-	Estimated initial state of charge at the beginning of event "k"
t	[s]	Time
t_{EOC}	[s]	Time at the end of charging period for the battery
Δt	[s]	Last portion of time during the constant voltage part of the charging event
t_{DRV}	[s]	Time at which the charge depleting driving mode begins
t_{CE}	[s]	Time at which the battery capacity is estimated
Q_k	[Ah]	Estimated capacity of the battery at the end of event "k"
Q_{nom}	[Ah]	Nominal capacity of the battery

T_{meas}	[°C]	Measured temperature
j	-	Index number for target value of battery capacity
M	-	Number of measurements made during the time period from t_{EOC} to t_{CE} at event "k"
N	-	Index number for the final target value of battery capacity
$\boldsymbol{Q_g[Q_{g1},..,..,Q_{gN}]}$	-	A vector of target battery capacity values
$\boldsymbol{SoC_j[SoC_j(t_{EOC}),..,..,SoC_j(t)]^T}$	-	A vector of SoC values at different instants for the target capacity value of Q_{g_j}
$\boldsymbol{OCV_{exp_j}[OCV_{exp_j}(t_{EOC}),..,..,OCV_{exp_j}(t)]^T}$	-	A vector of OCV_{exp} values at different instants for the target capacity value of Q_{g_j}
$\boldsymbol{SoC_{mat} = [SoC_1,..,..,SoC_N]}$	-	A matrix of SoC values at different instants and for different values of target capacity
$\boldsymbol{OCV_{exp_{mat}} = [OCV_{exp_1},..,..,OCV_{exp_N}]}$	-	A matrix of OCV_{exp} values at different instants and for different values of target capacity
$\boldsymbol{e_j[e_j(t_{EOC}),\dots,\dots,e_j(t)]}$	-	A vector of error values at different instants for the target capacity value of Q_{g_j}
$\boldsymbol{e_{mat}[e_1,\dots e_j,\dots,e_N]}$	-	A matrix of error values at different instants and for different values of target capacity
$\boldsymbol{E_j}$	-	Norm of vector e_j
$\boldsymbol{E[E_1,\dots E_j,\dots,E_N]}$	[mV]	A vector of calculated norms for different target values of battery capacity
α_1	-	Proportional constant for which the target capacity is maximum
α_2	-	Proportional constant for which the target capacity is minimum
CE	-	Capacity estimation

CC	-	Constant current portion of the charging event
CV	-	Constant voltage portion of the charging event
BOL	-	Beginning of life
EOL	-	End of life
EOC	-	End of charging
RMS	-	Root mean squared value
BMS	-	Battery management system
CCV	-	Closed circuit voltage
OCV	-	Open circuit voltage
$HPPC$	-	Hybrid pulse power characterization
$PHEV$	-	Plug-in hybrid electric vehicle

Chapter 1: Introduction

1.1 Introduction

Energy crisis, stringent emissions regulations and fuel economy mandates, and soaring prices of crude oil are some of the toughest challenges faced by the automotive industry today. In an attempt to counteract these challenges nearly every automotive manufacturer is researching new technologies to power the automobiles of today and the future. Of all the possible alternative forms of energy generation in vehicles, electricity seems to be the most promising. The biggest advantages it offers are efficient energy conversion and nearly zero emissions from the tail pipe. Hence, the needs and demands for hybrid electric vehicles, pure electric vehicles and fuel cell electric vehicles is growing. The source of electricity on-board such vehicles can be a battery pack or a fuel cell. It can be argued if the advanced powertrains of these vehicles will completely eradicate the need for internal combustion engines or not. Regardless, the growth of these vehicles is clearly evident. Because of their growing popularity, the critical components of such vehicles namely batteries and fuel cells have become a focal point of interest for researchers. Cost, energy density, power density, charging times, reliability, safety and lifespan are some hurdles that need attention.

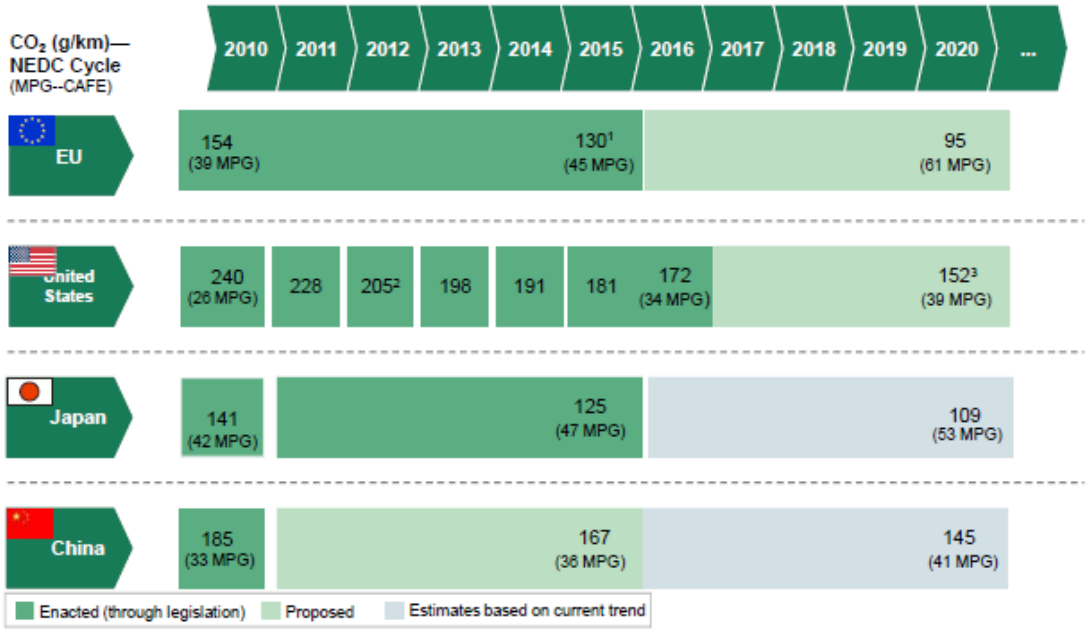

Figure 1: Fuel efficiency and emissions standards [2]

Fuel economy and emissions standards have been effectively used as means to reduce the demand for oil and harmful effects to the environment. The amount of fuel consumed by vehicles is directly correlated to the efficiency of the engine in converting the chemical energy in fuel to mechanical energy. It has been estimated that only 15-20% of the total energy coming from the fuel is converted into useful energy at the wheels of the vehicle [1]. Figure 1 shows the fuel efficiency and emissions standards and their projection into the future [2]. Numerous technologies have been developed over the years to gain significant improvements in fuel economy for conventional vehicles. These include multiple valves, variable valve actuation, engine downsizing, cylinder deactivation, stop-start systems, friction reduction and advanced transmission systems [3]. Though there has been reduction in tailpipe emissions and increment in fuel economy with the help of the

above mentioned technologies, researchers are now focusing more on alternative sources to power the transportation sector.

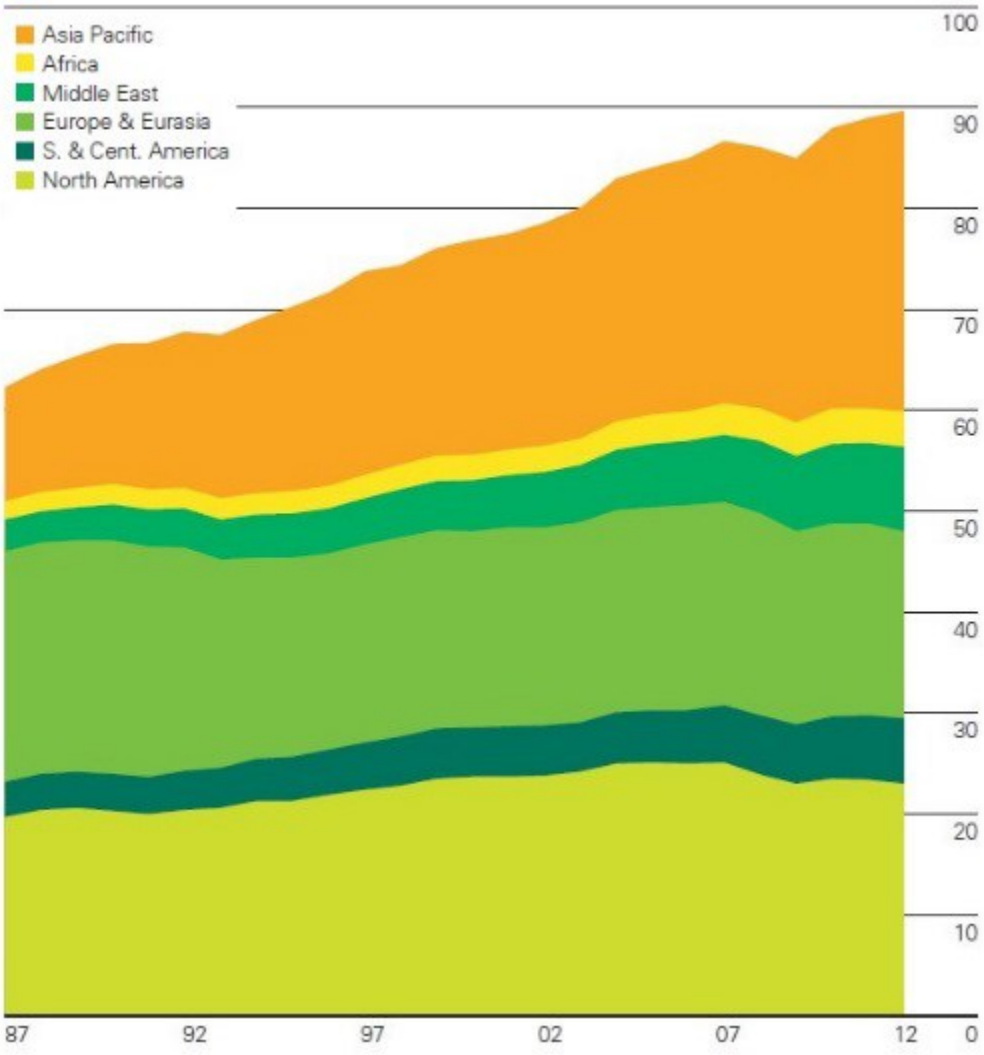

Figure 2: Oil consumption trends by region (million barrels daily) [5]

In 2009, the global transportation sector was estimated to be the second largest energy consuming sector following the industrial sector [4]. Most of this energy comes from

petroleum based fuels such as gasoline and diesel. It is well known that the global oil reserves are fast depleting and will become extinct sometime in the future. Figure 2 shows the oil consumption trends by region [5]. The global transportation sector also accounted for 23 and 22% of the total CO2 emissions in 2007 and 2008 respectively [6, 7]. This poses a real threat to the environment and the results can be catastrophic if the issue is neglected. The batteries and fuel cells used in advanced powertrain architectures offer some very distinct advantages. Firstly, these are renewable sources which can be used over and over again. Batteries can be charged externally and fuel cells can be refueled without any threat of depletion. Vehicles powered by fuel cells and battery packs have nearly zero tailpipe emissions. The well to wheel efficiency of a BEV and FCEV can be in the range of 21.3-66.5% and 31.2-41.6% respectively [8]. This is significantly higher as compared to conventional vehicles. However, some of the growing concerns with respect to batteries and fuel cells today are cost, durability, degradation, energy density, power density and safety. Figure 3 summarizes few specifications for different types of vehicles from a buyer's perspective. The initial buying cost for a BEV or an FCEV is proving to be one of the biggest hurdles when it comes to market appeal.

	ICE (VW GOLF 1.4TSI)	Hybrid (Toyota Prius III)	BEV (Nissan Leaf)	FCEV (Honda FCX Clarity)
Power supply	IC engine	ICE, electric motor	Battery and electric motor	PEM fuel cells and electric motor
Fuel	Petrol, diesel and alternative fuel	Petrol/diesel as main fuel	'Electricity'	Hydrogen
Top speed (mph)	124	112	94	100
Acceleration (s)	9.5	10.4	7	10
Range (miles)	552	716	73–109	240
Purchasing price	$29,400	$33,400	$41,250 (including $8,000 government incentive)	$80,000 (estimated)
Running fuel price (per mile)	$0.22	$0.14	From $0.02	From $0.07
Fuel economy (mpg or mpg equivalent)	45.6	72.4	99	81
Tailpipe CO_2 Emission (g/km)	144	89	0	0

Figure 3: Comparison of different types of vehicles from a buyer's perspective [8]

It has been noticed that batteries used in stationary storage devices like laptops, cell phones and other consumer electronics do undergo significant degradation with usage. Battery aging is a phenomenon that occurs due to loss in efficiency of the electrochemical reactions taking place at the cell level. This inefficiency translates itself into reduced energy storage capacity and poor performance or power loss. Considering a harsh environment like that of an automobile, battery aging can be expected to be more pronounce. These batteries are subject to rapid discharging and charging cycles during acceleration and regeneration events. They are also subjected to widely varying ambient conditions resulting in very high or low temperatures. Realizing the need to track battery aging, a lot of research and development is taking place at research universities, automobile manufacturers, battery manufacturers and government organizations. This research occurs at both micro level where, the behavior of cathode and anode particles is studied as well as at macro level where, a lot of experimental data is collected to study aging severity factors affecting the lifespan of batteries.

1.2 General Battery Terminology

1.2.1 Battery cell

A battery cell is the smallest unit of a battery pack. It typically consists of a cathode, anode and an electrolyte that facilitate the flow of current through an electrochemical reaction. A number of cells arranged in series and/or parallel constitutes a module and a number of modules arranged in series and/or parallel constitutes a battery pack. It should be noted that unless mentioned specifically in this thesis, the term battery refers to a battery cell.

1.2.2 Capacity

Battery capacity can be defined as the amount of charge that can be extracted from a fully charged battery until it's completely depleted [9]. It is a measure of the amount of usable energy the battery can store and has units of ampere-hour (Ah). The rated capacity is typically specified by the manufacturer for a given temperature and discharge current. It is important to note that the amount of energy a battery cell can store varies with temperature and discharging conditions and generally decreases as the cell is being used more and more. A term commonly used to quantify charging rate is C-rate. It gives an indication of how slow or fast a cell is charged. For instance, a cell with a nominal capacity of 15Ah will need 1 hour to be fully charged at 1C rate, half an hour to be fully discharged at 2C rate and so on.

1.2.3 Internal Resistance

The internal resistance of a battery cell opposes the free motion of electrons inside it and hence causes a loss in its ability to deliver power. It is also referred to as the ohmic resistance which by definition is a change in voltage when current is applied to the cell [9].

The cell internal resistance is sometimes also defined as a combination of ohmic, activation and diffusion polarization resistances and equates to the largest possible voltage drop in the cell [10].

1.2.4 State of Charge (SoC)

Battery state of charge gives an indication of the fraction of maximum charge remaining in a battery cell [9]. In other words, it denotes the amount a cell has been discharged and can be thought of as the dashboard gauge indicating the amount of fuel left in a conventional vehicle. Hence, a fully charged battery would have a SoC of 100% and a fully discharged battery would have a SoC of 0%.

1.2.5 Aging

Aging in general refers to the gradual loss in energy conversion efficiency with time and usage [9]. Once a battery is being put to use, it undergoes certain irreversible changes at the micro-level due to which the amount of energy it can store and the amount of power it can deliver gradually decrease. Some of the common factors affecting the rate of battery aging are temperature, state of charge and charging rate.

1.2.6 State of Health

Battery state of health is a highly subjective term and has been a specialized area for research for a number of years now. For the purpose of understanding the function of battery packs in vehicular applications, we study battery aging from two broad perspectives. These are the loss in cell capacity and the growth in cell internal resistance. Both these factors lead to poor performance and hence poor state of health of battery. A term very closely associated with state of health is end of life (EOL) and indicates a point

in battery life when it is no longer suitable for the desired application. For HEVs, PHEVs and BEVs, this is generally considered as a 20% loss in the cell capacity with respect to a new cell [9].

1.3 Literature Review

The automotive industry is taking steps towards reducing the need for oil and ensuring a cleaner environment. Powertrain electrification is playing a key role in this and hence research into advanced battery designs and smarter battery management systems is necessary to support advancement of powertrains. This literature review will present an overview of advanced vehicles and outline the state of batteries used in these vehicles. It will then establish the reasons for widespread acceptance of Lithium Ion batteries, explore the needs for battery modeling, identify the causes and effects of battery aging, list few important functions of the battery management system and cover some techniques that have been established for state of health assessment.

1.3.1 Overview of advanced vehicles and automotive batteries

Due to the problems caused by conventional vehicles, most of the automotive manufacturers are investing their resources to research renewable and energy efficient sources of energy generation on board vehicles. Some of the promising solutions to eliminate the concerns posed by conventional vehicles are hybrid electric vehicles (HEVs), plug-in hybrid electric vehicles (PHEVs), battery electric vehicles (BEVs) and fuel cell electric vehicles (FCEVs). Though it is debatable as to which one of these broad categories of low carbon vehicle markets will emerge as a front-liner in the future, it is largely

believed that all four categories of advanced vehicles are likely to play a major part [11, 12].

Generally speaking, a hybrid vehicle consists of more than one power sources. It could be a combination of petroleum based ICE with a battery pack or ultra-capacitor or a fuel cell with a battery pack or ultra-capacitor. These vehicles generally have one component each for energy storage and energy generation. These hybrids can come in different types based on their functionality such as micro hybrids, mild hybrids, medium hybrids and full hybrids [13]. Hybrid electric vehicles offer a good compromise between a fully electric and a conventional vehicle in a number of ways. Since an ICE is the main source of power in a hybrid vehicle, it never suffers from lack of range as in the case of a BEV. Also, since a HEV has a relatively smaller battery pack it is relatively cheaper as compared to a BEV. HEVs also give better fuel economy as compared to conventional vehicles because with the help of control strategies the engine is operated in the most favorable conditions. Plug in hybrid electric vehicles are yet another category of advanced vehicles in market today. The primary source of power in PHEVs is a battery pack and an electric motor, with the engine kicking on to assist when the battery state of charge reaches a minimum level. The advantage they offer over hybrid vehicles is the battery pack can be charged externally, helping in further increase in gas mileage.

BEVs use an electric motor to power the wheels and have a battery pack to store the energy required to drive the electric motor. The fuel in a conventional vehicle can be compared to a battery pack and the electric motor is equivalent of an engine. The first BEV was believed to have been built by Thomas Davenport way back in 1834, even before the conventional

vehicle was in existence [8]. However, due to lack of range the BEV could not become popular and became extinct by 1930s [14]. It should be noted that the requirements of battery packs for hybrid vehicles and electric vehicles are different. For a hybrid vehicle a battery pack with higher power density is desired while, for an electric vehicle a battery pack with a better energy density is desired. Range, cost, safety and lifespan are some of the challenges the automotive industry is trying to counter today to increase the popularity of BEVs [15]. According to organizations such as CARB, ANI, IEA, EPRI the cost of lithium ion battery is expected to reduce by one-third of its current price which, is approximately $857/kWh [8]. Few battery chemistries have had issues with thermal runaway and hence safety is still a concern. An internal combustion engine has a very long life and vehicles can go up-to 300,000 miles or more without the need to completely replace the engine. A lot of advancement in battery technology is needed if battery packs are to last anywhere as compared to internal combustion engines.

Fuel cell is an energy storage device that converts through a chemical reaction the chemical energy stored in a fuel and an oxidant into electricity, heat and water [8]. It was invented by Sir William Groove in 1839, even before the world knew of petroleum based fuels [8]. Fuel cells can offer higher energy densities and efficiencies than any other energy storage devices [8]. Consequentially, these are believed to be excellent sources of energy storage for the transportation sector in future [16, 17]. FCEVs are similar to BEVs and have some components in common like electric motor and other power electronic devices. The difference being that BEVs utilize the energy stored in battery packs and FCEVs utilize the energy stored in fuel cells.

A battery is an electrochemical device which converts chemical energy into electricity. Batteries have been at the heart of energy storage devices in consumer electronics and automobiles since a very long time. Automotive batteries have come a long way from being just a passive component in vehicle electric power system to being heart of a particular kind of vehicles like the BEVs. For a conventional vehicle, the energy storage device is the SLI battery where in S stands for starting, L for lighting and I for ignition [18]. Evident from its name these batteries are mainly used for cranking up the engine and providing power for auxiliary electrical systems in vehicles. However, the batteries used in advanced vehicles need to perform the task of providing traction along with the above mentioned functions. Batteries are generally classified according to their chemistries and the chemistry is decided by the materials making up its components mainly anode and cathode [19]. Lead-Acid, Nickel-Cadmium, Nickel-Metal Hydride and Lithium-Ion are some of the common battery types. Lead-Acid is known to be the first commercially available rechargeable battery [19]. It offers some distinct advantages of being easy to manufacture and cost effective. However, it also has some disadvantages such as being harmful due to lead content and poor energy densities. Nickel-Cadmium battery was invented in 1899 by Waldmar, Jungner [19]. It has an intermediate energy density and long cycle life, but suffers from memory effect [19]. Due to memory effect, the battery's maximum energy storage capacity reduces if recharged fully after partial discharges [19]. Nickel-Metal Hydride offer higher shallow-cycle life and are the best choice for HEVs where range is not a primary concern. Nickel-Metal Hydride batteries were mainly used in consumer electronics before the advent of Lithium-Ion batteries in early 1990s. Lithium-Ion batteries

have become extremely popular in consumer electronics and more recently in advanced vehicles due to their high energy densities, no memory effects and very less self-discharge. Figure 4 summarizes some characteristics of commonly used rechargeable batteries [20].

High Energy Design in Deep Cycle Application		Lead Acid	Nickel Metal Hydride	Lithium-Ion
Energy density	(Wh/kg)	35	55	>80
Power density	(W/kg)	150	230	1,000
Charge acceptance	(W/kg)	50	200	600
Life time (number of cycles)	at 80% swing at 5% swing	125 50,000	3,000 300,000	2,500 140,000
Cost level	USD/kWh	150	450	500

Figure 4: Characteristics of commonly used rechargeable batteries [20]

Batteries are going to play a major role in the coming years if the problems faced by automotive industry are to be solved. The desired characteristics of batteries for different types of vehicles are different. BEVs require batteries with higher energy densities while, HEVs require batteries with high power densities. Meanwhile, PHEVs require batteries with intermediate characteristics such that it can have a trade-off between the energy density required for a BEV and power density required for a HEV. It is believed that Ni-Cd and Ni-MH battery technologies do not show much potential for improvement. On the contrary, Lithium based chemistries such as Lithium-Ion and Lithium-ion polymer offer distinct advantages such as high energy density, low weight and cost and hence are attracting significant attraction from car manufacturers [21-27].

1.3.2 Need for development of lithium-ion batteries

The booming Information Technology industry in the late 1980s led to widespread use of portable electronic devices such as video cameras, mobile phones and notebook computers. This spurred an urgent need for deployment of rechargeable batteries in the field. Lithium-Ion batteries started evolving as main source of energy storage in the above mentioned devices in early 1990s. These batteries have an equally important role to play in the advancement of automotive powertrains. Figure 5 shows the comparison of different battery technologies in terms of their volumetric and gravimetric energy densities [28]. It is evident as to why Lithium based chemistry has become so popular for energy storage purposes. This is also reflected in Figure 6, where the annual sales amount for Lithium ion battery in 103 million is shown over the last 15 years [29]. Nearly every automobile manufacturer producing HEVs, PHEVs and BEVs is using Lithium-Ion batteries for energy storage in their vehicles [30].

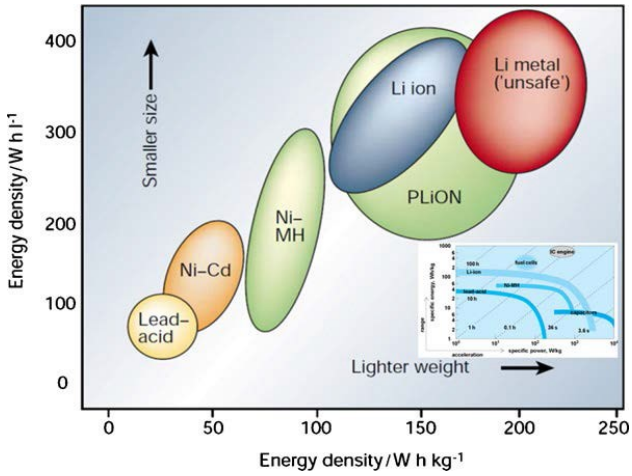

Figure 5: Comparison of energy densities for different battery chemistries [28]

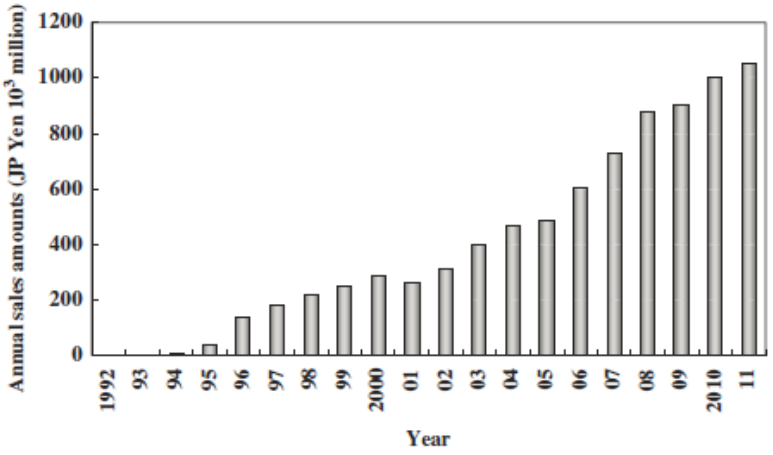

Figure 6: Annual sales amount for Lithium Ion batteries [29]

However, despite the clear advantages that Lithium-Ion batteries offer, several researchers echo concern over their longevity, cost and safety and believe these batteries aren't completely suitable for automotive applications as of today [31]. A general idea regarding safe operation of Lithium-Ion batteries is they should not cause fire or explosion when put to use [32]. However, it can also be argued as to why an internal combustion engine which runs on gasoline, a highly flammable substance is considered safe to power the vehicles. Hence, it should be noted that Li-ion cells are not considered safe when a hazardous event occurs during normal operating conditions for which these cells are designed [32]. A number of incidents involving fire and explosion in Lithium-Ion batteries have been reported [32]. In 2006, 10 million Sony batteries used in laptops were recalled due to them being vulnerable to internal contamination and risk of short circuit [33]. In 2012, EV batteries worth $55M were recalled by A123 systems, as these had manufacturing defects

[34]. As a result of such incidents, Lithium-Ion safety is still a concern and a lot of effort is being put in to make their operation risk-free. Battery lifespan is yet another issue which needs attention [35]. A lot of the aging that occurs in Lithium-Ion batteries is contingent on the conditions under which the battery is used, with high temperatures and deep discharge being very harsh on the batteries accelerating their degradation. Hence, predicting the lifespan of these batteries is a very difficult task. Cell imbalance also leads to rapid degradation in these batteries. A cell with higher aging rate over discharges as compared to other cells. This triggers a cycle of events which can lead to severe degradation at the pack level leading to poor performance characteristics under load. Hence, a lot of techniques have to be employed at the pack level to overcome cell imbalance resulting from temperature and capacity variation within cells. Though it is estimated that only around 0.08 kg of Li is used per kWh of storage capacity [36], one key roadblock is that batteries contain materials whose production can cause harmful environmental impacts [37]. This necessitates the need to recycle Lithium-Ion batteries and to improve the energy density of these batteries to reduce the demand for materials used in their production.

1.3.3 Battery modeling

Because battery aging is a complicated phenomenon difficult to understand in a laboratory setting [38], battery models have to be widely used to get an understanding of the aging phenomenon occurring in batteries. Thanks to advancement in computing technology over the last few decades, battery modeling and simulation have become an easier and inexpensive task. Fundamental or physics based and empirical or phenomenological are the two category of models generally used to simulate behavior of battery cells [39].

Physics based models are highly accurate but require a lot of computing power while, empirical models are relatively less accurate but cheap in terms of computation requirements. While physics based models aim to understand the behavior of materials at the micro level, empirical models gauge the performance of battery cells in terms of inputs and outputs. Regardless of the type of model considered, in general the goal of these models is to predict and estimate few important states of a battery cell like state of charge, open circuit voltage (OCV), terminal voltage and temperature. An accurate prediction of these states can provide information about available power and energy from batteries. The Battery Management System often relies on battery models to provide information regarding battery state of health, state of charge and available power and energy. Hence, the accuracy of BMS depends to a great deal on the accuracy of battery models it uses.

Electrochemical models are used to describe the mass, energy, and momentum transfer of different species in a battery cell. They are generally represented as a system of partial differential equations that need to be solved to get an estimate of various parameters. The advantages such models offer over phenomenological models is they can not only predict macroscopic quantities such as cell voltage, but also the spatial distribution of microscopic properties such as concentration, potential, current, and temperature [40]. One such electrochemical model for Lithium polymer cells has been developed and parameters were identified using experimental data [40]. An estimate of cell voltage and lithium cell concentration was obtained using the model under varying aging protocols. The authors use results from the electrochemical model to investigate processes that hinder cell performance and learn more about optimal cell design.

Since, electrochemical models are very complex and involve identification of a large number of parameters, a fractional model has been developed based on simplifications of an electrochemical model [41]. Fractional differentiation enables a reduction in the number of model parameters and hence it offers some advantages while, ensuring the parameters of an electrochemical model (like diffusion coefficients, maximum solid phase concentration) are still used [42]. Such models in conjunction with state observers or estimators such as a Kalman Filter can be used to estimate the State of Charge of battery cell [42]. Electrochemical battery models can also be used to simulate the response of batteries in undesirable conditions such as an accident or collision. Batteries are generally tested for such conditions using an actual nail penetration test [43], which is time and money consuming. One such electrochemical battery model has been developed in order to simulate nail penetration into a battery pack which could result in a short circuit posing risk of fire and explosion [43]. The authors employ an electrochemical model to accurately model the short circuit phenomenon that can occur in lithium-ion batteries. They also go on to accurately predict the temperature variation in a cell in the event of such an incident. Out of all the phenomenological models developed, Randle equivalent circuit models are most common [39]. The equivalent circuit model is a simpler model capable of accurately estimating the dynamics of a battery cell under varying operating conditions. Such a model consists of an ideal voltage source, an internal resistance term and a number of RC circuits. The total number of RC circuits decides the order of the equivalent circuit model. The simplest example can be a zero order model which only has an internal resistance term. These are lumped parameter models wherein the parameters are generally identified using

vast amount of experimental data. These parameters are generally a function of battery operating conditions such as state of charge, temperature, current etc. and are used to approximate all the dynamics occurring inside the cells. In one such empirical model, a first order equivalent circuit model was used to estimate the state of charge of lithium ion batteries under varying operating conditions [44]. The authors use a two-step approach for accurate state of charge estimation. In the first step they use a low pass filter to clean the measured current data and then employ coulomb counting technique to estimate the state of charge. In the second approach, they utilize a first order equivalent circuit model to estimate the cell open circuit voltage and interpolate the experimental curve of open circuit voltage vs. state of charge to get an estimate of the latter. They then propose a combined algorithm which enables accurate state of charge estimation under varying temperature conditions and driving cycles.

Battery models can also be used to get an estimate of cell internal resistance, a critical parameter that quantifies a battery's state of health. In one such technique developed, a first order equivalent circuit model is used for online estimation of internal resistance and open-circuit voltage of lithium-ion batteries [45]. The authors propose the use of an adaptive algorithm to update the parameters estimated by the first order equivalent circuit model. The adaptive algorithm utilizes knowledge about the open circuit voltage and internal resistance from tests conducted in the laboratory. They gone on to show that the open-circuit voltage and internal resistance can be extracted accurately in real driving conditions using such a methodology. In summary, it can be said that battery models play a very significant role in understanding the complex phenomenon of battery aging and

provide a reliable mode for simulation of hybrid and electric vehicle components. While electrochemical models can give very accurate results, for most engineering purposes computation always poses a limit and hence equivalent circuit battery models are given first priority. This thesis aims to develop an algorithm for capacity and resistance estimation that can be implemented in real time. Hence, cheap computation and ease of implementation are two critical objectives of this thesis. Keeping in mind the same, a first order equivalent circuit model has been used to develop an algorithm for capacity and resistance estimation in this thesis. The model will be described in great detail in section 2 of chapter 2.

1.3.4 Battery aging: causes and effects

Battery aging has emerged as a growing field of study over the last few decades. The portable electronics industry and the need for electrification of powertrains in automotive industry are the two main drivers leading to its growth. Battery aging can be classified into two main categories: Cycle aging and Calendar aging. While, cycle aging is an artifact of actual usage of the battery under load, calendar aging leads to capacity loss due to storage. While, the rate of cycle aging is determined by a number of factors like charging patterns, temperature and state of charge, calendar aging rate is determined by storage conditions.

It is believed that aging in lithium-ion cells occurs mainly due to reactions of materials with electrolyte solution at the interfaces of positive and negative sides and self-degradation of these active materials due to usage [46]. The rate of these degradation mechanisms depends on the type of materials and their purity, manufacturing processes employed for their production, battery cell design and lastly on the kind of use the cell is

put to [46]. Regardless of the mechanism responsible for battery aging, it has been well established that battery aging results in energy and/or power losses. It has also been observed that the phenomenon responsible for aging at the interface are highly dependent on cell operating variables such as voltage and temperature [46]. In order to better understand the aging mechanisms in lithium-ion batteries, researchers have tried to study the aging occurring at positive and negative sides separately. One such work has been conducted to study the impact of calendar aging on lithium-ion batteries [47]. The authors propose that during rest thermodynamic stability governs the rate of aging. They also propose that negative electrode stability is the dominant factor because of the strong affinity of an organic electrolyte to react with lithium electrode. Ironically, this situation gives a better lifespan to lithium-ion batteries through the formation of a protective layer given a right electrolyte is present. This concept of a solid electrolyte interface (SEI) [48] has been well studied and universally accepted. According to this concept, any breakage in the protective film could lead to corrosion of lithium and subsequent energy loss. Due to large surface area provided by the porous negative electrode in lithium ion batteries, this breakage of SEI is more critical and a major source of aging [47]. The authors also suggest that the seal provided by SEI isn't airtight and some amount of lithium corrosion is always taking place. At the positive electrode, the interaction between positive electrode material and the electrolyte solution becomes the dominant factor for aging. The rates of reactions at the positive electrode depend on operating conditions like the cell voltage and temperature. Hence, the aging at positive electrode depends a great deal on the state of charge and temperature. It has been observed that calendar aging at high state of charge

and temperature cam accelerate the aging process in lithium-ion batteries [47]. To summarize battery aging in lithium ion batteries, it can be said that with a correct choice of electrolyte aging at the negative electrode can be controlled. Consequently, mechanisms governing aging at the positive electrode dominate the aging characteristics.

In yet another work published, similar thoughts about mechanisms governing battery aging are echoed [49]. The authors believe separate mechanisms govern the rate of aging at negative and positive electrodes. The two principal effects of battery aging are capacity fade and internal resistance growth. Loss of active lithium leads to battery capacity fade while, growth of passive films at interfaces can lead to resistance growth [49]. It has also been observed that capacity fade and resistance growth result from a number of processes that depend on each other [50]. This makes the independent study of these processes nearly impossible and makes battery aging an even more complex phenomenon. Because battery aging depends on a multitude of factors and is a relatively slow phenomenon, suitable experiments have to be designed to accelerate the aging process.

1.3.5 Battery management system and its functions

Batteries used to provide traction in vehicular applications are considered to be the most critical component of these vehicles just, like an internal combustion engine is for a conventional vehicle. Consequently, the functionality of these batteries must be properly controlled by a management system. The battery management system in advanced vehicles consists of sensors, actuators and controllers which have to perform specific functions. Some of the important sensors in a BMS are current, voltage and temperature sensors. The temperature sensor could be for a single cell, for a module, for the ambient conditions and

for the coolant inlet and outlet. A BMS used in an electric vehicle can also have input signals such as accelerate pedal sensor, brake pedal sensor and flag variables such as start key ON/OFF etc. to know about the condition of the vehicle. The outputs of the BMS could be commands to different controllers present for various functions such as thermal management, cell balancing, safety management and on-board diagnostics [51].

Design specifications of a BMS can be different based on the intended use and requirements. Regardless, some of the common functions for a BMS in an electric or hybrid vehicles are battery parameter measurement, state estimation, on-board diagnostics, safety management, cell equalization, thermal management, information storage and communication [51]. Parameter measurement include current and voltage measurement to ensure operation within limits and prevent over-charging/over-discharging. This information is also passed on to other controllers responsible for thermal management, safety, cell equalization etc. State estimation can indeed be considered as the most important function of BMS. This includes state of charge and/or state of health estimation. This important function will be explored in detail in section f of chapter 1. On-board diagnostics keeps track of any faults in sensors and ensures a fault code is set whenever it detects any component not functioning properly. Safety management and thermal management are necessary to avoid any risk of thermal runaway, short-circuit etc. It has been noted earlier that lithium ion batteries are prone to risk of fire or explosion if operated beyond their limits and hence these functions are equally critical. Cell equalization includes ensuring all the cells in a module and a pack are at the same state of charge, temperature and state of health. A failure to do so could result in a chain of events which could

ultimately cause the battery to function very poorly. Information storage and communication is essential because the BMS is comprised of a number of components interdepending on each other for full functionality.

Actual BMS in a vehicle may not have all the hardware and software functions outlined earlier. However, considering the urgent need to develop batteries with very good range and lifetime, keeping a track of battery state of health has become inevitable. Since, this thesis presents an algorithm for capacity and resistance estimation, two parameters used to quantify battery state of health, some methods developed in the literature to achieve the same are reviewed in the next section.

1.3.6 Battery state of health monitoring

The cost of battery pack and management system is the biggest reason for the high price of electric and/or hybrid vehicles today. It is necessary to optimize the performance of battery pack without which the pack will have to be overdesigned to compensate. Battery state of health monitoring includes keeping track of the energy and power that can be extracted from the pack at any point in its life. Good knowledge about battery state of health can thus help in optimal energy management and optimal sizing of battery packs in hybrid and/or electric vehicles. Moreover, information on the battery state of health can also help in predicting the remaining useful life of batteries, which can consequently increase the reliability of these vehicles. A lot of work published in the literature considers state of charge estimation as a mean to assess battery state of health [52, 53]. A part of literature also considers capacity fade and resistance growth as two parameters to quantify

the state of health of batteries [54, 55]. Hence, it can be said that state of health estimation amounts to estimating the state of charge, capacity or internal resistance of batteries.

One such approach to estimate the state of charge is reviewed here [53]. The author proposes an algorithm based on kalman filtering, to track the state of charge, state of health and available power for a lithium-ion polymer battery pack. The advantages of using kalman filtering based methods are it provides automatic error bounds on the estimated states. Since cells in a battery pack used in hybrid or an electric vehicle are never in an equilibrium state the cells' open-circuit voltage vs. state of charge curve cannot be used for state of charge estimation based on voltage measurements. They employ a model for the battery cell based on dynamics and update the model parameters at every sampling interval by minimizing the error between estimated cell voltage and measured cell voltage. This way an accurate estimate of the cell state of charge can be obtained at each time step. To go a step further, they utilize the present cell conditions to get an estimate of the maximum charge/discharge power that could be delivered/absorbed for a given time without exceeding the limits on cell voltage. Based on the algorithm proposed, estimated of state of charge, cell current, internal resistance were obtained with good confidence. The authors claim that even though the algorithm is mathematically advanced, it can be implemented in a micro-processor with less computing needs.

A method for capacity estimation of lithium-ion batteries used in PHEVs and BEVs has been developed in [56]. The method utilizes an equivalent circuit battery model to estimate the battery capacity separately during a driving event and a plug in charging event. The open circuit voltage vs. state of charge curve and the cell capacity vs. temperature curve

along with a second order equivalent circuit model are used to obtain the cell capacity as a function of a single parameter. The introduced parameter is then estimated using a recursive least squares algorithm. The authors successfully validate the algorithm by using experimental data from accelerated aging tests conducted in the laboratory.

A lot of work published for estimation of state of charge, cell capacity, internal resistance and cell voltage has been carried out in laboratory setting and not real time [57, 58 and 59]. Real time implementation enforces a strict criteria in terms of ease of implementation, cost of implementation and computing power. The work developed in this thesis aims to overcome these hurdles and establish an algorithm to estimate the cell capacity and internal resistance that can be implemented in real time. The results from the algorithm in conjunction with experimental data obtained in the laboratory can then be used for prognosis and life predictions.

Chapter 2: Background

2.1 Experimental Activities

Battery lifespan is one of the most critical factors considered while designing battery cells for vehicular applications. Because batteries are designed to have a long life, understanding the gradual aging phenomenon requires collection of huge amounts of data over long periods of time. The data utilized to conduct research in this project was collected at The Ohio State University Center for Automotive Research Battery Aging Lab. The experiments were engineered and carried out for the CAR industrial consortium project. The cells used in all the experiments were LGChem P1 pouch type Lithium ion polymer cells shown in Figure 7. These cells have a nominal discharge capacity of 15Ah and are similar in style (smaller in scale) to those used in Chevrolet Volt, a range extender vehicle manufactured by GM. Some of the specifications for this cell are listed in Table 1.

Figure 7: LGChem P1 Lithium-Ion Polymer Battery Cell

Rated Discharge Capacity (Ah)	15
Maximum Discharge	60A to 2.8V
Nominal Voltage (V)	3.75 V
Mixed Cathode	Mn spinel and layered
Mixed Anode	Graphite and Amorphous Carbon

Table 1: LGChem Pouch Type Cell: Specifications

2.1.1 Testing procedures

As noted earlier, the experimental data utilized in this project was collected at the OSU Center for Automotive Research, Battery Aging Lab that was created in 2008. The laboratory contained a number of aging stations, each carefully monitored for safety. In particular the datasets used in this project were collected on eight different aging stations over a period of time from February 2012 to present date. A total of 18 cells were aged according to different aging protocols engineered, to test the severity of aging against different factors. Besides the cells used for aging characterization, a few cells were explicitly used for system identification purposes. This included characterizing the battery capacity as a function of temperature, battery model identification and establishment of the OCV vs. SoC curves for these cells. The experiments were conducted at different temperatures and the temperatures were accurately controlled. Since, battery testing is a field of study in itself and is not the main focus of discussion in this thesis, not much is described about the details of testing hardware and software. However, for a more detailed understanding of battery testing capability at The Ohio State University Center for Automotive Research, the reader can refer to [39]. In that document, Alexander K Suttman

a former graduate student at The Ohio State University has provided details on standard testing procedures and battery aging lab.

Battery testing and collection of vast amount of data is critical to getting the maximum out of them for vehicular applications. As a result, battery testing procedures are very standard and are defined by national research laboratories in conjunction with The U.S Department of Energy. Detailed description of all the testing procedures can be found in [60] and the same guidelines were adopted in the testing conducted at The Center for Automotive Research Battery Aging Lab. A number of initial characterization tests were conducted on each test cell prior to starting the actual aging campaign. These tests included characterization of energy and power through Capacity Tests, Hybrid Pulse-Power Tests (HPPC) and Electrochemical Impedance Spectroscopy (EIS) Tests. These tests not only provided a means for baseline energy and power measurements, but also helped in de-greening the battery. De-greening is often described as characterizing the initial drop/rise in capacity when it's charged for the very first time. This is important because, even though the cell nominal capacity as listed by the manufacturer was 15Ah, some of these cells had capacities higher or lower than that value. Once, the initial energy and power capabilities for all the fresh cells were known, the actual aging campaign was run on them according to different aging protocols. In addition to initial characterization, in-order to keep track of cell capacity and internal resistance, the capacity and HPPC tests (also referred to as assessment tests or reference performance tests) were run at regular intervals through-out the aging campaign. The entire aging campaign was to be run until the End of Life (EOL) criteria for cells was met. For battery cells used in PHEVs and BEVs, this end of life criteria

is generally defined as the point when the cell capacity drops to 80% of its initial value. This is because for a PHEV or a BEV, range and hence cell capacity are of prime importance. Hence, a threshold on the cell capacity is set in order to decide the criteria for these cells to be considered usable for such applications. Due to equipment availability limitations and the fact that some of these aging protocols would require cells to be aged for a long period of time, the EOL criteria couldn't be met for all the cells.

The capacity tests was the first characterization test being conducted to measure the actual capacity of the cell. This test measures cell capacity in ampere-hours at a constant current corresponding to a fixed C rate. The test is conducted by first charging the cell to a full state of charge and letting it rest for a period of time. This is followed by discharge at a constant current until the low voltage limit as recommended by the manufacturer is reached [60]. This way the number of ampere-hours that can be extracted from a fully charged and relaxed battery cell can be estimated. For all the experiments considered in this project, the capacity tests were conducted at a current rate of 1C and at 30 °C. With a nominal capacity of the cell being 15Ah, this corresponded to a constant current of 15A. In addition, the tests were conducted three times to establish repeatability and the average capacity was considered as a reliable estimate. An example of current and voltage data for one such capacity test is shown in Figure 8 and Figure 9.

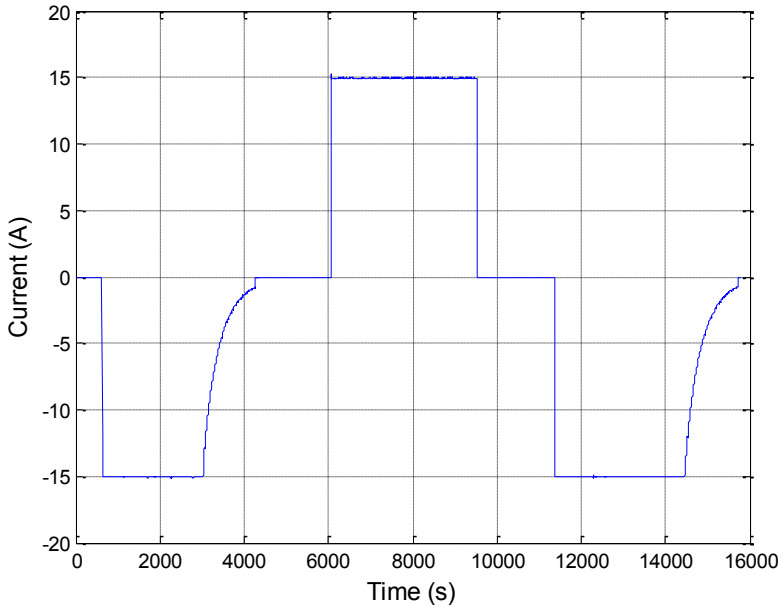

Figure 8: An example of input current profile during a capacity test

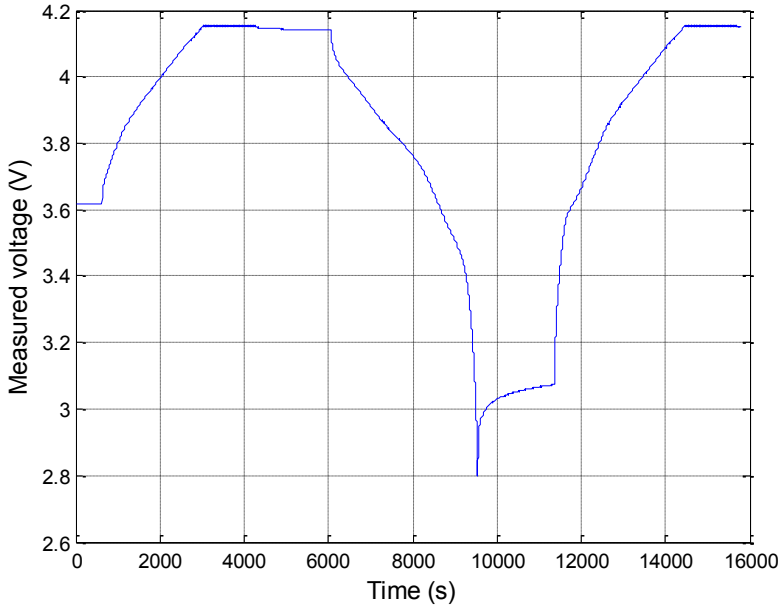

Figure 9: An example of voltage response during a capacity test

Once, the initial capacity was measured, HPPC tests were conducted to assess discharge and recharge power capability of the cell over its usable voltage range. This test can provide an estimate of the charge sustaining available power and energy and charge depleting available energy [60]. Besides, it can also be used to get an estimate of the cell internal resistance as a function of the state of charge by using a simple Ohm's Law relationship from the voltage curves. These resistance estimates can be used for characterizing resistance growth and developing aging models for hybrid vehicles to assess their performance. HPPC is a standard test conducted in every battery aging campaign and is very well defined in the DOE battery test manual [60]. Current and voltage data for one such HPPC test are shown in Figure 10 and Figure 11. Actual aging protocols were run on battery cells after the initial characterization was completed. The aging protocols engineered for this project are described in greater detail in section the next section on aging design of experiments.

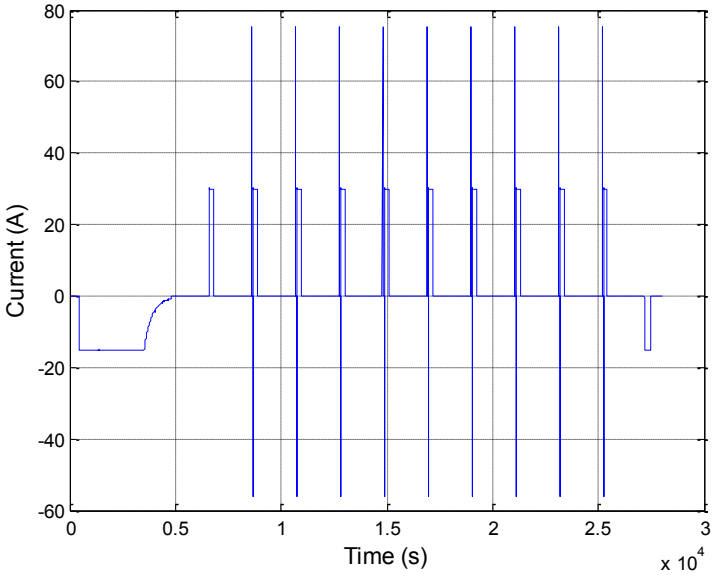

Figure 10: An example of input current profile during a HPPC test

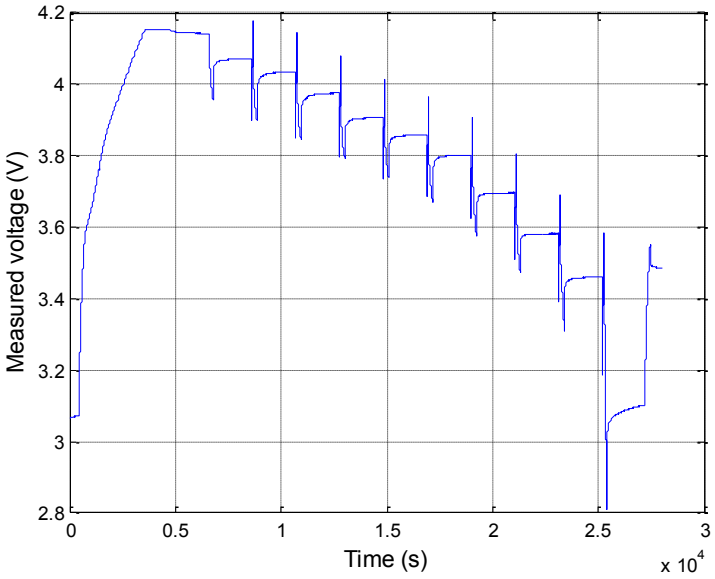

Figure 11: An example of voltage response during a HPPC test

2.1.2 Aging design of experiments

It was echoed earlier that battery aging is not an easy phenomenon to understand. Hence, a lot of experimental data has to be gathered to assess the criticality of various factors that contribute to battery aging. Looking at the time constraints and equipment availability, a design of experiments (DOE) with 16 aging cases was engineered to gather significant aging data. In addition, few cells were also used for battery modeling and vehicle simulation purposes. A complete aging cycle for any experiment typically consisted of a sequence of events in the following order: battery operation in a particular mode (representative of usage in actual vehicle), charging the battery back to a predefined maximum state of charge and lastly a rest period of thirty minutes to allow the cell to attain some equilibrium. The aging profiles were prescribed in power mode and not current mode. This meant, the vehicle performance was always preserved regardless of state of charge or temperature. The four severity factors considered during DOE were: mode of operation, depth of discharge or SoC_{min} during charge depleting phase, charging type and temperature. Due to equipment availability issues, these factors were not varied independently and the aging was partial (not yielding fully aged batteries). Hence, the overall aging campaign and DOE was a compromise between available resources and getting maximum information in PHEV relevant scenarios. Current and voltage data for an aging cycle representing the factors considered during aging DOE are shown in Figure 12 and Figure 13. In particular, the figures show data from a CD:CS (1:1) blend mode of operation at 30 °C, corresponding to scenario 3 in Table 2. The work outlined in this thesis utilized data from aging scenarios one and three mentioned in Table 2.

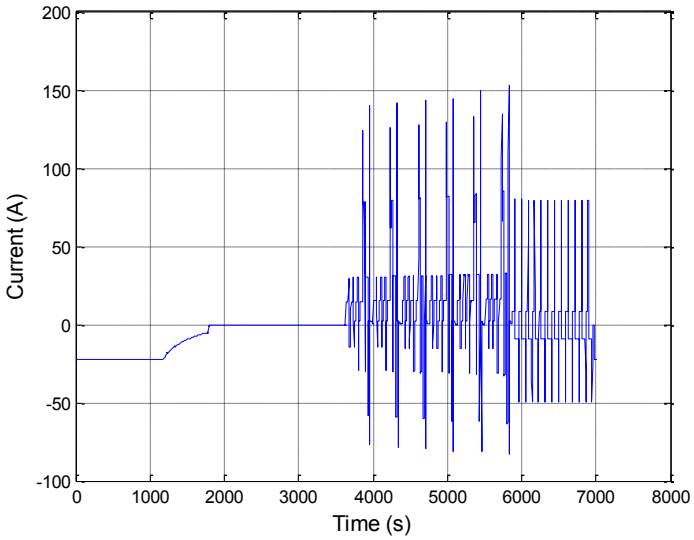

Figure 12: An example of input current profile during a PHEV like aging cycle

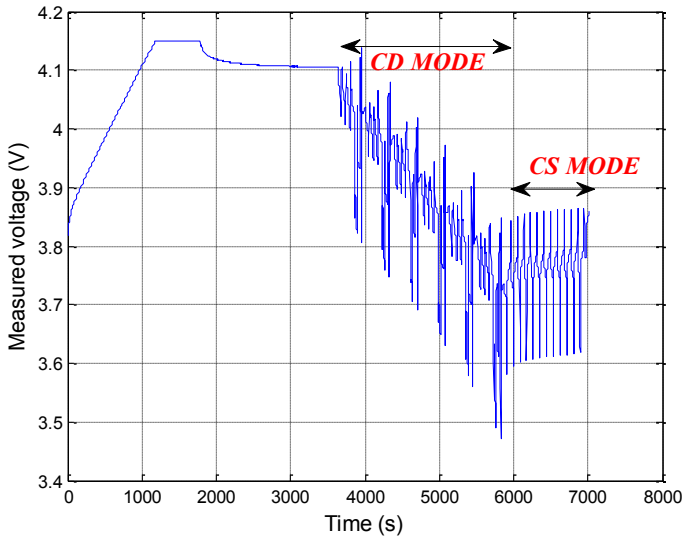

Figure 13: An example of voltage response during a PHEV like aging cycle

Aging scenario	Remarks
1	a) Effects of SoC_{min} and charging rate during charge depleting mode of operation at a single temperature of 30 °C. b) Three experiments addressing the effect of SoC_{min} at a fixed charging rate and three experiments addressing the effect of charging rate at a fixed SoC_{min} c) A total of nine experiments.
2	a) Effects of SoC_{ave} during charge sustaining mode of operation at a single temperature of 30 °C. b) No effect of charging rate. c) A total of three experiments.
3	a) Combined effect of charge depleting/charge sustaining operation at various temperatures. b) Fixed SoC_{min} of 30% and a fixed medium charging rate at different temperatures. c) A total of four experiments.
4	a) Electro-thermal modeling and characterization

Table 2: Summary of factors considered during aging DOE

A battery pack is an integral part of a PHEV, HEV or a BEV, each utilizing the energy stored in it in a different way. A PHEV uses the battery in a completely charge depleting mode with the IC engine not running until a minimum state of charge as decided by the control algorithm is reached. Following this charge depleting mode of operation, the battery is used in a charge sustaining mode with the state of charge remaining nearly constant around the minimum value and the IC engine kicking in to provide more power if needed. However, for a HEV the battery is mainly operated in a charge sustaining mode and the state of charge is nearly constant. For a BEV, the battery is always operated in a

charge depleting mode. Hence, in-order to represent all these different scenarios in which a battery can age in an actual vehicle, the three different modes of operation considered in the DOE were: pure charge depleting, pure charge sustaining and a blend mode of charge depleting – charge sustaining with different amount of time spend in each mode. For the blend mode of operation, two ratios of 1:1 and 1:3 were chosen to indicate the amount of time the battery spend in charge depleting and charge sustaining modes. Note that 1:0 and 0:1 indicates charge depleting and charge sustaining respectively. Charging the battery can happen in a number of different ways depending on the amount of charge needed and the charging time at hand. A PHEV or a BEV can be fully charged overnight at a slow pace or they could be partially charged at a faster speed in a couple of hours. Also, it has been observed in the literature [47] that, fast charging can affect the rate of aging and hence three different charging levels were chosen during the DOE. The charging event for all the cells aged during the aging campaign was done through a standard CC-CV protocol as recommended by various battery test manuals [60]. Three different CC current magnitudes were chosen to replicate different real world charging scenarios. These were fast, medium and slow depending. Some of the specifications of these current levels are outlined in Table 3.

Charging type	Protocol	Charging rate	Voltage limit (V)	Time at voltage limit (s)	Rest time (s)	Resting voltage (V)
Slow	CC/CV	C/3 (5A)	4.15	Negligible	1800	4.117
Medium	CC/CV	1.5C (22.5A)	4.15	600	1800	4.116
Fast	CC/CV	5C (75A)	4.15	600	1800	4.087

Table 3: Charging types and corresponding specifications

The minimum state of charge value in any particular mode of aging operation is a critical factor. The effect of deep discharge and battery operation in low state of charge region on battery aging has been well documented in the literature [47]. Three different minimum state of charge values of 45, 35 and 25% were chosen to assess the severity of depth of discharge. These were relevant for battery operation during charge depleting and charge sustaining operation. For the initial DOE, most of the experiments were conducted at a fixed temperature of 30 °C. This was assuming that the thermal control system would carefully monitor the temperature of the battery pack and keep it fixed around this chosen value. In-order to assess the effect of higher temperatures on the performance of lithium-ion batteries, a couple of experiments were engineered at a later date, to occur at elevated temperatures of 45 and 55 °C. A complete summary of the DOE and the ampere-hour throughput at the end of experiment is outlined in Table 4.

Experiment number	Mode of operation	Charging type	SoC_{min} (%)	Temperature (°C)	Ampere-hour throughput at end of experiment (Ah)
1	CD	FAST	45	30	24292
2	CD	FAST	35	30	28140
3	CD	FAST	25	30	30704
4	CD	MEDIUM	45	30	24361
5	CD	MEDIUM	35	30	53489
6	CD	MEDIUM	25	30	27596
7	CD	SLOW	45	30	12364
8	CD	SLOW	35	30	13984
9	CD	SLOW	25	30	12712
10	CD	MEDIUM	35	45	14792
11	CD	MEDIUM	35	55	7625
12	CS	-	45	30	17477
13	CS	-	35	30	20080
14	CS	-	25	30	16385
15	CD-CS(1:1)	MEDIUM	35	10	19944
16	CD-CS(1:1)	MEDIUM	35	30	50054
17	CD-CS(1:3)	MEDIUM	35	30	44149
18	CD-CS(1:1)	MEDIUM	35	45	21315

Table 4: Complete overview of experimental activities and aging DOE

2.2 Battery Model

2.2.1 Battery model classification

It was noted in chapter 1, section 2.3 on battery modeling, that a number of battery models have been established for simulating the response of battery cells used in various applications. These can be broadly classified into two categories: Phenomenological or Physics based and Empirical or Input-Output based [39]. Electrochemical models and particle filter models are some common physics based approaches used by researchers. These models focus on electrochemical reactions taking place at the cell level and define

these reactions by using partial differential equations. The parameters that need to be identified in-order to solve these models are actual physical quantities. Such models are more suited for understanding material properties and hence are used for material selection and characterization, for cell cathode and anode [43]. One of the biggest downfalls of these models is they are computationally expensive. Though a lot of work has taken place over the years to reduce the computation time of such models and still retain their physics based approach, they are still second priority for on-line implementation. On the contrary, a lot of battery modeling work has been dedicated to understanding the cell from an input-output perspective. Equivalent circuit models and impedance models are few common empirical approaches used by researchers. These are computationally less expensive, require less calibration effort and are easily reproducible for different battery chemistries. Hence, these are better suited for state estimation, control system implementation, system identification and other system level simulation. A brief summary of different battery modeling approaches is shown in Figure 14. This thesis aims to develop an algorithm for capacity and resistance estimation that can be implemented in real time. Hence, cheap computation and ease of implementation are two critical objectives. Keeping in mind the same, a first order equivalent circuit model has been used to develop an algorithm for capacity and resistance estimation in this thesis.

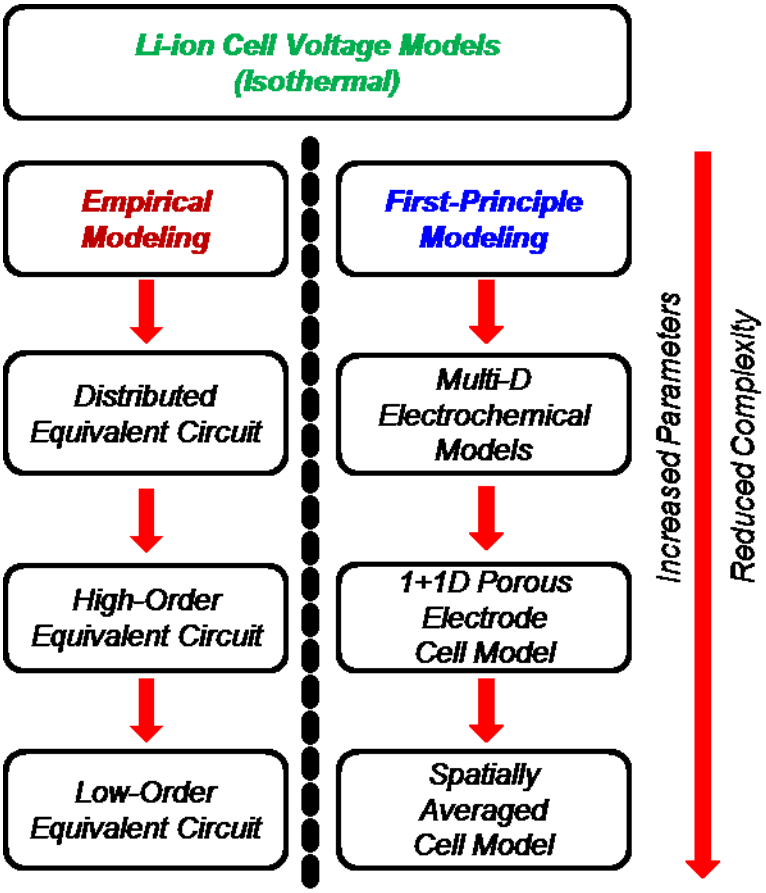

Figure 14: Lithium-Ion battery model classification [67]

2.2.2 Equivalent circuit battery model

As noted earlier an equivalent circuit battery model can be used to simulate the voltage response of a battery cell under different operating conditions. These models consist of an ideal voltage source, an internal resistance and a number of RC circuits in series [39]. The number of RC branches decide the order of the battery model and a higher order model generally predicts the battery dynamics better. The simplest equivalent circuit model is a Zeroth order model. Such a model consists of an ideal voltage source and an internal resistance term and is devoid of any RC circuits. As a result, it is very easy to calibrate and

develop such a model using experimental data. However, it cannot capture all the cell dynamics and as a result gives inaccurate voltage response. For goals such as algorithm development, system identification and control system development first and second order battery models are considered accurate enough. Though a lot of calibration effort is required to come up with accurate battery models, they are still useful considering the fact that battery aging is such a complicated phenomenon. The inputs to these battery models are generally some physical quantities like current, temperature and the battery state of charge with the output generally being an estimate of the voltage at the output terminals of the battery (V_{est}), also referred to as the closed circuit voltage (CCV). The operation of such a battery model is depicted in Figure 15.

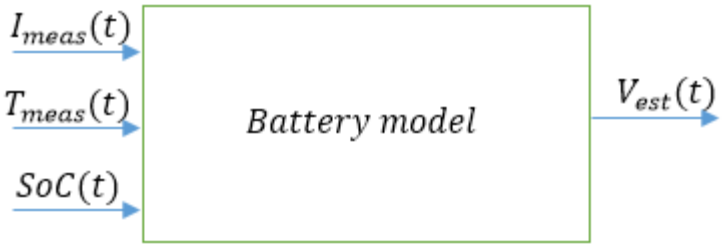

Figure 15: Output voltage estimation using a battery model

Although, many types of battery models exist, including electrochemical models, particle filter models, it should be noted that the algorithm presented in this thesis does not rely on specific model type. It only requires a battery model which can estimate the dynamic voltage at all instants. In other words, the algorithm requires a battery model that can capture the cell dynamics reasonably well. As a trade-off between model simplicity and

accuracy, a first order equivalent circuit model has been used for capacity and resistance algorithm development in this thesis. Such a model consist of an ideal voltage source, an internal resistance term and an RC circuit and can be depicted using an electrical circuit as in Figure 16. The model parameters namely E_0, R_0, R_1, C_1 are generally functions of state of charge, current magnitude and direction and temperature [39]. For the particular model considered in this project, the parameters are scheduled as shown in equations 2.6-2.8, below. The model dynamics can be descried using Kirchhoff's Law and are described in equations 2.1-2.5 below.

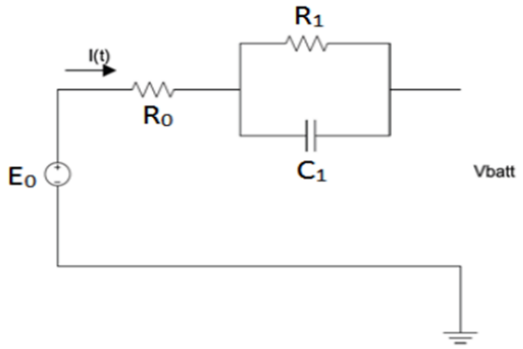

Figure 16: First order equivalent circuit model

$$V_{batt} = E_0 - IR_0 - V_{c_1} \tag{2.1}$$

$$V_{dyn} = -IR_0 - V_{c_1} \tag{2.2}$$

$$\frac{dV_{c_1}}{dt} = \frac{I}{C_1} - \frac{V_{c_1}}{R_1} \tag{2.3}$$

$$SoC(t) = \int_{t_0}^{t} \frac{I(\tau)d\tau}{Q_0} \tag{2.4}$$

$$E_0 = f(SoC, T) \tag{2.5}$$

$$R_0 = f(\text{sign}(I), T) \tag{2.6}$$

$$R_1 = f(\text{sign}(I), \text{abs}(I), T) \tag{2.7}$$

$$C_1 = f(\text{sign}(I), \text{abs}(I), T) \tag{2.8}$$

Where,

$E_0 = \text{Open Circuit Voltage (V)}$

$R_0 = \text{Internal resistance of the cell } (\Omega)$

$R_1 = \text{Dynamic resistance of the RC} - \text{circuit } (\Omega)$

$C_1 = \text{Dynamic capacitance of the RC} - \text{circuit (farad)}$

$V_{batt} = \text{Measured Voltage at the output terminals (V)}$

$I = \text{Input current (A)}$

The open-circuit voltage is generally determined as a function of battery state of charge and temperature by conducting several experiments. Once, the OCV is experimentally established as a function of SoC and temperature, the forward battery model can be implemented to obtain an estimate of the terminal voltage. Cell dynamics can be accurately modeled using the first order ECM. The open circuit voltage (OCV_{exp}) when added to dynamic voltage estimated by the model will give an estimate of the actual voltage at the output terminals of a battery (V_{est}). This is generally how a battery model functions and we will refer to it as forward battery model implementation. It can be depicted as in Figure 17 and equation 2.9.

$$V_{est} = OCV_{exp} + V_{dyn} \tag{2.9}$$

Where,

V_{dyn} ⇒ Dynamic voltage estimated by the battery model

OCV_{exp} ⇒ Experimentally determined battery OCV

V_{est} ⇒ Estimated voltage at the output terminals

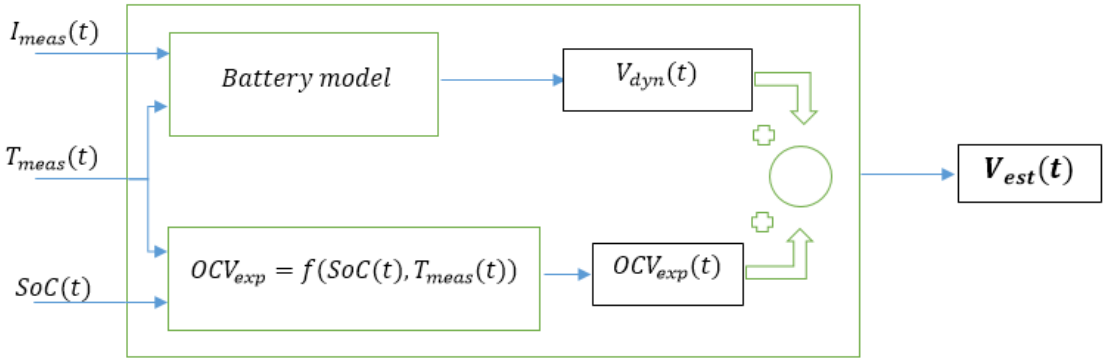

Figure 17: Forward battery model: Output voltage estimation

Since, the algorithm presented in this thesis relies on open-circuit voltage estimation, the battery model is implemented in an inverted form such that using the known measured voltage, an estimate of the open-circuit voltage estimation can be obtained. This is depicted in Figure 18 and equation 2.10.

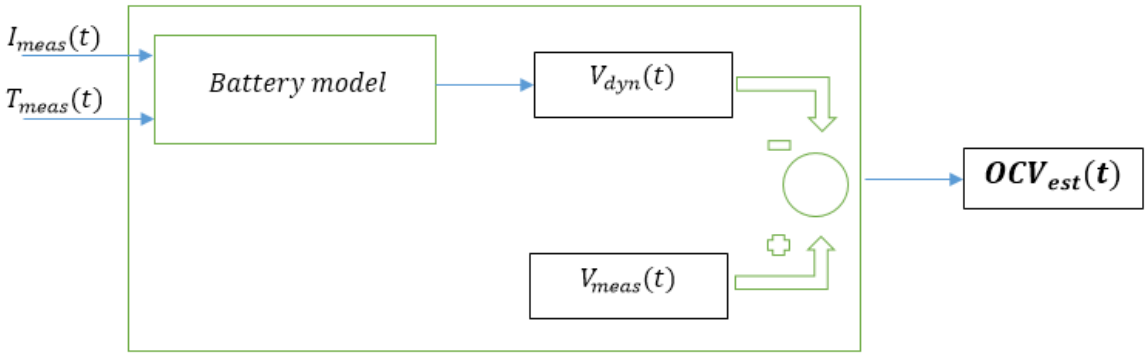

Figure 18: Inverse battery model: Open-circuit voltage estimation

$$OCV_{est} = V_{meas} - V_{dyn} \quad (2.10)$$

Where,

V_{dyn} ⇒ Dynamic voltage estimated by the battery model

V_{meas} ⇒ Measured voltage at the output terminals

OCV_{est} ⇒ Estimated battery OCV

2.2.2.1 Model identification and calibration

The battery model parameter identification is a critical step in determining the accuracy of a battery model. Model calibration is generally done by conducting a number of experiments, in order to identify the parameters of a model and to establish their dependency on other factors like battery SoC, current, temperature etc. For the model considered in this project, the parameter identification was carried out at fixed test temperature and the procedure was repeated at various temperatures. The identification current profile was engineered to traverse through the entire SoC range both while charge as well as while discharge. Battery modeling, calibration and validation is an extensive field of study and not the main focus of this thesis. A comprehensive and detailed

discussion about equivalent circuit models can be found in [61-66]. However, an example of an input current profile for parameter identification is shown in Figure 19 and the model response on the identification current dataset is shown in Figure 20.

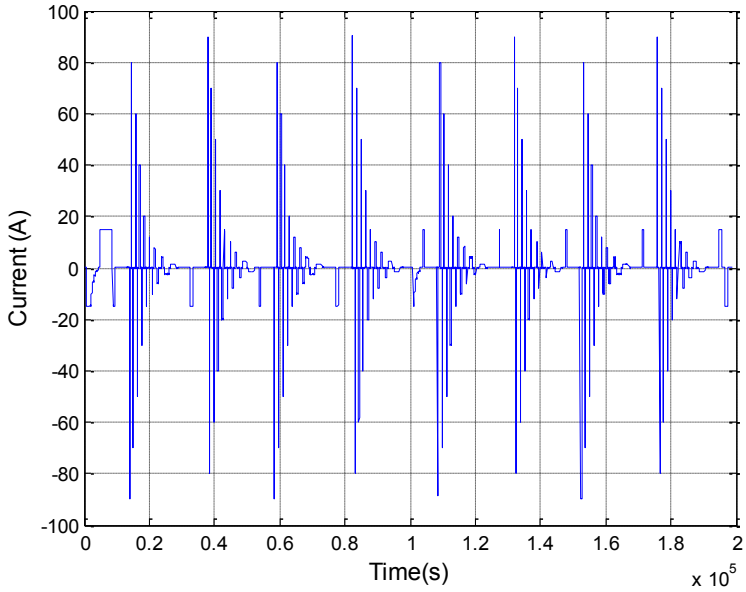

Figure 19: A typical current profile used for model calibration

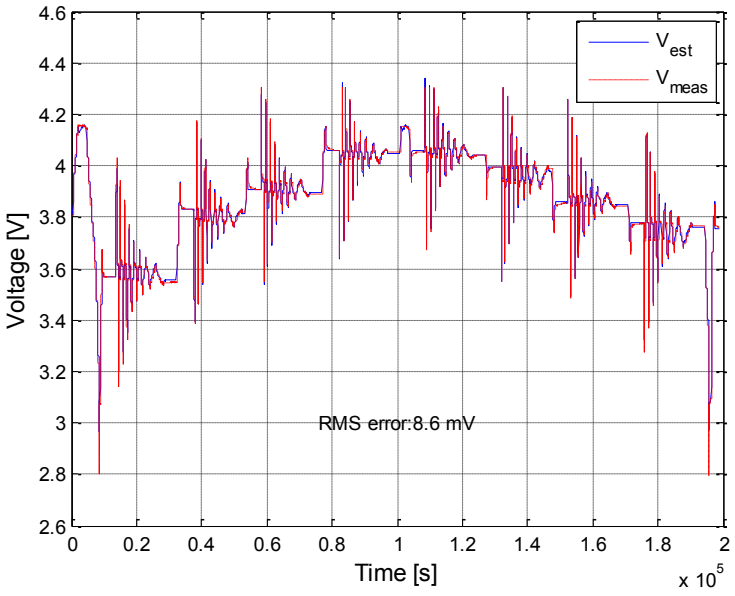

Figure 20: Typical example of battery voltage response to current profile used for calibration (red: measured, blue: estimated by model)

As seen in Figure 20, the RMS error between measured voltage and the estimated voltage, for the current input used to identify the battery model parameters is 8.6 mV, which shows that the model gives a really good estimate of output voltage. Another important quantity is the battery open circuit voltage (OCV) which is the voltage across the battery output terminals when there is no current flowing through it. Generally, the battery OCV is experimentally determined as a function of the battery state of charge (SoC) and temperature (T), irrespective of aging level or battery state of health. For the battery model considered in this thesis, this experimental procedure was carried out at five different temperatures of -10, 5, 15, 30 and 50 °C respectively. The test generally consists of soaking the cell temperature to desired identification temperature followed by charging the cell at 1C current using a standard CC/CV protocol. This is followed by discharging the cell at a

constant current rate of 1C until the minimum voltage is reached. The cell is then recharged at a constant current rate of 1C until the maximum voltage is reached. An initial estimate of OCV is obtained by taking the average of charge and discharge voltage curves as a function of ampere-hour and hence SoC. This initial OCV is further refined by using a multi-parameter optimization using identification datasets [61]. The final OCV curves obtained as a function of SoC at different temperatures are shown in Figure 21.

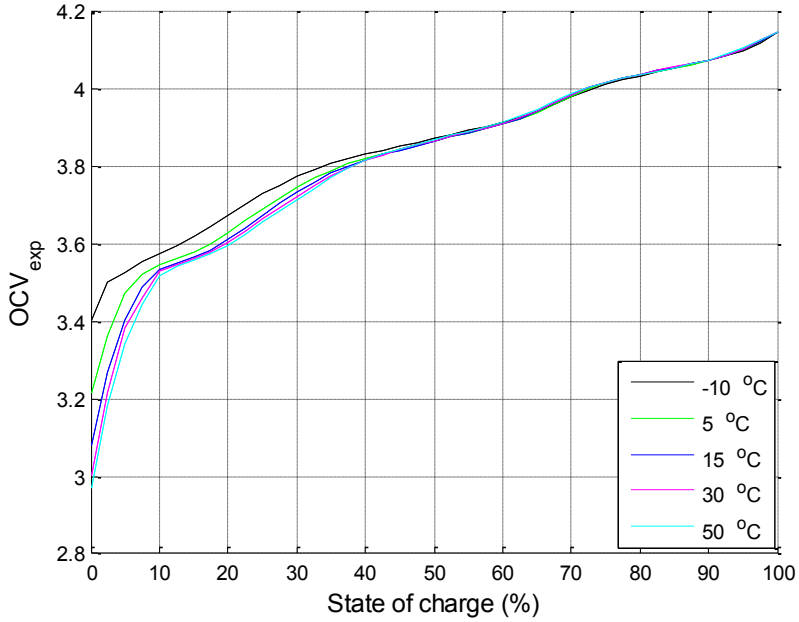

Figure 21: OCV_{exp} curves at different temperatures

It is widely observed that capacity measurements are sensitive to changes in temperature [47] and hence the capacity tests were conducted at different temperatures for cells meant for identification purposes to establish the relationship between capacity and temperature. Such a relationship for the LGChem cells considered in this project is shown in Figure 22.

The capacity values in Figure 22 are normalized with respect to a nominal capacity of 15 Ah.

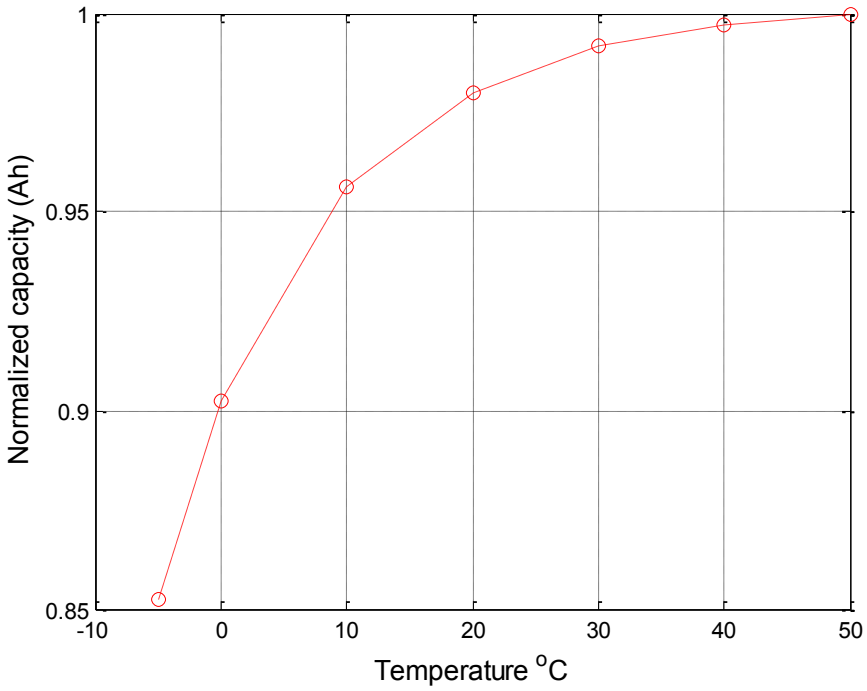

Figure 22: Effect of operating temperature on battery capacity (normalized)

2.2.2.2 Model validation

Once calibrated, response from the model must also be compared with measured data for a different set of inputs. This is known as model validation. The validation was performed on a different dataset, with the current and power profile engineered to represent a PHEV like driving profile, which would typically be a charge depleting mode of operation from a higher state of charge to a lower state of charge. An example of input current of such a representative power profile is shown in Figure 23 with the corresponding model voltage

response shown in Figure 24. It can be observed from the figure that, though the model does yield some significant error locally, it does a very good job on the entire trajectory.

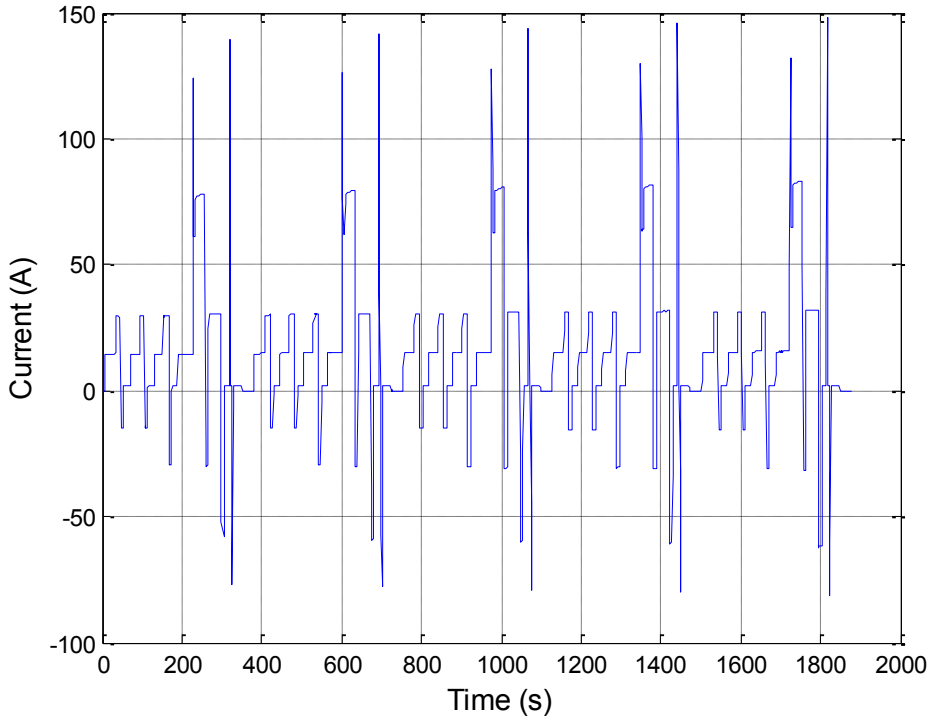

Figure 23: A typical PHEV current profile used for validation

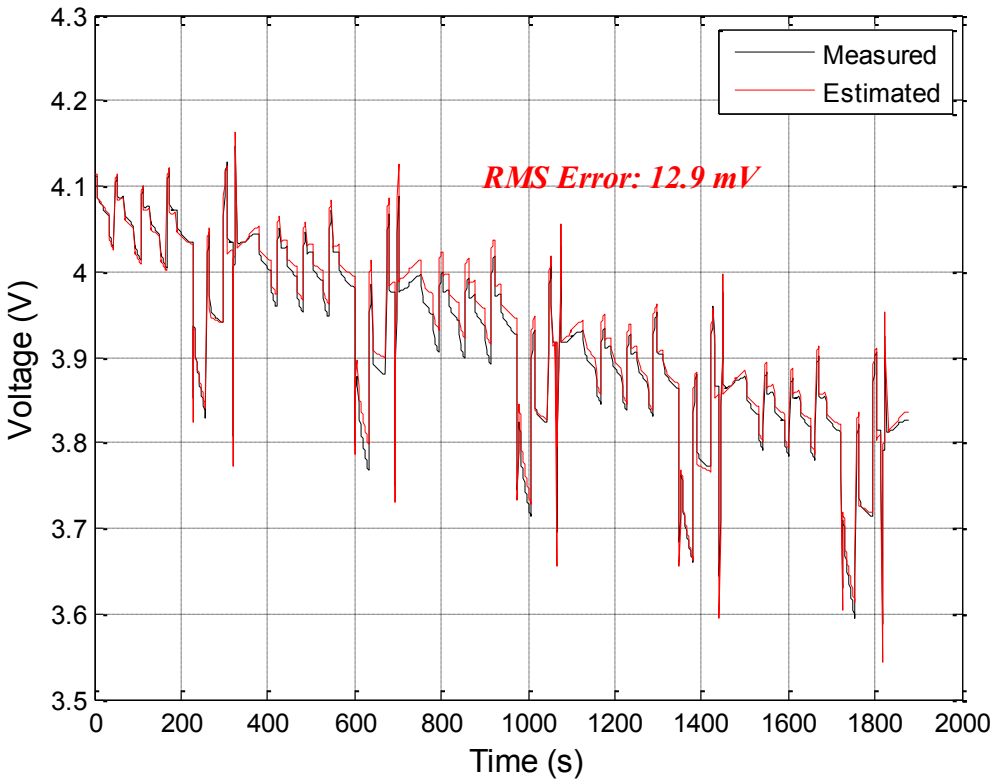

Figure 24: Typical example of battery voltage response to current profile used for PHEV current validation profile (blue: measured, black: estimated by model)

2.3 Resistance and Capacity Estimator: Needs and Wants

Energy loss and power loss are generally used to characterize battery state of health, with capacity fade and internal resistance growth contributing to those losses respectively. While several approaches have been established for quantifying the resistance growth and capacity fade under varying operating conditions in the laboratory environment, very few of these are actually implementable in real vehicles. This thesis focuses on developing an algorithm for capacity estimation of batteries, that can be implemented in real time on-board a hybrid, PHEV or an electric vehicle.

Battery State of health estimation on board a HEV, PHEV or a BEV is important for several reasons. Optimal energy management, optimal sizing of energy storage systems, safety, thermal management, diagnosis, prognosis and a long operating life of a battery are just a few of those reasons [51]. It was noted in chapter 1, section 1.5 that state of health estimation amounts to either SoC estimation, resistance estimation or capacity estimation. In addition to the above mentioned reasons, the state of health estimation is also very critical due to monetary reasons. The cost of a battery pack in a BEV has been estimated to be anywhere between 35-50% of the cost of the entire vehicle [31]. Hence, efforts need to be made to ensure long life of battery packs. Consequently, it also becomes paramount to track the state of health in-order to understand the factors that cause it to age faster and take measures to design better packs.

Numerous algorithms have been established in the literature to estimate state of charge, capacity and internal resistance of battery cells [44, 45]. These algorithms are generally model based and utilize techniques like kalman filters, extended kalman filters, particle filters, neural networks and fuzzy logic [49]. At best, these are only capable of providing accurate results offline or in a laboratory. A lot of computation would be required if they were to be imbedded on-board real vehicles. Unfortunately, such luxury is unavailable and hence these algorithms are practically impenetrable. Capacity estimation techniques employed in the field by various OEMs is a matter of great interest but most of it is proprietary and not disclosed in the open literature. However, some of the characteristics of an ideal capacity estimator can be easily thought of and the same are outlined in the upcoming paragraphs.

For ease of implementation, it is desirable that the capacity estimator relies only on readily available measurements from the CAN bus or the BMS like current, voltage and temperature. The advantages of this is twofold; firstly it ensures ease of implementation and secondly it utilizes dynamic variables that can directly give an indication of battery state of health. Most of the capacity estimation algorithms rely on either fully discharging the battery or letting it rest for a long period. Even the capacity test performed in laboratory requires the cell to be charged and discharged completely. This is not feasible in an actual vehicle. Hence, it is desirable that any proposed technique relies on the measured quantities and doesn't affect normal vehicle operation. As noted earlier, many of the algorithms developed are computationally expensive, hence limiting their use in the field. So, it is desirable that the capacity estimator is computationally cheap and can be imbedded in a microprocessor. In terms of memory requirements, it's best if the proposed technique can function independently at any given point during the life of the battery, without having to rely on much past information. The utilization of battery pack in an actual vehicle is contingent on a number of factors like type of driving cycle, powertrain architecture, driving habits etc. Hence, an ideal capacity/resistance estimator should be tolerant of data drops. Furthermore, such an ideal capacity/resistance estimator should also provide inherently clean estimates. Clean and smooth estimates will require less post-processing and filtering and hence can help gain more insight into battery aging. Over discharging and operation in low state of charge region have been identified as two causes of reduced battery lifespan [50]. Therefore, the capacity estimator should not require discharging the battery to its full or prolonged operation at low state of charge values. It should be able to

give a reliable estimate with normal vehicle and battery operation. A lot of research is taking place in the area of battery cell design and selection of materials for cathode and anode. These materials and the components that make up the cell decide the kind of chemistry the cell would fall into. It would be best for a capacity estimator if it requires very less calibration effort and is universal in nature. In other words, an ideal capacity estimator should be adaptable to various lithium-ion chemistries. To summarize the above mentioned points, a list of the desired qualities for an ideal capacity/resistance estimator are outlined below:

1) It shouldn't be affected by normal vehicle operation wherein the current, voltage and sometimes temperature are dynamic variables.
2) It should be cheap from a computation stand point so that it can be imbedded in a microprocessor.
3) It should not require the battery to be charged fully or discharged below its normal SoC limits, to avoid shortening of battery lifespan through overcharging and over discharging.
4) Robust enough to provide relatively accurate estimates in the presence of sensor noise.
5) Adaptable to various lithium ion chemistries.
6) It should require as little calibration effort as possible.

2.4 Motivation for Proposed Approach

It has been observed with many Li-ion chemistries that with cells subjected to repeated cycling do experience aging effects which manifest themselves in 2 main categories: capacity loss and power capability loss. Capacity loss is usually assessed in the laboratory by performing constant current discharge at a set current level and temperature from a fully charged condition down to some cut-off voltage level. These levels and charging and discharging protocols are specified by the battery manufacturer. Figure 25 shows a prototypical example of voltage as a function of Ah discharged (analogous to time at constant current). With increasing battery aging, the capacity decreases. While the absolute numbers vary, this effect is observed for all battery chemistries. Notice that the voltage as a function of Ah curves appear to retain their nominal shape, albeit shrunk by the aging due to the decreased capacity. This is the direct measurement of the capacity feasible only in the laboratory under controlled and fixed conditions which are never experienced in the intended applications in which the batteries are deployed. Hence it is not a field-achievable method.

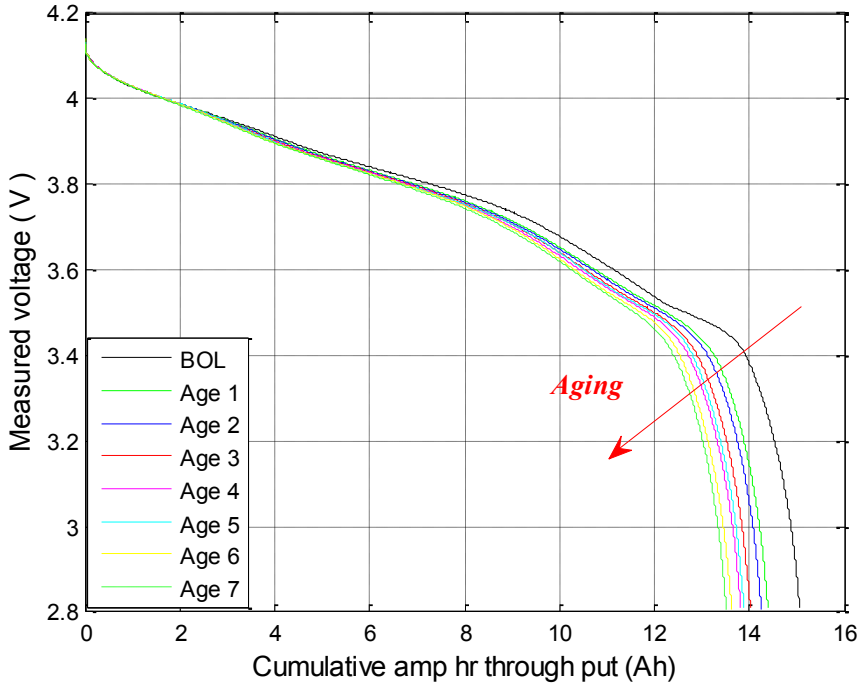

Figure 25: Measured voltage as a function of ampere-hour discharge at different aging levels

However, it has been observed for many batteries that the same curves can be re-plotted in a different set of axes, where the abscissa is not Ah discharge, but rather State of Charge (SoC) calculated on the current (aged) capacity at any point in life. In this representation the starting point and ending point of every curve is the same regardless of age, *i.e.*, the battery is always fully discharged from a SoC of 100% down to 0%. This is shown in Figure 26 for the same data set shown in Figure 25. Notice that the curves in this set of axes are nearly self-similar (*i.e.,* same shape) regardless of aging state. While the specific shape of the curve depends directly on the battery chemistry, this self-similarity property has been observed for many different types of batteries.

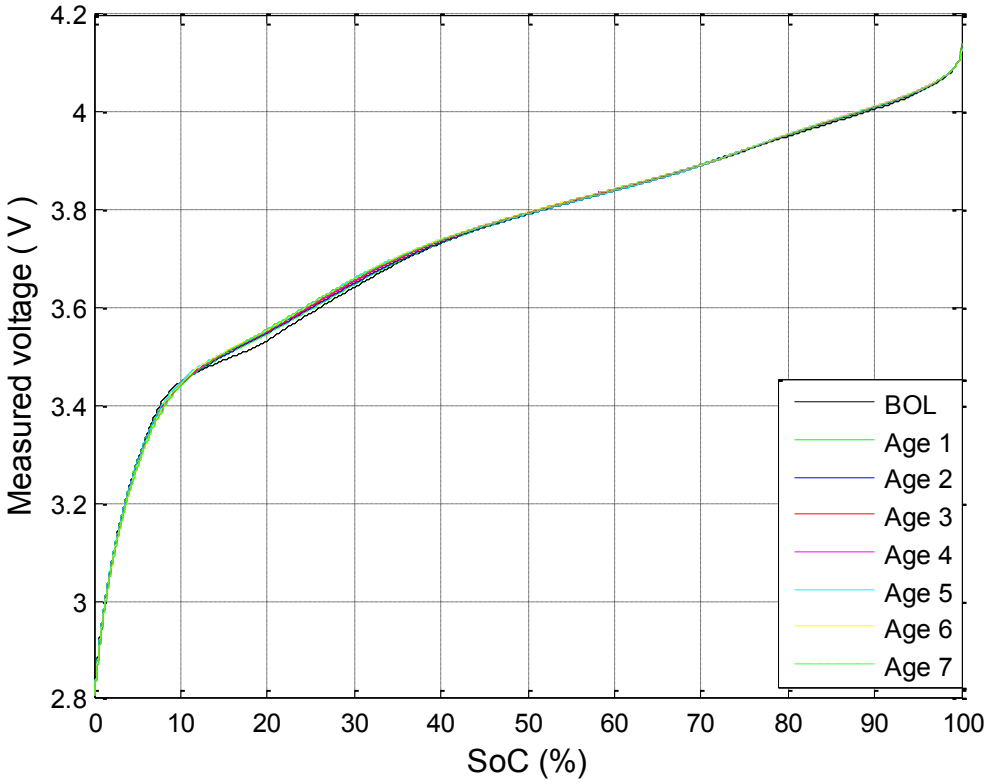

Figure 26: Measured voltage as a function of SOC based on capacity at different aging levels

This is the motivation for the approach proposed in this thesis, to effectively use this property to estimate the battery capacity at any age which best makes the curve self-similar to the Beginning of Life (BOL) curve. The challenge and main contribution of the work performed through this project is to perform the same estimation process not under controlled laboratory conditions (constant current and temperature), but under actual usage conditions while the battery is used in a vehicle (*i.e.,* during the actual aging process).

2.5 Thesis Objectives

A lot of experimental activities are being carried out The Ohio State University Center for Automotive Research, Battery Aging Laboratory. The primary goal of this thesis is to utilize data collected in the laboratory to gain insight into battery aging. This necessitates the need for development of an algorithm which can estimate the two parameters critical to quantifying battery state of health: Capacity fade and resistance growth. The idea is not too utilize advanced techniques and immense processing power, but to develop an algorithm that meets all the needs and wants of an ideal capacity/ resistance estimator as outlined in section 3. After, having developed a suitable technique, the objective should be to implement the algorithm on a number of different aging protocols to test the validity of the algorithm. One of the important needs of an ideal capacity estimator as highlighted in section 3 was it should rely on conventional measurements made in an actual vehicle. However, actual measurements are bound to be noisy and hence the developed algorithm should be tested for sensitivity to noise in sensors. It should also be robust enough to provide reliable estimates in the presence of deviation in other parameters that govern the algorithm. Consequently, sensitivity and robustness analysis should be conducted. Raw results from any capacity estimation algorithm cannot be used deduce much useful information about battery state of health. It would require some post processing, filtering etc. in-order to gain more insight into battery aging. Hence, suitable criteria must be set for post-processing the raw results such that the final results after post-processing can be fed into a state of health estimator to make end of life predictions. All the above mentioned objectives of this thesis and the chapter numbers highlighting them are listed below:

1) Utilize large amount of data available from battery aging lab to gain more insight into battery aging.
2) Develop and test an algorithm that can estimate capacity and resistance and which is implementable in real time (Chapter 3 and 6).
3) Conduct sensitivity analysis to gauge the performance of the algorithm in presence of sensor errors and variation in parameters governing the algorithm. (Chapter 4).
4) Develop and explore suitable techniques for post-processing of raw results (Chapter 5).
5) Based on capacity and resistance estimation results obtained for various different aging protocols, summarize the effect of severity factors on battery aging (Chapter 7).

Chapter 3: Algorithm Development and Methodology

3.1 Framework of the Algorithm

Capacity estimation using the algorithm can be done on event basis, beginning with a fresh cell until the end of life criterion for the cell is met. For algorithm implementation, an event is defined as the time period when the vehicle is in driving mode and battery is being used in charge depleting mode. This requirement is imposed due to the idea on which the capacity estimation technique is based and will be justified after the algorithm is described in detail in the coming sections. In other words, an event constitutes a part of the aging cycle when the cell is aged in charge depleting mode of operation. A PHEV generally operates in charge depleting mode until the minimum state of charge limit is reached, beyond which it operates in charge sustaining mode. In such a scenario, the data from charge depleting portion of driving event can be utilized to implement the algorithm. The end of life criteria is generally regarded as a 20% loss in the cell capacity with reference to its initial capacity [9]. Beyond this 20 percentage degradation, the cell is not considered suitable for use in vehicular applications. However, it can still be used for stationary storage applications. For on-board applications, the initial capacity can be considered as the nominal capacity as listed by the cell manufacturer and for battery cells subjected to aging campaigns, this capacity is experimentally determined through initial characterization tests. During these capacity tests, the cells are charged to a full state of charge and allowed

to rest for a certain amount of time. They are then subjected to constant discharge current until the terminal voltage reaches a prescribed lower limit. In this way, an estimate of the amount of charge that can be extracted from a fully charged cell can be obtained. The lower limit of voltage is recommended by the manufacturer and is regarded as the zero percentage state of charge point. This procedure is usually repeated 2-3 times to get a mean value for the cell capacity. However, these capacity tests are not practically feasible in an actual electric or a hybrid vehicle. The algorithm presented in this thesis aims to achieve the capacity estimation process onboard a vehicle using dynamic measurements and during normal vehicle operation.

The overall framework of the algorithm in input-output form is presented in Figure 27. Inputs to the algorithm are the measured quantities of current, voltage and temperature, battery model parameters, initial state of charge and a target vector of battery capacity. An estimate of the cell capacity is obtained at the end of each event starting from the BOL until the EOL criteria is met. Assuming on average a person makes two trips every day and the battery pack sustains its life for a period of 7-8years, the capacity estimator can facilitate two capacity estimates per day and around 5000 in total. In this way, the cell capacity can be continuously tracked as it ages.

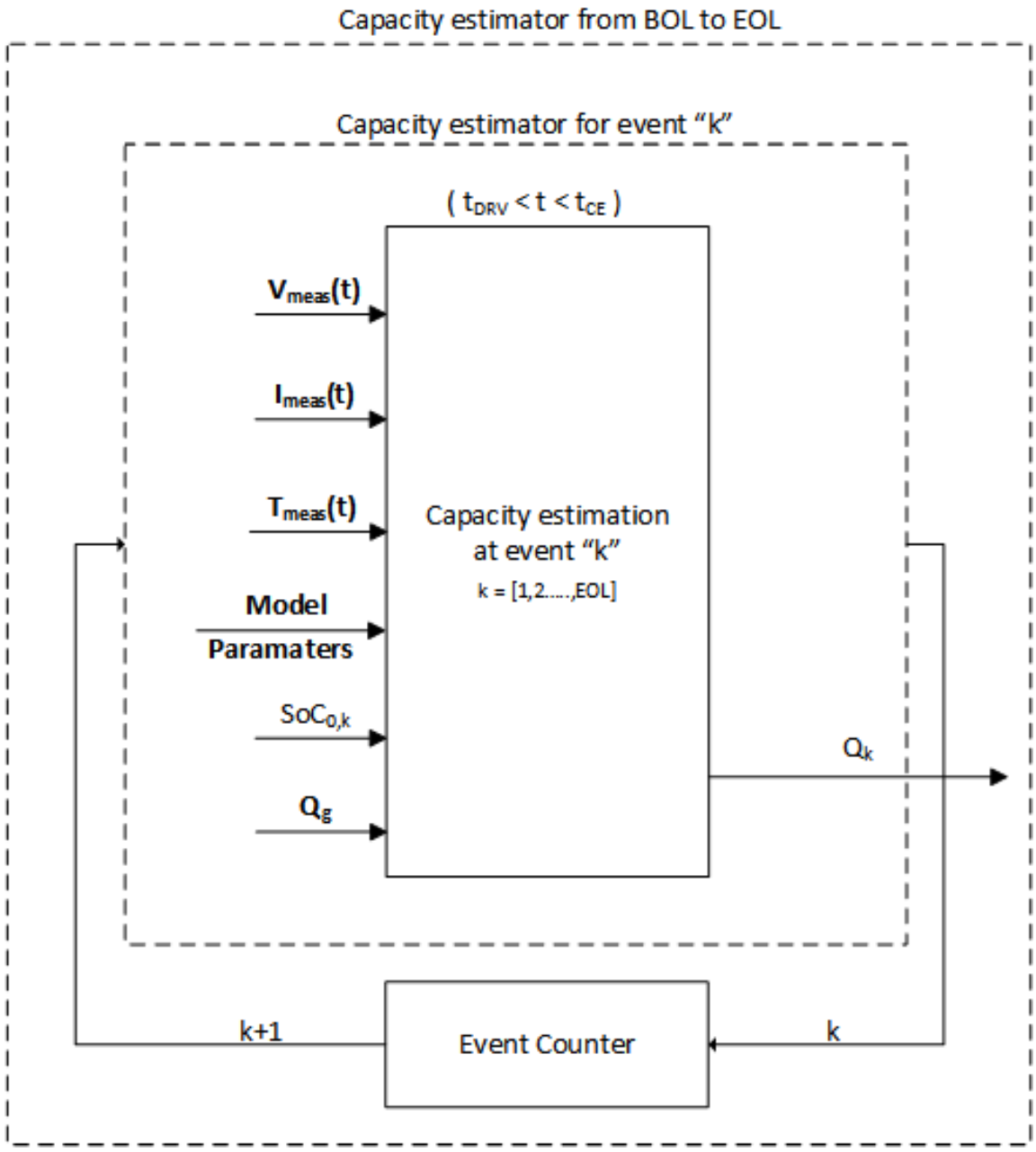

Figure 27: Block diagram for capacity estimation from BOL to EOL

The algorithm relies on measurements made by the BMS hardware components such as current, voltage and temperature sensors. These sensors have a key role to play for the

BMS to maintain full functionality and are present in some way shape or form in every BMS. These could be placed at the pack/module/cell level or even at multiple locations depending on the BMS hardware architecture. The algorithm also requires a battery model that can estimate the dynamics of a cell reasonable well. In the more common battery model implementation, the dynamic voltage when added to experimentally determined battery open circuit voltage gives an estimate of the battery terminal voltage. The algorithm presented here implements the battery model in an inverted manner, thus yielding an estimate of the open circuit voltage under dynamic conditions. This open circuit voltage will then be compared with the experimentally determined OCV described in Figure 26, (chapter 2) to give an estimate of the battery capacity as it ages. The algorithm doesn't pose any limitations on the type of model needed for implementation. It could be a complex electrochemical model or a relatively simple equivalent circuit model. As noted in section 2 on battery modeling in chapter 2, a first order equivalent circuit battery model is used in this project. The algorithm also requires the battery SoC at the beginning of each event. Because keeping a track of state of charge is so critical to monitoring battery state of health and ensuring safe operation, it is assumed that the BMS on-board a vehicle can provide an accurate initial state of charge value. However, in the laboratory this value is not known as the battery state of charge is not tracked. Hence, a method to estimate the same has been developed and is described in step 1 of section 3 later. A target vector of battery capacity is also an input to the algorithm. This can be chosen to be an array of capacity values that the cell would most likely achieve through-out its life. For instance, this can be a vector of capacity values ranging from 1.1 times the initial capacity to 0.8 times the initial capacity.

The output of the algorithm is a capacity estimate at the end of each event. Hence, the battery capacity can be tracked as it ages. For ease of understanding, a convention for font is maintained throughout all the flowcharts in this thesis. All vector quantities will be marked in bold, scalar quantities in normal font and matrices will be italicized and marked in bold. In Figure 27, the measured quantities of current, voltage and temperature and the battery model parameters are vectors of time. The quantity Q_g is a target vector of battery capacity, while $SoC_{0,k}$ and Q_k are scalars.

It is important to note, that the capacity estimator functions only when the vehicle is in operation and the battery is being used in charge depleting mode. Hence, the time duration when the measured inputs of current, voltage and temperature are utilized is from the beginning of a charge depleting driving event to the end of it.

for $k = 1$ *to EOL*
    if battery is being used in charge depleting mode
        - *Carry out capacity estimation for event "k"*
    end
end

The above pseudo code describes the algorithm in brief. The capacity estimation is done during the driving period where the battery is used in charge depleting mode, using the measured values of current, temperature and voltage, the battery model parameters and the initial state of charge value. This is repeated for all events till the end of life criteria is met.

3.2 Detailed Algorithm Description for a Specific Driving Event

While the previous section presented the algorithm from an input-output standpoint, this section explains the detailed working of the algorithm for a particular event. The capacity estimation is achieved through 7 major steps. These are Input pre-processor, SoC calculator, Experimental OCV calculator, Dynamic voltage calculator, Estimated OCV

calculator, Error calculations and Error minimization and capacity estimation respectively. These are depicted in the detailed flowchart in Figure 28. The upcoming sections will explain each of these steps in detail. It should be noted again that, a font convention to differentiate between vectors, matrices and scalars is followed throughout all the flowcharts in this thesis.

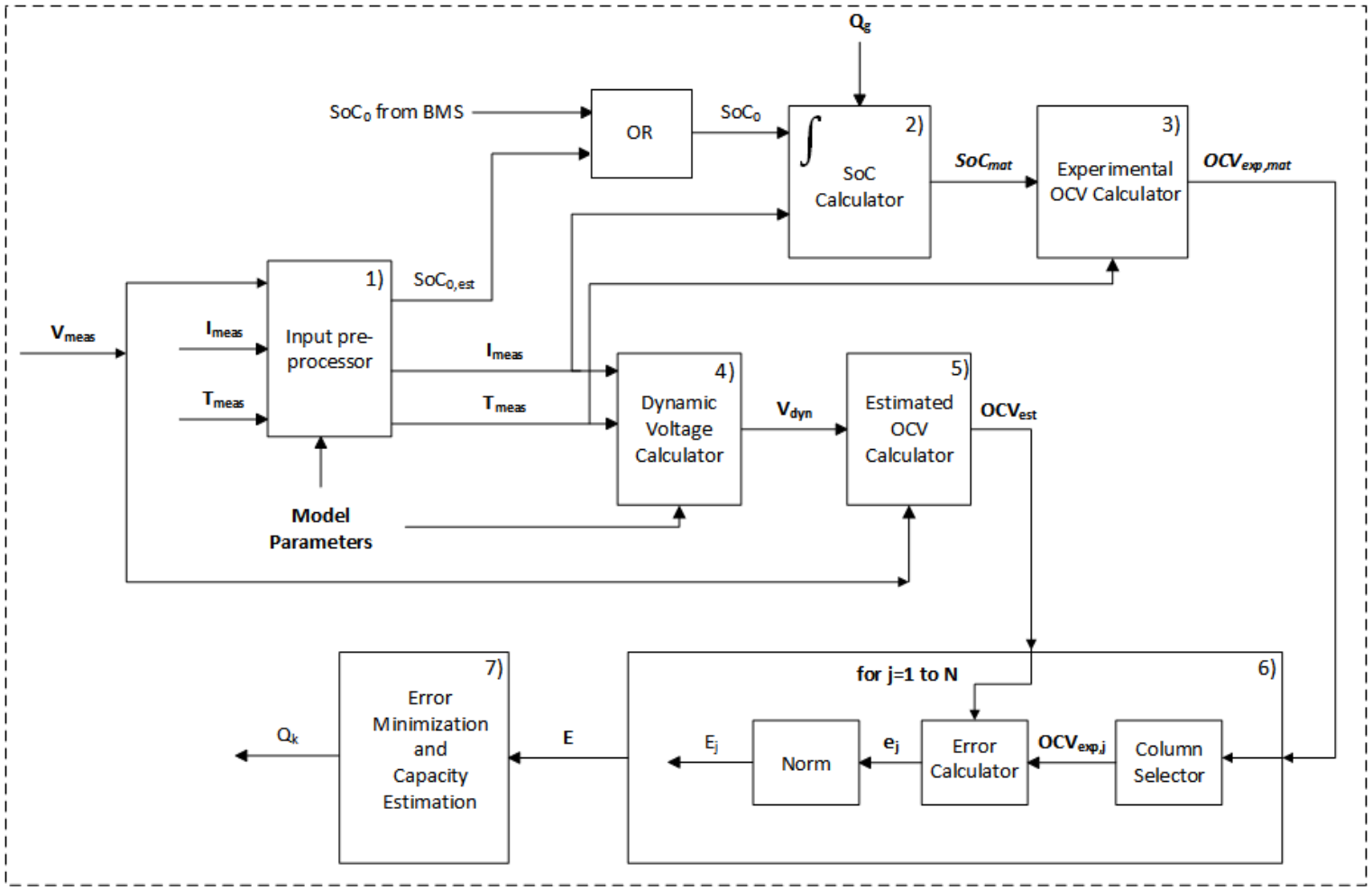

Figure 28: Detailed flowchart for capacity estimation at event “k”

3.2.1 Input pre-processor

As mentioned earlier, state of charge is not continuously tracked in the laboratory environment and this first step essentially describes a method to estimate the initial state of charge value using dynamic measurements. The inputs to this step are raw data of current, voltage and temperature and the battery model parameters with an estimate of the initial SoC value as an output. In the battery aging laboratory at the Center for Automotive Research, raw data is collected at a frequency of 10 Hz. Another step that could be embodied in this first step could be down sampling of the measured quantities. It can be recalled from the section on needs and wants of capacity estimator that low computation time and memory requirements were key desired traits. In fact, in the next chapter on sensitivity analysis it is established that the algorithm is insensitive to frequency of data acquisition and hence for on-board applications it would be a very good step to utilize down-sampled data.

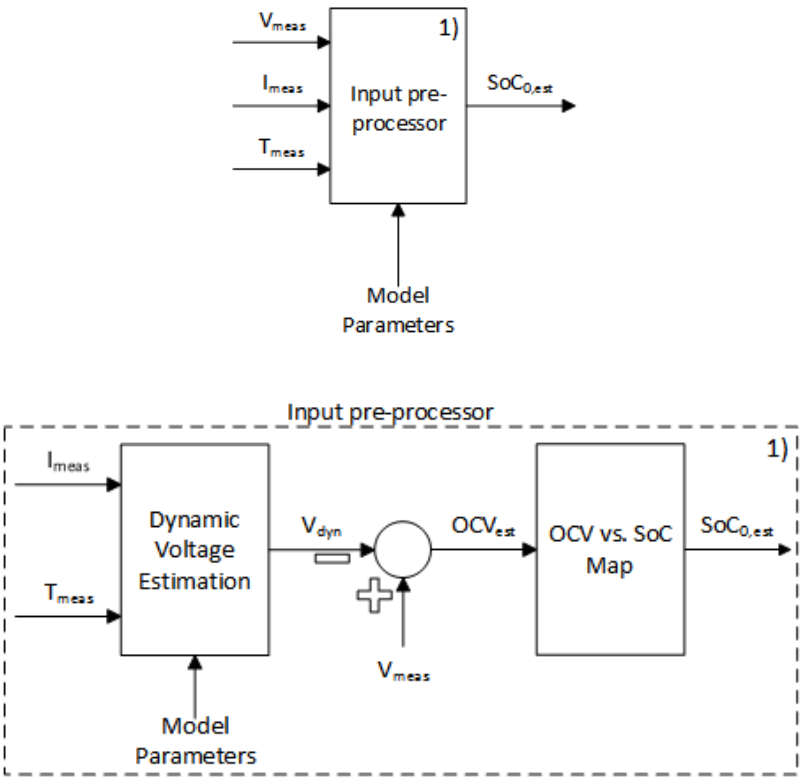

Figure 29: Block diagram for input pre-processing to estimate SoC_0

As mentioned in the introduction, capacity estimation is achieved on event basis and for practical purposes, this event is defined as any duration when the battery is used in charge depleting mode. For experiments conducted in the laboratory, this event is a portion of a complete aging cycle and is well defined by fixed aging protocols. To show the input profiles of current, voltage and temperature for one such event, an aging cycle from experiment number 4 described in Table 4 is selected. Note that for algorithm implementation, the data during charge depleting mode of driving operation is utilized. The upper and lower limits of SoC (i.e. SoC_{max} and SoC_{min}) during the charge depleting mode of driving operation, within which the data is utilized can vary. These limits define the

scope of data and sensitivity analysis will be carried out to see the effect of changing these limits on the results of the algorithm.

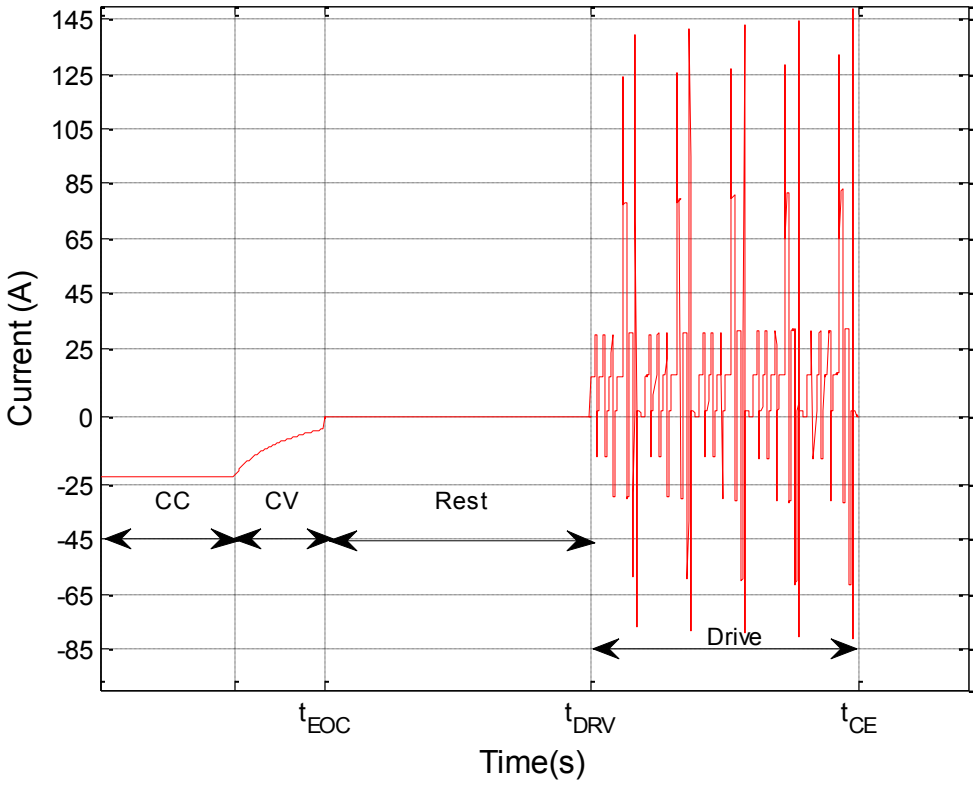

Figure 30: Sample input profile for a complete aging cycle

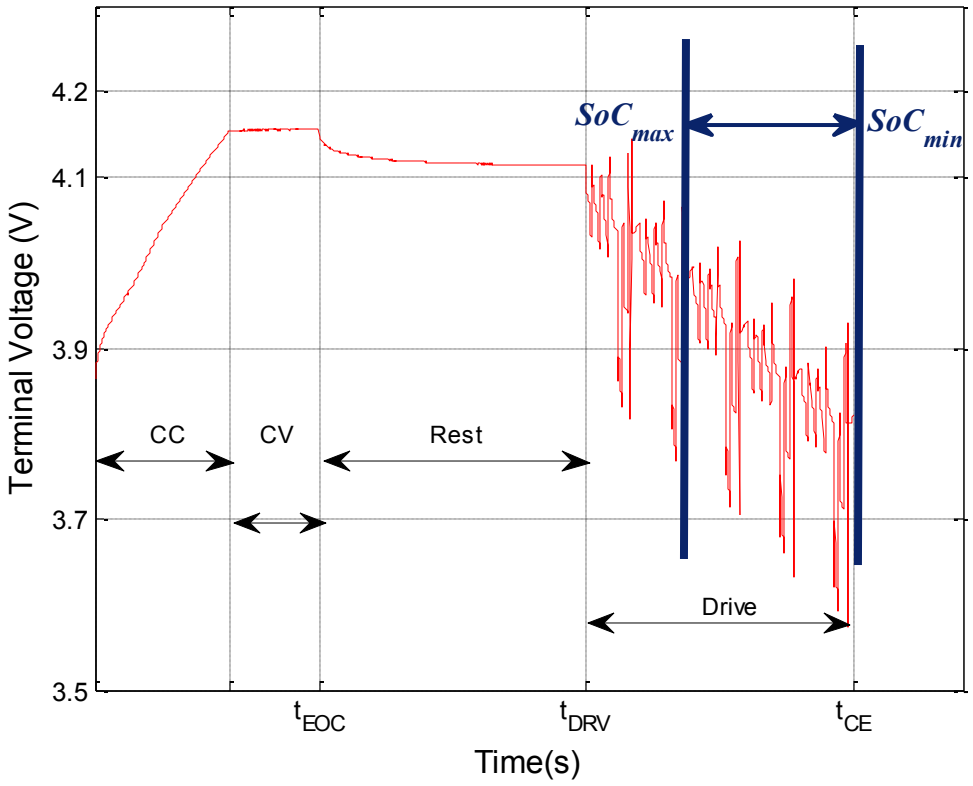

Figure 31: Sample voltage response to a PHEV like aging cycle

An aging cycle as depicted in Figure 30 and Figure 31 consist of three major steps: charging the cell using a CC-CV protocol, an intermediate rest period and the aging/driving period. During the CC portion of charging, the cell is subjected to a constant current with the magnitude being determined by the C-rating. As was described in the aging campaign section of chapter 2, the design of experiments aimed to study the effect of charging level on battery aging. This charging level determines the C-rating and consequentially the current magnitude during the constant current portion. For the experiment considered above, this C-rating happened to be 1.5C and hence a constant current of 22.5A. This is

followed by a CV charging portion, wherein charging is continued until the current drops to zero. The voltage during this period remains nearly constant. Charging is followed by an intermediate rest period, during which the battery cell is allowed to come to a state of equilibrium. For the aging cycle considered in Figure 30, there was a rest period of 30 minutes. Although, this period is not enough for the cell to attain a complete equilibrium state, it can be observed from the figure that the cell voltage does decrease exponentially, thus indicating the relaxation process. Following this charging and rest steps, the cell is subjected to aging. The current profile is engineered to represent a PHEV like current profile during CD mode of vehicle operation. It is to be noted that, the temperature was maintained constant at a fixed value of 30° C for the aging described here.

The battery model parameters are dynamic variables, generally a function of cell operating parameters like voltage, SoC, temperature, current magnitude and direction etc. As noted earlier, any type of battery model can be employed to accomplish capacity estimation using the algorithm described in this thesis. However, for simplicity and to reduce memory requirements and computation time a first order equivalent circuit model is chosen for the work presented in this thesis. For such a model, three parameters namely internal resistance, RC resistance and RC capacitance are evaluated. For more about the specifics of the battery model, please refer to chapter 2.

As mentioned earlier, the algorithm for capacity estimation relies on accurate initial state of charge estimation. Since, the algorithm relies on data collected in the laboratory measured SoC values are not available and hence an approach is presented to estimate the SoC_0 value (Figure 29). However, in a hybrid or an electric vehicle the BMS can provide

the SoC value at every instant which can be used in order to implement the algorithm in real time. The method adopted in this thesis makes use of the established OCV vs SoC map. The OCV is experimentally determined as a function of the battery state of charge (SoC) and temperature (T), irrespective of aging level or battery state of health. This map is unique for different battery chemistries and combinations of anode and cathode. The OCV vs SoC map established for the battery cells considered in this thesis was shown in Figure 26.

It is known that the current during the rest period is zero. According to this, the battery dynamic voltage should be zero and hence the measured voltage can be assumed to be equal to the battery OCV during resting period. This approximation can be used to interpret the OCV vs SoC map and hence get an estimate of the SoC_0 value. In Figure 32 and Figure 33, the OCV (approximated as the terminal voltage) and the corresponding SoC is plotted during the rest period. The end value of SoC is thus the $SoC_{0,\,est}$ value. It can be observed, that using such an estimation method yields a relaxed initial state of charge value where the battery voltage is almost constant and consequently the state of charge has attained an almost constant asymptotic value.

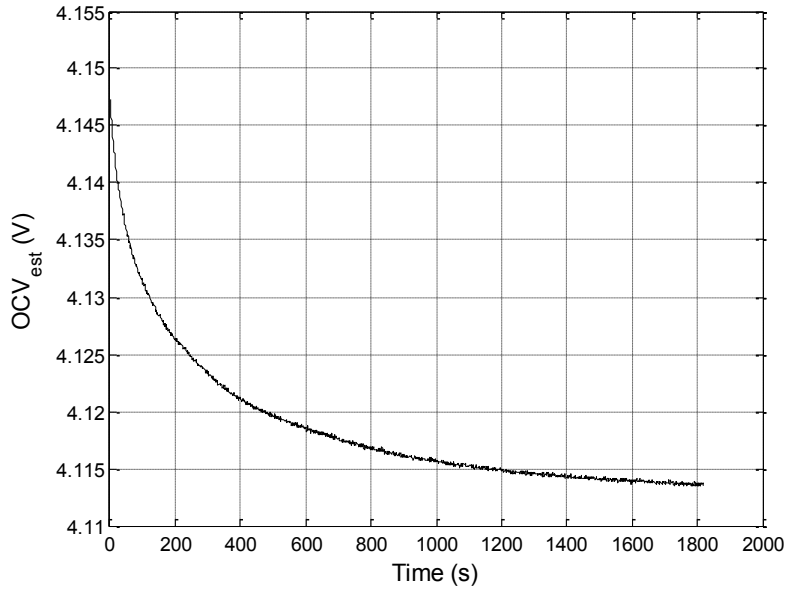

Figure 32: OCV trajectory during rest period for a sample aging cycle

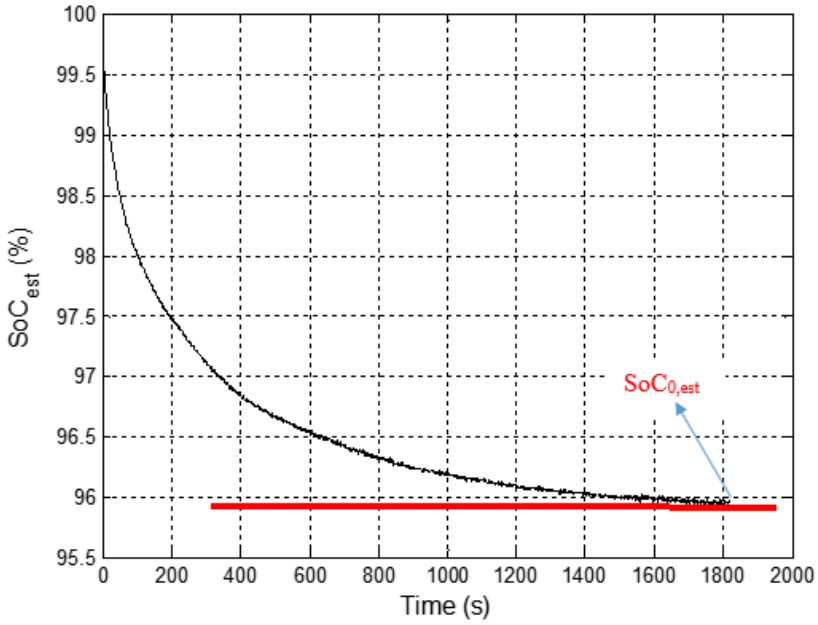

Figure 33: SoC trajectory during rest period for a sample aging cycle

It can also be observed from Figure 33, that the SoC_0 value is accurately estimated within $\pm$ of a fraction of percentage. It will be later established in the sensitivity analysis chapter that this much of an error in SoC_0 estimation approach does not impact the capacity estimation algorithm.

3.2.2 SoC calculator

Inputs to this step are the measured current, SoC_0 value and the target vector of battery capacity Figure 34. The output is a matrix of SoC values. For each value of target capacity, coulomb counting [51] is adopted to calculate the battery state of charge starting from SoC_0 value. The target value of cell capacity is used to normalize the state of charge and is described in equation below. The output is a SoC value at each instant of time and for each value of Q_g resulting in a matrix of SoC values.

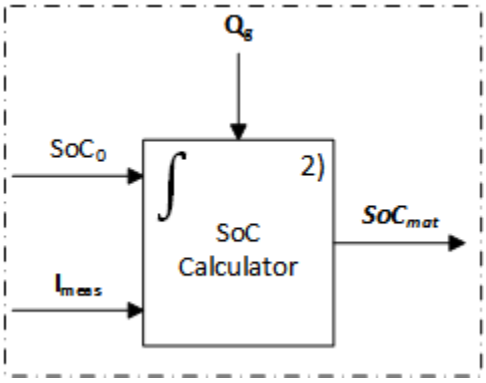

Figure 34: Block diagram for SoC calculations

The output SoC_{mat} constitutes the SoC matrix, with SoC_j being a column vector of time, calculated using the j^{th} value from the target battery capacity vector Q_g. In Figure 35, the SoC values are represented as a function of time for three different target capacity values.

It can be seen, that the SoC values are different for the three vectors. The green curve corresponds to the lowest cell capacity while, the blue one corresponds to the maximum cell capacity. In the same way, SoC can be calculated for the remaining values of target capacities.

$$SoC_j(t) = SoC_0 - \int_{t_{DRV}}^{t_{CE}} \frac{I_{meas}(\tau)d\tau}{Q_{g_j}} \quad (3.1)$$

$$SoC_{mat} = [SoC_1 \quad .. \quad SoC_j \quad .. \quad SoC_N] \quad (3.2)$$

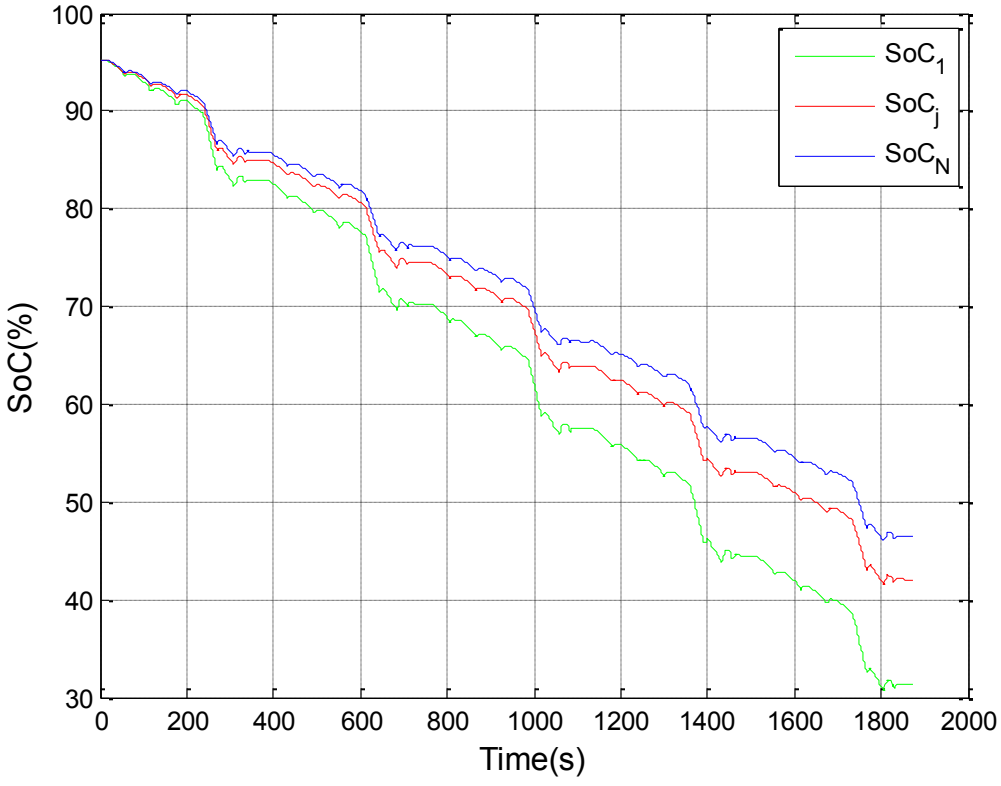

Figure 35: Representative example of SoC as a function of time at event "k" for three different target capacities

for $j = 1$ *to length of vector* Q_g

- *Select the guessed battery capacity based on index* j

for $l = 1$ *to* M

- *Calculate* SoC_j *at time* $t = t_{DRV+l}$ *using coulomb counting starting from* $SoC_{0,k}$ *and normalizing using guessed capacity* Q_{g_j}.

end

- $SoC_j = A\ vector\ of\ SOC\ values\ of\ length\ M\ corresponding\ to\ the\ guessed\ capacity\ Q_{g_j}$

end

$SoC = [SoC_1 \ldots \quad SoC_j \ldots \quad SoC_N] - A\ matrix\ of\ SoC\ values\ of\ size\ M * N$

3.2.3 Experimental OCV calculator

Once the SoC values are calculated, OCV_{exp} can be calculated by interpolating the experimentally established map for OCV as a function of SoC and temperature (Figure 26). The result thus is a value of OCV_{exp} at every instant of time and for each guessed value of Q_g resulting in a matrix of OCV_{exp} values (Figure 36, Figure 37). Recall the measured voltage curves obtained as a function of state of charge during capacity tests (Figure 25). It was observed that the curves were self-similar and hence implied that OCV was strictly a function of SoC and temperature and independent of the capacity. The OCV_{exp} determined in this step is equivalent to those curves, the difference being the current capacity here is not known and the OCV curve obtained here is under dynamic conditions (current not constant). As a result, we are able to obtain OCV as a function of cell capacity and SoC under dynamic conditions. It is relevant noting that the algorithm relies on comparison of OCV form two different approaches and hence, the OCV obtained in this step will be used to compare with the OCV estimated using a battery model in step 5.

Lastly, the target capacity value that yields minimum error between the OCV calculated from two approaches will give the best estimate of cell capacity at any given age.

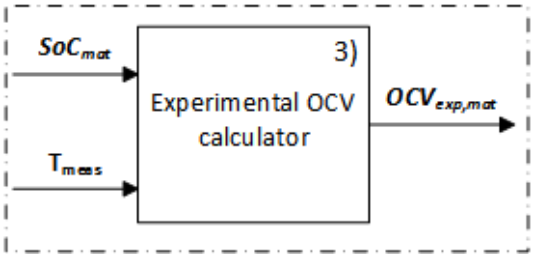

Figure 36: Block diagram for OCV_{exp} calculations

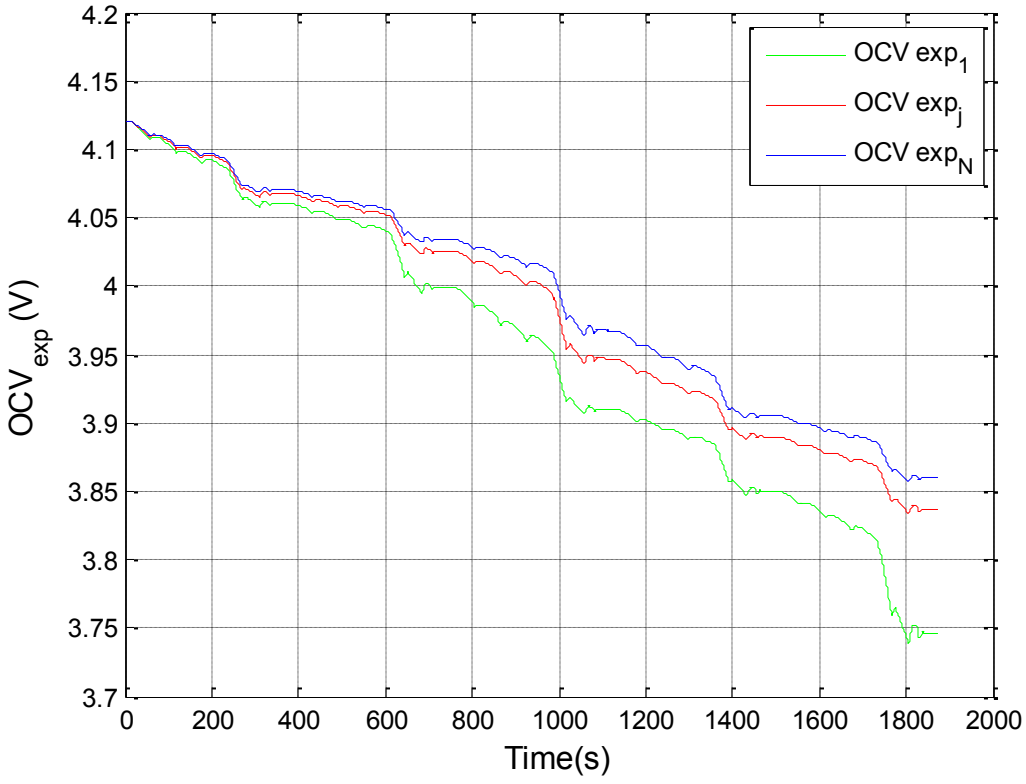

Figure 37: Representative example of OCV_{exp} as a function of time at event "k" for three different target capacities

for $j = 1$ *to length of vector* Q_g

- $Select\ the\ guessed\ battery\ capacity\ based\ on\ index\ j$

for $l = 1$ *to* M

- $Calculate\ OCV_{exp}\ at\ time\ t = t_{DRV+l}\ using\ experimentally\ established\ OCV_{exp}\ as\ a\ function\ of\ SoC\ and\ temperature.$

end

- $OCV_{exp_j} = A\ vector\ of\ OCV_{exp}\ values\ of\ length\ M\ corresponding\ to\ the\ guessed\ capacity\ Q_{g_j}$

end

$$OCV_{exp} = [OCV_{exp_1} \ldots \quad OCV_{exp_j} \ldots \quad OCV_{exp_N}] - A\ matrix\ of\ OCV_{exp}\ values\ of\ size\ M * N$$

3.2.4 Dynamic voltage calculator

In this step the cell dynamic voltage is calculated as shown in equations 3.3 and 3.4 below, using the measured data of current and temperature. The inputs to this step are current, temperature and model parameters (Figure 38). These parameters are scheduled on current magnitude and direction and temperature. It should be noted that, the battery model parameters are specific to a particular type of model used for implementing the algorithm. The algorithm does not impose any limitation on the type of model used. The only constraint is the model used should give an accurate estimate of the dynamic voltage which when subtracted from the measured voltage can give an estimate of the cell OCV. Since, V_{dyn} and V_{meas} are independent of the battery cell capacity, the output of this step is a vector of time (Figure 39).

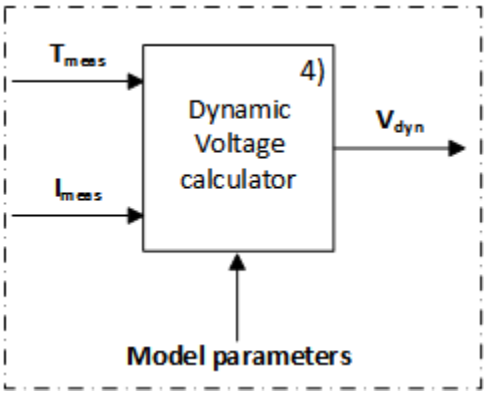

Figure 38: Block diagram for dynamic voltage estimation

$$V_{dyn} = -IR_0 - V_{c_1} \tag{3.3}$$

$$\frac{dV_{c_1}}{dt} = \frac{I}{C_1} - \frac{V_{c_1}}{R_1} \tag{3.4}$$

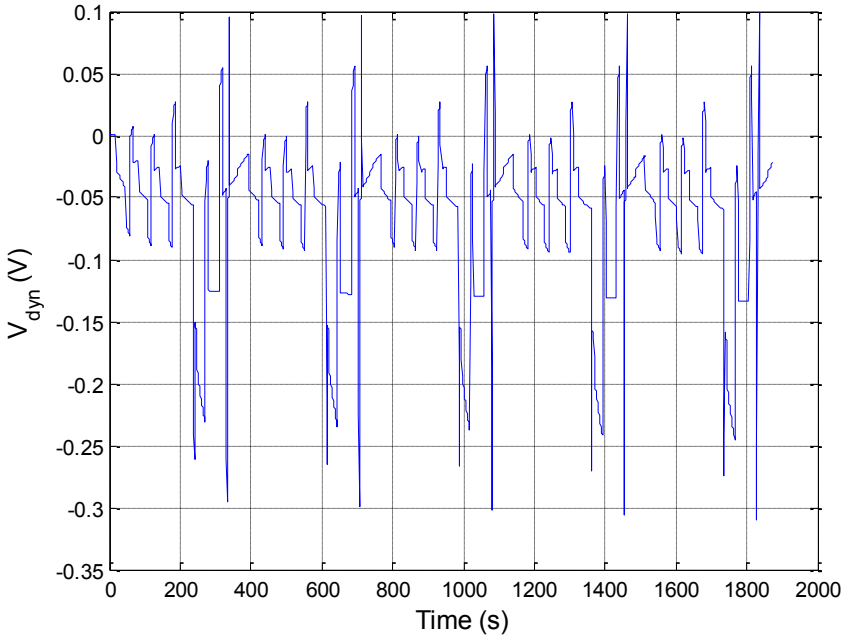

Figure 39: Representative example of dynamic voltage estimation (V_{dyn}) as a function of time at event "k"

for $l = 1$ *to* M

- $Calculate\ V_{dyn} at\ time\ t = t_{DRV+l}\ from\ the\ battery\ model\ using\ measured\ values\ of\ current\ and\ temperature$

end

- $A\ vector\ of\ values\ of\ V_{dyn}\ of\ length\ M$

3.2.5 Estimated OCV calculator

In this step, the dynamic voltage calculated in step 4 is subtracted from the measured voltage to get an estimate of the cell OCV (Figure 40, Figure 41). This is essentially the battery model inversion described in chapter 2 and can be represented as in equation 3.5 below. It is to be noted that, this OCV is different from the one calculated in step 3. In the 3rd step, OCV was calculated using an experimentally established look-up table. In this step, the battery model is used to get an estimate of OCV. Error between OCV calculated in step 3 and in this step will be minimized to get an estimate of cell capacity. This is the main motivation behind the proposed algorithm. It is to utilize dynamic measurements to get an estimate of the OCV (step 5) and compare it with OCV independent of the cell capacity or age by utilizing the self-similarity property of lithium-ion batteries.

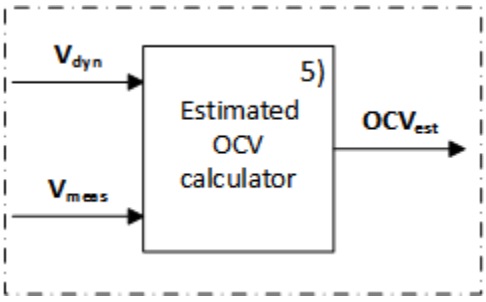

Figure 40: Block diagram for OCV_{est} Calculation

$$OCV_{est} = V_{meas} - V_{dyn} \quad (3.5)$$

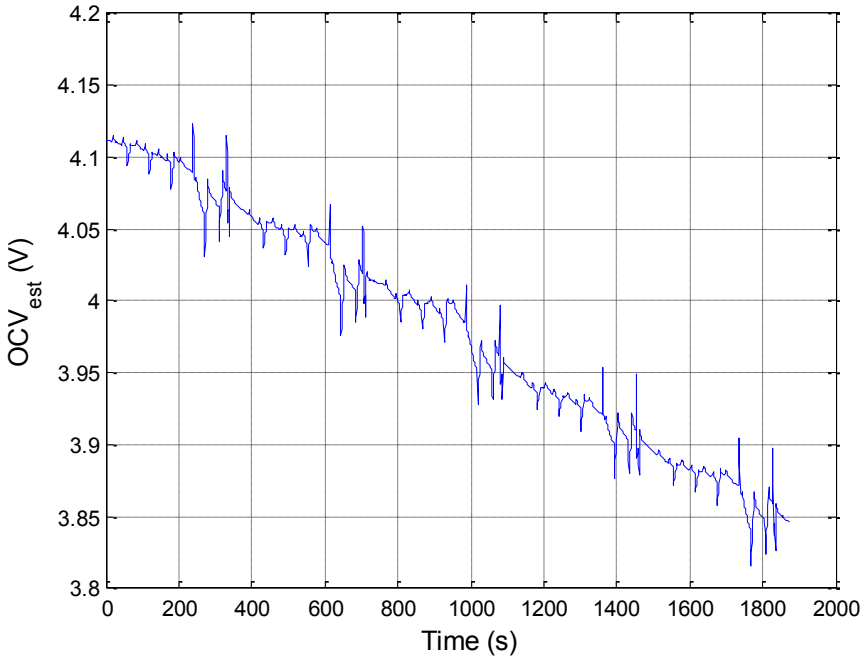

Figure 41: Representative example of OCV estimation (OCV_{est}) as a function of time at event "k"

for $l = 1$ *to* M

- $Calculate\ OCV_{est}\ at\ time\ t = t_{DRV+l}\ by\ subtracting\ V_{dyn}\ at\ time\ t = t_{DRV+l}$
  $from\ V_{meas}\ at\ time\ t = t_{DRV+l}.$

end

- $A\ vector\ of\ values\ of\ OCV_{est}\ of\ length\ M$

3.2.6 Error calculator

In this step, comparison is made between the OCV calculated from both the approaches earlier (Figure 42). First, a column from the $OCV_{exp,mat}$ is selected corresponding to the j^{th}

value of target capacity vector. This $OCV_{exp,j}$ is subtracted from the OCV_{est} to give a vector e_j (Figure 43) as shown using equation 3.6 below. A norm is then used to reduce the vector e_j to a scalar quantity (equation 3.7) and thus quantify error over a large scope of data with a single value. Different norms can be used for this step and for this thesis the root mean square or the RMS value is used to quantify the magnitude of the error and is shown in equation below. This gives the scalar error E_j (equation below) corresponding to the j^{th} value of target battery capacity. This is repeated for all the N target values of battery capacity. Hence, the output of this step is an error vector E (equation 3.8).

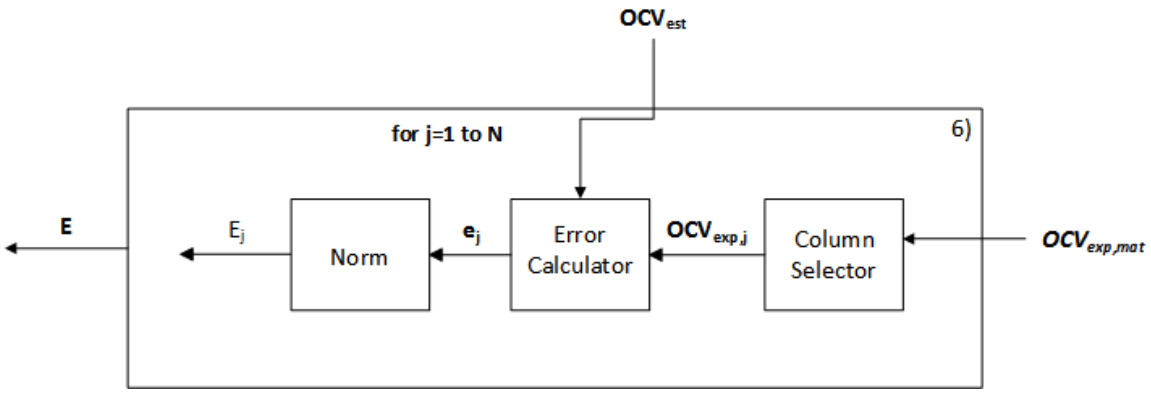

Figure 42: Block diagram for error calculations

$$e_j = OCV_{est} - OCV_{exp_j} \tag{3.6}$$

$$E_j = RMS(e_j); j = 1{:}M \tag{3.7}$$

$$E = [E_1, \dots E_j, \dots E_N] \tag{3.8}$$

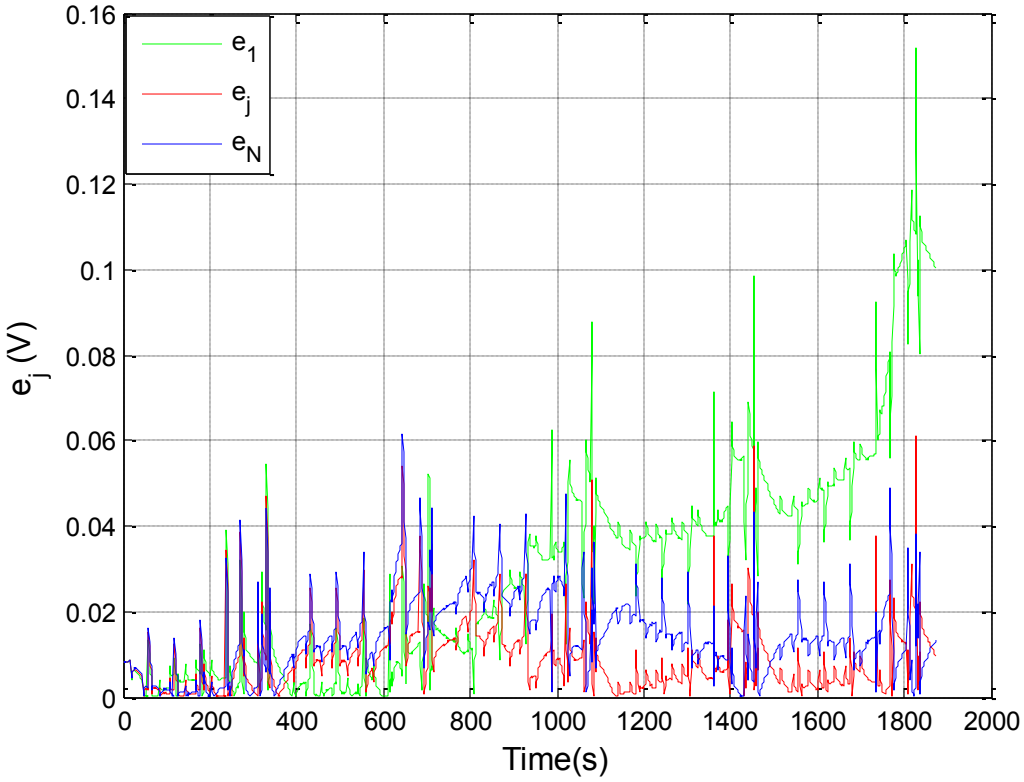

Figure 43: Representative example of error between OCV_{exp} and OCV_{est} as a function of time at event "k" for three different target capacitites

The three curves represent the error vectors of time for three different target capacities (Figure 43). In this way, the error vectors for all the target cell capacities can be calculated. By using a certain norm (like RMS), the error vector can be converted into a scalar quantity. Hence, the final output of this step is an error vector E, with each element corresponding to a particular target value of cell capacity. The result thus is an error vector as a function of the guessed cell capacity. When this error is minimized an estimate of the cell capacity can be obtained. It can be seen that the technique relies on error calculated over a wide

scope of data (thousands of points) and hence is capable of getting rid of point wise measurement errors and battery model errors.

for $j = 1$ *to length of vector* Q_g
    for $l = 1$ *to* M
        - $Calculate\ error\ e_j\ at\ time\ t = t_{DRV+l}$
    end
    - $e_j =$ $A\ vector\ of\ error\ values\ of\ length\ M\ corresponding\ to\ the\ guessed\ capacity\ Q_{g_j}$
    - $E_j = Norm\ of\ vector\ e_j\ corresponding\ to\ the\ guessed\ capacity\ Q_{g_j}$
end

- $e_{mat} = [e_1 \dots \quad e_j \dots \quad e_N] - A\ matrix\ of\ error\ values\ of\ size\ M * N$
- $E = [E_1 \dots \quad E_j \dots \quad E_N] - A\ vector\ of\ norms\ of\ vector\ of\ length\ N$

3.2.7 Error minimization and capacity estimation

In this step, minimization techniques are used to get the best estimate of capacity, the one which would result in the lowest value of error E. The most straight forward method is to look for the minimum value in the vector E and select the corresponding target capacity as the best possible estimate of the capacity at event k (Q_k). Other minimization techniques can be used as well to get the best possible estimate.

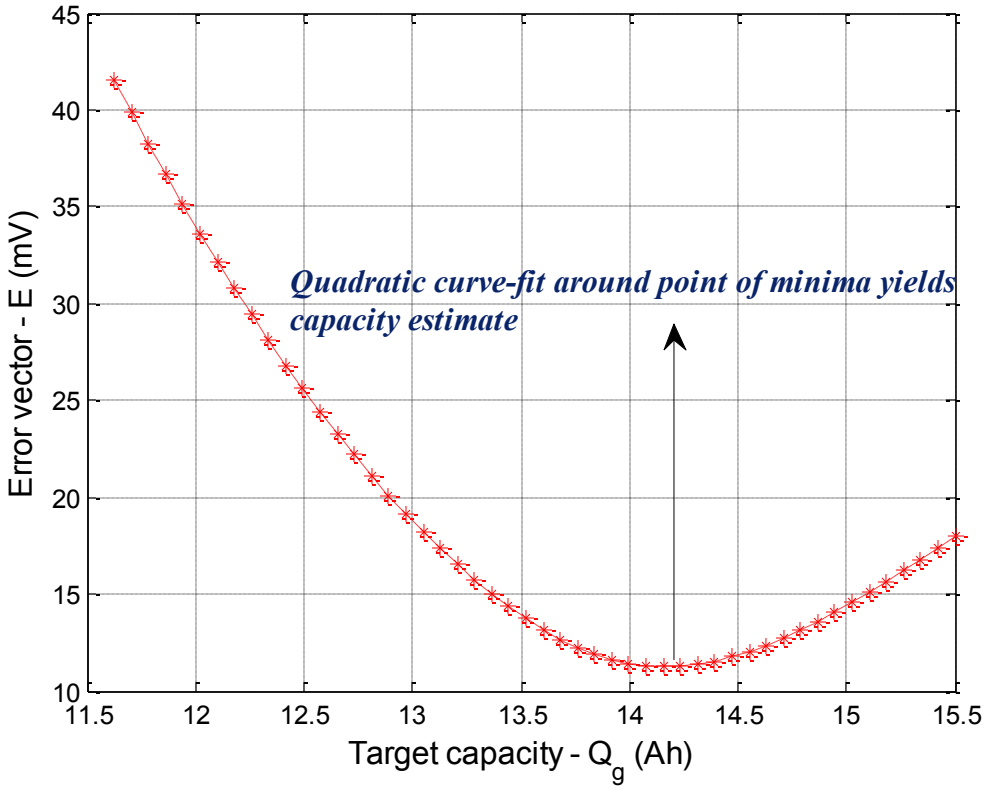

Figure 44: Estimated capacity at event "k" (Q_k) calculated using error minimization

In this thesis, the capacity is estimated by doing error minimization around the point where the error E is minimum. It is well known that any function can be assumed to be quadratic near its point of minima and hence using a quadratic curve fit near the point of minima a better estimate of capacity can be obtained. For the work presented in this thesis, two points on either side of the point of minima are chosen to enable a quadratic curve fit. It can be observed from Figure 44 that the error is very well behaved and the minimum error obtained is around 10 mV. This is a very good estimate of the OCV considering an error of 9 mV was obtained on model calibration (Figure 20). The inherent clean and well

behaved nature of the algorithm could be attributed to the fact that error calculation is done over a wide scope of data and not on individual measurements. Hence, even if there are large errors present locally, considering a couple of thousand points cancels the individual errors resulting in very well behaved error as a function of cell capacity. Another important observation from the figure above is that because the error is so well behaved, the algorithm does not require a large number of target capacities to be considered. For instance, in the figure shown 30 target capacity values were considered. However, it was observed that the results were almost inseparable with the number being reduced to 10. This is highly desirable, because larger the number of target capacities, larger would be the requirement for computation and memory.

3.3 Matrix Representation

In Figure 45, the algorithm is depicted from a vector-matrix stand point. The measured quantities of current, voltage and temperature are vectors of time, and hence have a dimension of [M*1]. The value M depends on the length of the driving period. This can vary a lot in the field depending on the duration of trip. However, in the experiments conducted in the laboratory it is fixed for a particular type of aging protocol. Since, the battery model parameters are scheduled on current and temperature, these are vectors of time as well with dimension [M*1]. The SoC_0 value is a scalar quantity while, SoC_{mat} and $OCV_{exp,mat}$ are matrices of dimension [M*N]. The value of N corresponds to the length of target capacity vector. This parameter can be changed in order to get better accuracy with the error minimization process. However, since it is observed that the error as a function of target cell capacity is nearly a quadratic function, the value of N does not really affect

the estimation algorithm. The dynamic voltage calculated in step 4 and the estimated OCV calculated in step 5 are vectors of time and have dimension [M*1]. In step 6 (error calculator), the instantaneous error e_j is a vector of time with dimension [M*1] while, E_j the norm is a scalar quantity. Hence, the output of this step E is a vector of dimension [1*N]. This error when minimized as a function of the guessed capacity vector gives a single estimate of the cell capacity Q_k. It is interesting to note that, a single capacity estimate is obtained at the end of each event from a large number of dynamic measurements.

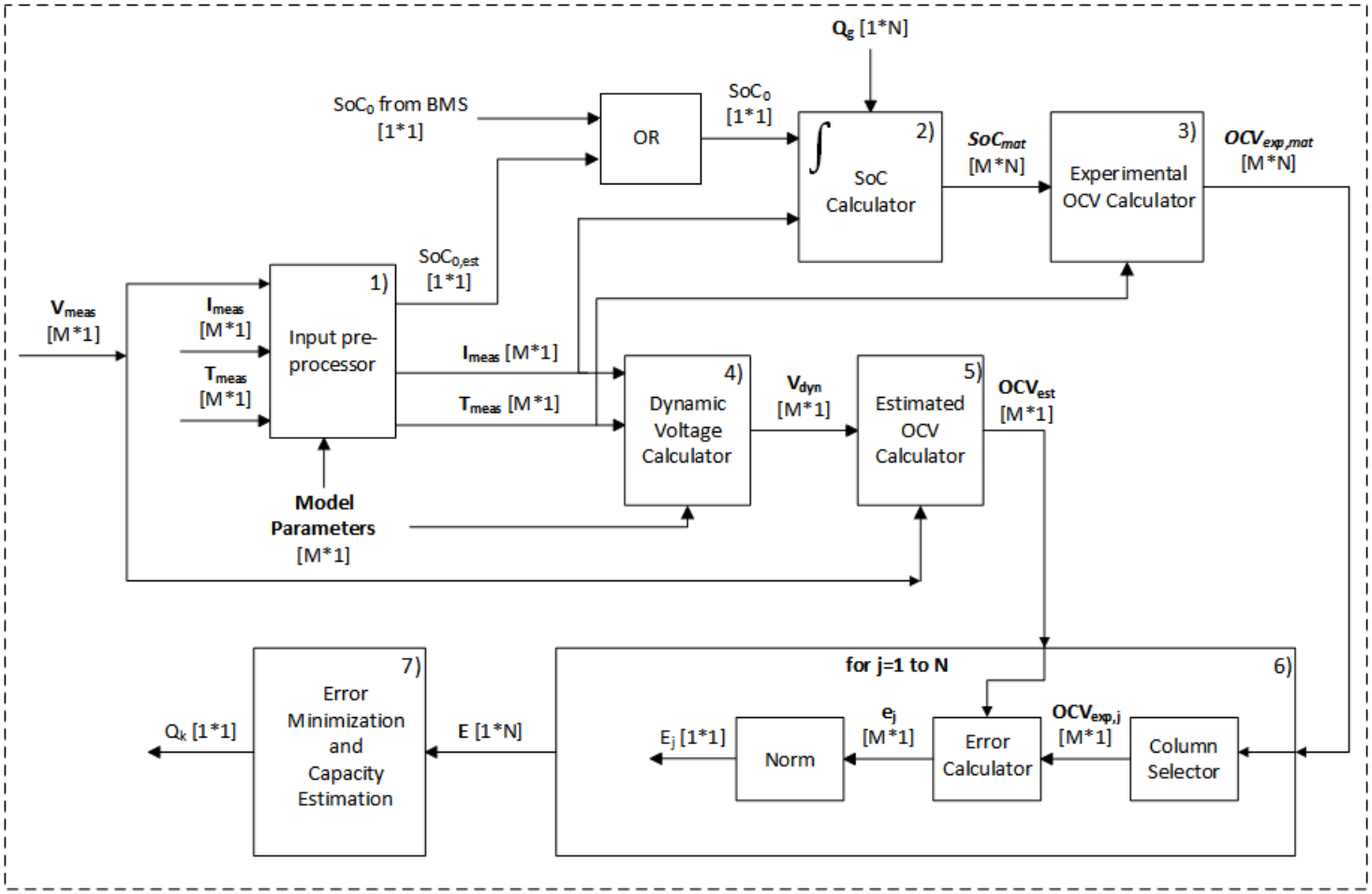

Figure 45: Detailed flowchart for capacity estimation at event “k” using vector-matrix notation

3.4 Key Advantages

In chapter 2, key attributes of an ideal capacity estimator were outlined. These are recalled here, in order to realize the capabilities of the algorithm proposed in this chapter. These needs and wants are as follows:

1) It shouldn't be affected by normal vehicle operation wherein the current, voltage and sometimes temperature are dynamic variables. Recalling step 1 of the algorithm described in this chapter, it can be concluded that because the algorithm directly relies on dynamic measurements made in a vehicle, it doesn't interfere with normal vehicle operation. The only requirement imposed is the battery operation in charge depleting mode, which is bound to happen in a PHEV or a BEV as these vehicles are primarily used to reduce fuel costs and exhaust emissions.

2) It should be cheap from a computation stand point so that it can be imbedded in a microprocessor. Going through all the steps involved in the capacity estimation algorithm, it is clear that the algorithm requires simple mathematical operations and does not rely on any advanced technique. The algorithm doesn't rely on any past information and hence memory requirements are low. Moreover, for real time implementation, the algorithm can be further refined to reduce the memory requirements by optimizing the number of computations made at each time step.

3) It should not require the battery to be charged fully or discharged below its normal SoC limits, to avoid shortening of battery lifespan through overcharging and over discharging. Capacity tests performed in laboratory require full discharge and recharge in order to get

accurate estimates of cell capacity. These measurements are intrusive and do not occur in the field. The algorithm presented does not require any such discharge or recharge beyond the limits specified by the controller. The DOE summarized in Table 2 involved battery aging over a number of different protocols and the algorithm will be implemented on each of these protocols spanning various minimum state of charge levels.

4) It should be robust enough to provide relatively accurate estimates in the presence of sensor noise and insensitive to other parameter variations. Because the algorithm relies on error minimization over a wide scope of data, it can be believed that it should be fairly insensitive and robust in the presence of errors. This analysis is conducted in great detail in the next chapter

5) It should be adaptable to various lithium ion chemistries. The self-similarity property that forms the basis if the proposed algorithm has been observed for a number of lithium-ion chemistries. Some of these might have the voltage curves self-similar only across a certain state of charge region while, others might be self-similar across the entire state of charge range. Nonetheless, this algorithm can be implemented because it doesn't rely on point wise measurements.

6) It should require as little calibration effort as possible. For the implementation proposed in this thesis, we utilize a first order equivalent circuit battery model which is not very hard to calibrate and develop. It only requires scheduling the model parameters on battery operating conditions at the BOL, a task that can be achieved with fewer experiments and little calibration effort.

Chapter 4: Robustness and Sensitivity Analysis

In order to assess the robustness and sensitivity of any algorithm, it is critical to see its performance in the presence of errors in sensors and to study its sensitivity against various parameters involved. Sensor errors are very commonplace in a dynamic environment like an automobile. It is necessary to gauge the performance of any algorithm in the presence of such errors. Based on the results from a healthy system and a faulty system, residuals can be generated. These residuals can then be used to conduct fault diagnosis and develop fault strategies. Though, an extensive study on fault diagnosis and residual analysis is not the focus of this thesis, preliminary robustness and sensitivity analysis is conducted in this chapter. There are a number of parameters involved that can be tweaked in order to implement the algorithm in real time. These parameters though not dynamic variables like measurements from sensors, can affect the results of the algorithm. Hence, sensitivity of the algorithm against these parameters is carried out as well.

For the algorithm presented in this thesis, sensor errors can be present in the form of noise and/or bias in one or more of the three sensors concerned, namely current, voltage and temperature. Also, the parameters that can have an effect on the results of the algorithm have been identified as SoC_0, scope of data during the charge depleting event used for capacity estimation, frequency of data acquisition and the battery model resistance. In order to see the effects of sensor faults, noise and bias of different magnitudes will be injected.

In order to gauge the sensitivity of the algorithm against the parameters involved, the parameters will be deviated within certain percentage of their nominal value and results will be analyzed.

4.1 Parameter Sensitivity

4.1.1 Sensitivity of the algorithm towards SoC_0

As noted earlier, the algorithm requires an initial state of charge value as an input for capacity estimation. This value can be readily obtained from the BMS in an actual vehicle. However, it is desirable to see the performance of the algorithm if SoC_0 value as given by the BMS is inaccurate. For this purpose, the SoC_0 is deviated by $\pm$ 5% from its nominal value and the estimated capacity is noted. This is done for a number of different aging cycles through the life of the cell. The nominal value of SoC_0 is as estimated using the method described in step 1 of the algorithm development chapter. A number of different cycles throughout the life of the cell are chosen and the sensitivity analysis is carried out for all these cycles. The results of the analysis are presented in figure below. Note that, the actual SoC_0 value for the aging protocol considered is somewhere around 96% as estimated by the method described earlier in chapter 3. Therefore, whenever the deviated value of SoC_0 is greater than 100%, it is forced to stay at a maximum at 100%. This way the physical limits of SoC are not voided.

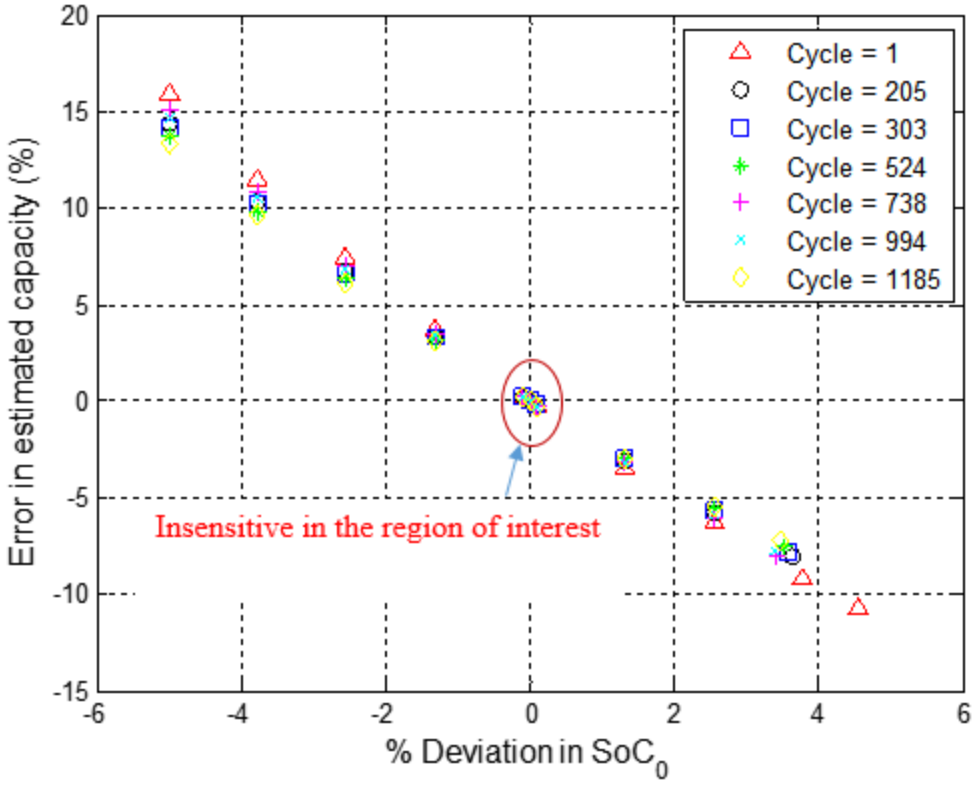

Figure 46: Percentage error in estimated capacity vs. deviation in SoC_0 for a number of aging cycles

In Figure 46, percentage change in estimated capacity is plotted against the corresponding percentage deviation in SoC_0 value for a number of different cycles. The percentage change in estimated capacity is calculated with respect to the capacity estimated using a nominal SoC_0 value. Three observations can be made from the results seen in figure above. Firstly, the behavior of algorithm towards deviation in the SoC_0 value is linear. In other words, if there was to be a general relation in terms of the sensitivity of the algorithm against deviation in SoC_0, it could be defined with a straight line equation. This is advantageous because, in case of a known error in the SoC_0 value, the corresponding error in estimated

capacity can be calculated. This makes implementation of the algorithm in real time easier. Secondly, it can also be observed that, the algorithm is insensitive to the aging level of the cell. All the cycles considered in the analysis depict the same general behavior. Lastly, it can also be seen that with positive deviation in SoC_0 value, the estimated capacity is lower than the nominal value.

Looking at the results one might suspect that the capacity estimation algorithm is indeed sensitive to the SoC_0 value. For around $\pm$2% variation in SoC_0, the percentage change in estimated capacity is around -+ 5%. However, it is expected that the SoC_0 value given by BMS in an actual vehicle would be fairly accurate because a $\pm$ 5% variation in SoC_0 can cause the BMS to loose functionality in a number of aspects. Any error in state of charge estimation can directly affect the health of battery and in some cases can also lead to unsafe operation. In addition to the above, recall from Figure 33, where the SoC_0 estimation method was presented, it was observed that the relaxed SoC value was very close to being constant. In other words, the SoC_0 estimated can be assumed to be within a fraction of percentage of the true value and hence the algorithm is insensitive to such deviation in SoC_0.

4.1.2 Sensitivity towards scope of data used

It was noted earlier that the capacity estimator functions only when the battery is used in a charge depleting mode. However, in an actual vehicle this scenario can occur in a number of different ways depending on the driving needs. For example in one case, the battery might be used in charge depleting mode starting with a SoC value of 100% down to 80%. In another case, it might be used in charge depleting mode starting with a SoC value of

70% down to 30%. Therefore, it is critical to look at the results obtained from the algorithm for a number of such scenarios. This way, thresholds can be set on the scope of data and driving conditions, viable for doing capacity estimation using the algorithm onboard a vehicle. For the experiments conducted in the laboratory, there were a number of different charge depleting profiles (refer to the section on aging campaign in chapter 2). To maintain consistency, the same experiment considered earlier in chapter 3 is chosen to carry out the sensitivity analysis.

4.1.2.1 Effect of SoC minimum

In this section, the sensitivity of the algorithm against scope of data is studied by varying the lower limit on the SoC value. Hence, the capacity is estimated using data from initial SoC_0 value down to different SoC_{min} values. Note that this is done for a number of aging cycles throughout the life of the cell. For the results shown in Figure 47, the SoC_0 happened to be around 95%. Four different SoC minimum values are considered. These are 80, 70, 60 and 50% respectively. In order, to estimate the capacity, measured data of current, voltage and temperature starting from the SoC_0 value down to the respective minimum SoC value are considered. In this way, the scope of data considered becomes shorter as the SoC minimum increases. In Figure 47, the estimated capacity is plotted against the minimum SoC value for all the cycles considered. It can be seen from the results, that the algorithm is sensitive to the scope of data used. For example, if we look at the results of cycle 1, the estimated capacity decreases from around 14 to 12.25 as the SoC minimum increases from 50 to 80%. Cycle 1 indicates a new cell for which the actual capacity is expected to be around 15 (nominal capacity for the cell). Hence, it can be said that the capacity estimation

becomes inaccurate as the scope of data is reduced (SoC_{min} = 80%). However, it is interesting to note that the same behavior is observed for all the cycles.

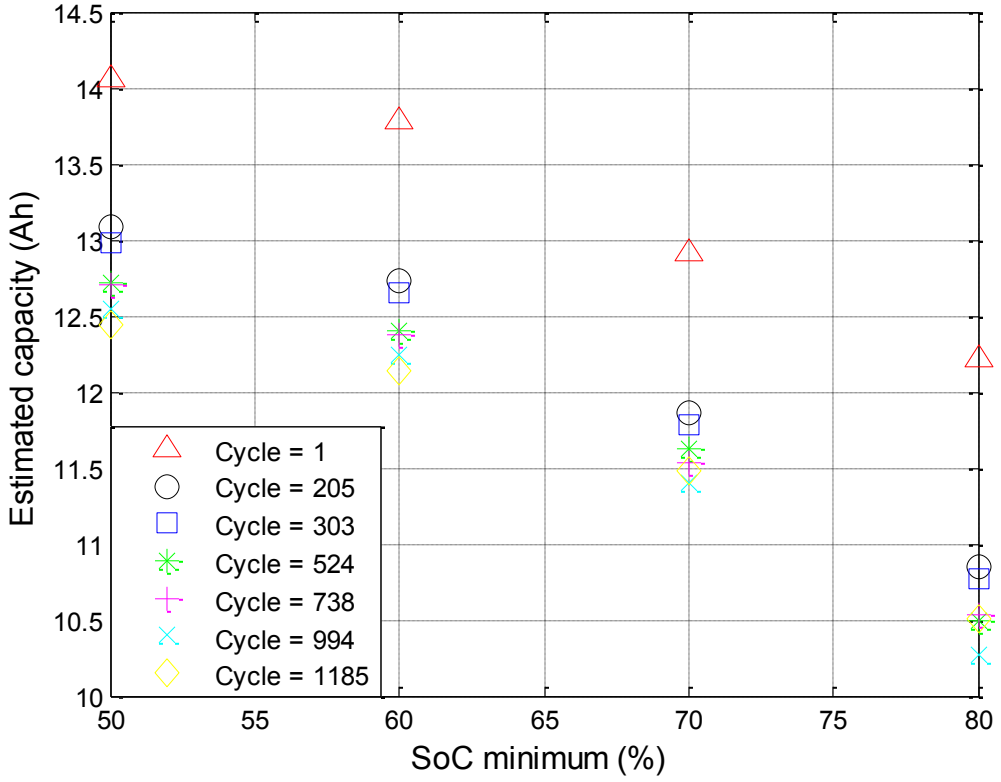

Figure 47: Estimated capacity vs. SoC minimum for a number of aging cycles

The same results can be re-plotted by calculating the percentage capacity loss with respect to the capacity estimated at the BOL for different SoC minimum values (Figure 48). On the Y-axis, the capacity loss for a particular SoC minimum value, is calculated with respect to the capacity estimated at the BOL or cycle number = 1 for that particular SoC minimum value. This is done for all the four different SoC minimum values considered. It can be

seen that, barring the case when the SoC minimum value is 80%, the nature and magnitude of capacity degradation as the cell ages is almost same. This is a desirable characteristic because it shows that, as long as the scope of data considered is not too short the percentage degradation remains the same and the algorithm is fairly insensitive to the scope of data used for capacity estimation. Therefore, in an actual vehicle the capacity estimation algorithm should not be run when the vehicle has been used for a very short trip. Although, this is a very qualitative idea, it can be implemented effectively if certain factors (like the range of battery pack and the type of vehicle under consideration) are known.

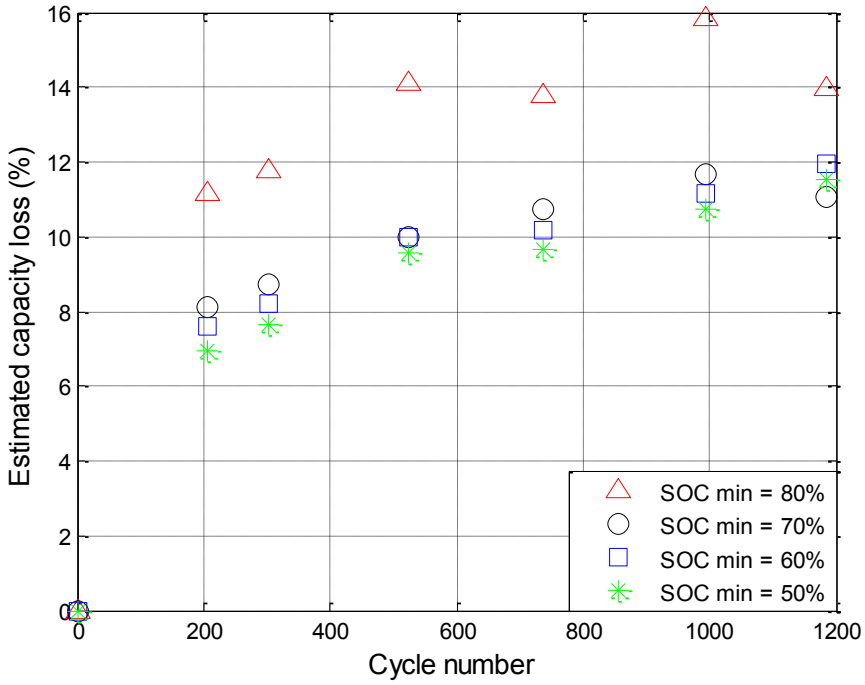

Figure 48: Estimated capacity loss vs. cycle number for different SoC minimum values

4.1.2.2 Effect of SoC maximum

In this section, the sensitivity of the algorithm against scope of data is studied by varying the upper limit on the SoC value. Hence, the capacity is estimated using data from different SoC values down to a fixed SoC_{min} value. This SoC_{min} is chosen to be 50%. Note that this is done for a number of aging cycles throughout the life of the cell. Four different SoC_{max} values are considered. These are 60, 70 80% and the actual SoC_0 value as estimated using the method described in chapter 3. This actual SoC_0 value happens to be around 95% for all the cycles of this particular experiment considered. In order, to estimate the capacity, measured data of current, voltage and temperature starting from the SoC_{max} value down to the minimum SoC value (50%) is considered. In this way, the scope of data considered becomes shorter as the SoC maximum decreases. In Figure 49, the estimated capacity is plotted against the maximum SoC value for all the cycles considered. It can be seen that the algorithm is sensitive to the scope of data used. For example, if we look at the results of cycle 1, the estimated capacity decreases from around 14 to around 11.5 as the SoC maximum value decreases from 95% to 60%. As in the case when the SoC minimum value was varied, it is evident here as well that the estimation becomes more inaccurate as the scope of data is reduced (SoC_{max} = 60%). However, plotting the same results in a different form will reveal interesting points.

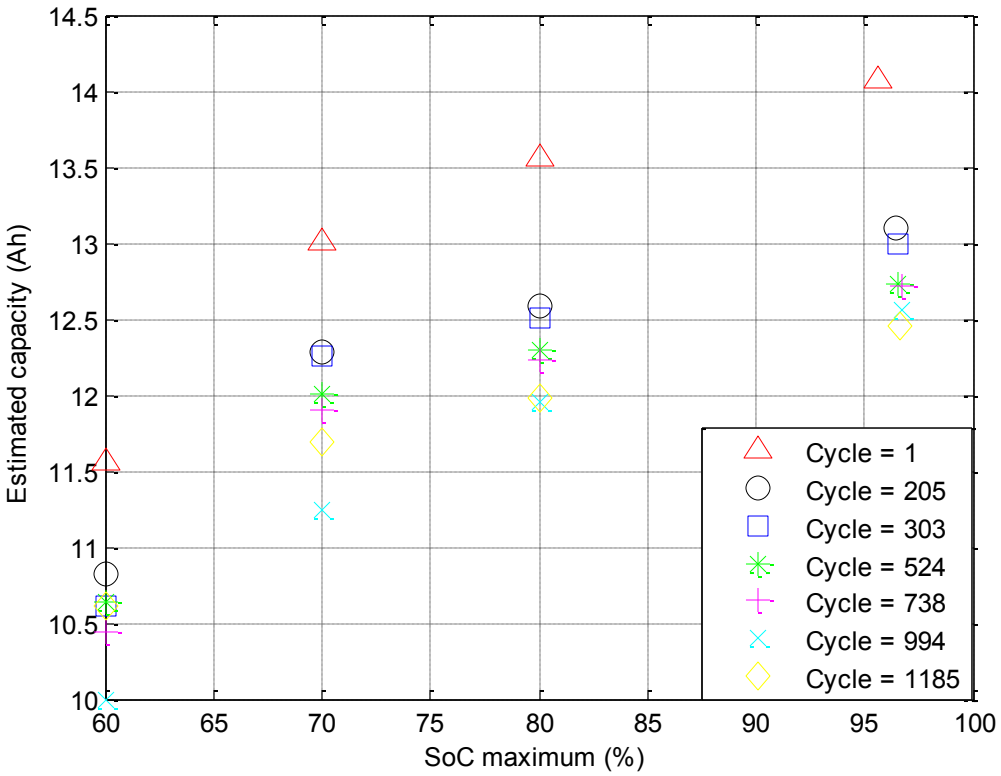

Figure 49: Estimated capacity vs. SoC maximum for a number of aging cycles

The same results can be re-plotted by calculating the percentage capacity loss with respect to the capacity estimated at the BOL for different SoC minimum values (Figure 50). On the Y-axis, the capacity loss for a particular SoC maximum value, is calculated with respect to the capacity estimated at the BOL or cycle number = 1 for that particular SoC maximum value. This is done for all the four different SoC maximum values considered. It can be seen that, barring the cases when the SoC maximum value is 60% or 70%, the nature and magnitude of capacity degradation as the cell ages is almost same. This leads to the same

conclusion that, as long as the scope of data used to carry out the capacity estimation is not too short the algorithm is insensitive to it.

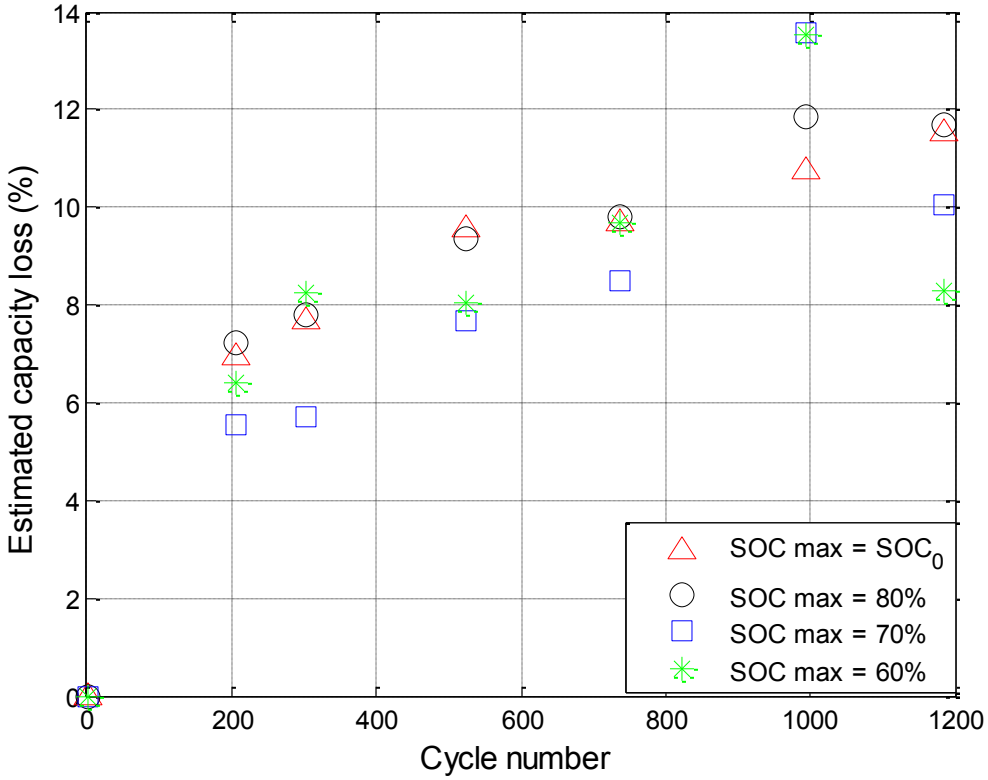

Figure 50: Estimated capacity loss vs. cycle number for different SoC maximum values

4.1.3 Sensitivity towards frequency of data acquisition

The frequency of data acquisition is another parameter of importance. For the experiments conducted in the laboratory, data was collected at a frequency of 10 Hz. In order to see the effect of down sampling the measured data, three other frequencies of 1, 2 and 5 Hz were used. The capacity was estimated using the algorithm for each of these frequencies and the

percentage change in estimated capacity is calculated with respect to the value obtained for 1 Hz. This is done for a number of different cycles. The frequency of 1 Hz is chosen because it requires the least computation time for the algorithm to run.

In Figure 51, percentage change in estimated capacity is plotted against the frequency of DAQ for a number of different cycles. The maximum percentage change in estimated capacity is 1%, which happens to be for cycle 738 and a frequency of 10 Hz. However, the same results can also be re-plotted to show the capacity degradation (Figure 52).

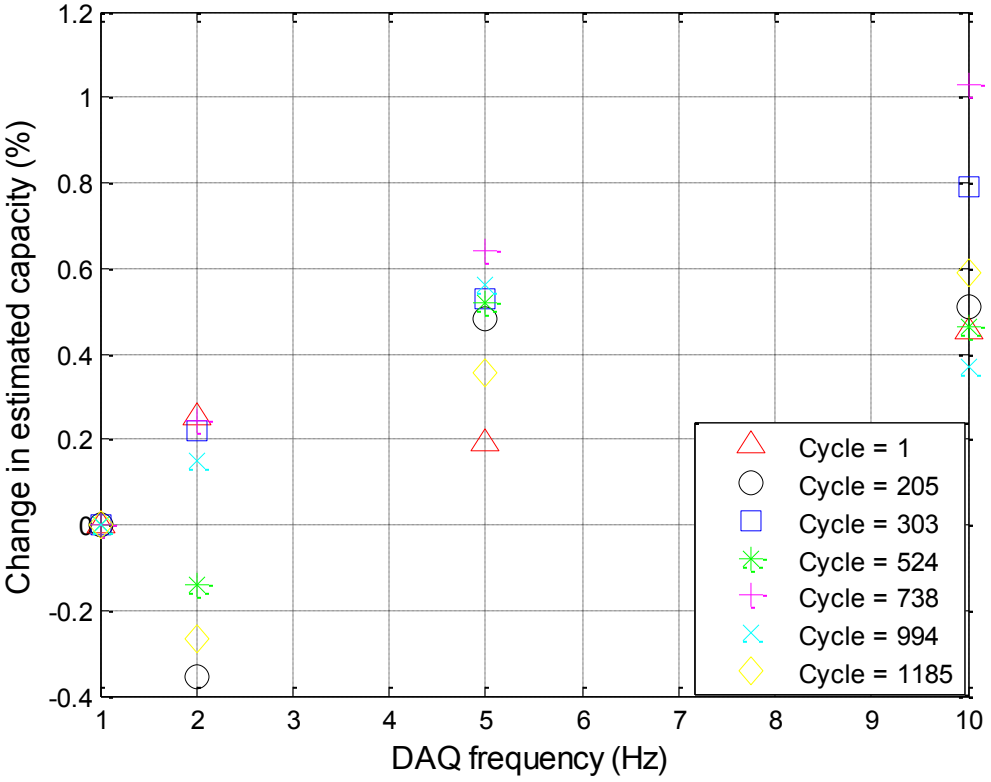

Figure 51: Percentage error in estimated capacity vs. frequency of DAQ for a number of aging cycles

It is evident, that the algorithm is insensitive to the frequency of data acquisition because the nature and magnitude of capacity degradation with respect to the initial value is same for all the different frequencies considered. Hence, a value of 1 Hz will be used to implement the algorithm throughout this thesis. This is done to shorten the computation time and memory requirements, two factors highly desirable of a capacity estimator.

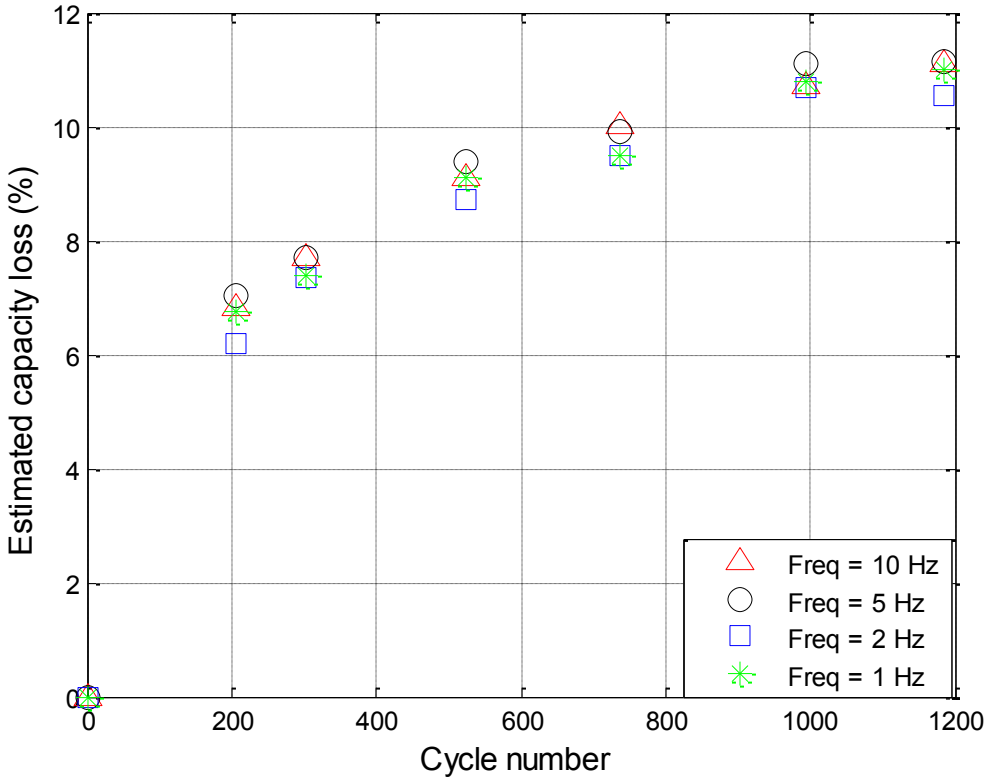

Figure 52: Estimated capacity loss vs. cycle number for different DAQ frequencies

4.1.4 Sensitivity towards resistance parameter variation

Cell internal resistance is another parameter which changes as it ages. For the algorithm presented, a constant internal resistance value obtained using model calibration is used throughout the life of the cell. However, it is important to see the effect of changing resistance value on the estimated capacity because in an actual vehicle the internal resistance is bound to be a dynamic quantity. $\pm$ 10% variation in the resistance with respect to the nominal value obtained using model calibration, is considered for this sensitivity analysis. The capacity is estimated for each of these different resistance values and the percentage change in estimated capacity is calculated with respect to the capacity obtained using the nominal resistance value. This is done for a number of aging cycles throughout the life of the cell. In Figure 53 the percentage change in estimated capacity is plotted against the percentage deviation in the resistance value.

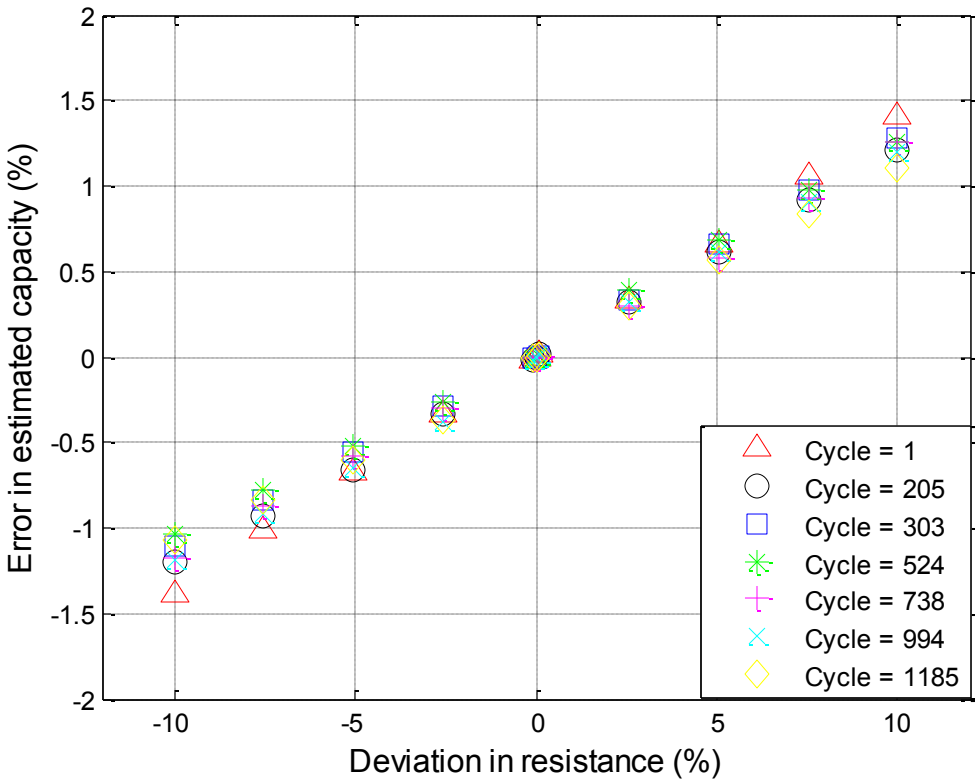

Figure 53: Percentage error in estimated capacity vs. deviation in internal resistance for a number of aging cycles

It can be observed, that the nature of capacity change is similar for all the cycles considered. Also, it can be seen that the algorithm is fairly insensitive to the resistance parameter because a 10% variation in the resistance parameter results only in a 1.5% change in the estimated capacity. It can also be concluded from the figure, that the algorithm shows a linear behavior with respect to the resistance parameter. This is advantageous because if a method to track the internal resistance can be developed the error in capacity estimation can be calculated and hence accounted for.

4.2 Sensor Sensitivity

Since the algorithm relies on measurements made in an actual vehicle like current, voltage and temperature, it becomes critical to observe the effects of error in these measured quantities on the output of the algorithm, the estimated cell capacity. These errors can come across in the form of noise or bias in the respective sensors present in the BMS. In this section, errors in the form of noise and bias in the current, voltage and temperature sensors are considered.

4.2.1 Error in voltage sensor

4.2.1.1 Effect of noise

In this section, sensitivity of the algorithm against noise in voltage sensor is analyzed. This is done by generating an array of normally distributed random numbers with zero mean and different standard deviations. This noise is added to the actual measured voltage obtained from the experimental data. A number of different standard deviations are chosen such that the maximum standard deviation equals 3% of the maximum voltage for the battery cell. For the lithium ion cells under consideration, this maximum voltage is 4.15V. Hence, a maximum standard deviation of 0.1245V is chosen. Percentage change in capacity is calculated with respect to the capacity estimated without any noise. This is done for a number of different cycles. In figure below, the percentage change in estimated capacity is plotted against the standard deviation of the injected noise.

It can be observed from Figure 54, that the algorithm is fairly insensitive to noise in the voltage sensor. Even for noise with standard deviation of 1% (corresponds to 0.0415V which is quite large), the percentage change in estimated capacity is only about 2%. Any

error in voltage sensor is bound to affect the accuracy of algorithm because, measured voltage is used to calculate the estimated OCV which when compared with the experimental OCV generated the error matrix. However, it is important to note that any noise in the voltage sensor of the BMS will affect its functionality and hence it is assumed that the BMS has embedded strategies to diagnose faults and errors in sensors. The percentage change in estimated capacity for cycle 1, when the standard deviation is greater than 2% is constant because, the estimated capacity is at its upper threshold value equal to the nominal capacity. This threshold comes from the target capacity vector, which was chosen to be a number of values between the nominal capacity and 75% of the nominal capacity. Hence, the capacity estimated from the algorithm cannot be greater than this nominal capacity.

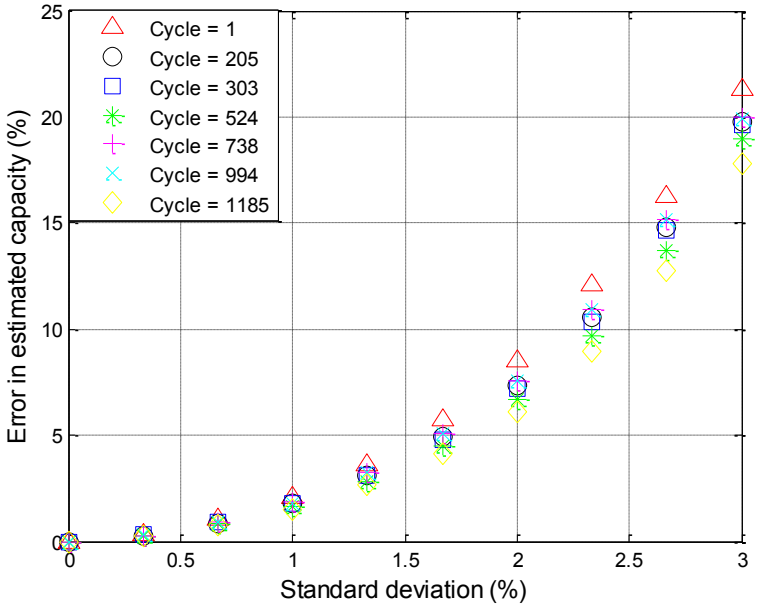

Figure 54: Percentage error in estimated capacity vs. standard deviation of noise in voltage sensor for a number of aging cycles

4.2.1.2 Effect of bias

In this section, sensitivity of the algorithm against a bias in voltage sensor is analyzed. A constant bias of different magnitudes is added to the actual measured voltage from the experimental data. The magnitudes are so chosen such that the maximum magnitude equals 0.3% of the maximum voltage. Hence, a maximum bias of 0.0125V is chosen. As before, percentage change in capacity is calculated with respect to the capacity estimated without any bias. This is done for a number of different cycles. In figure below, the percentage change in estimated capacity is plotted against the bias.

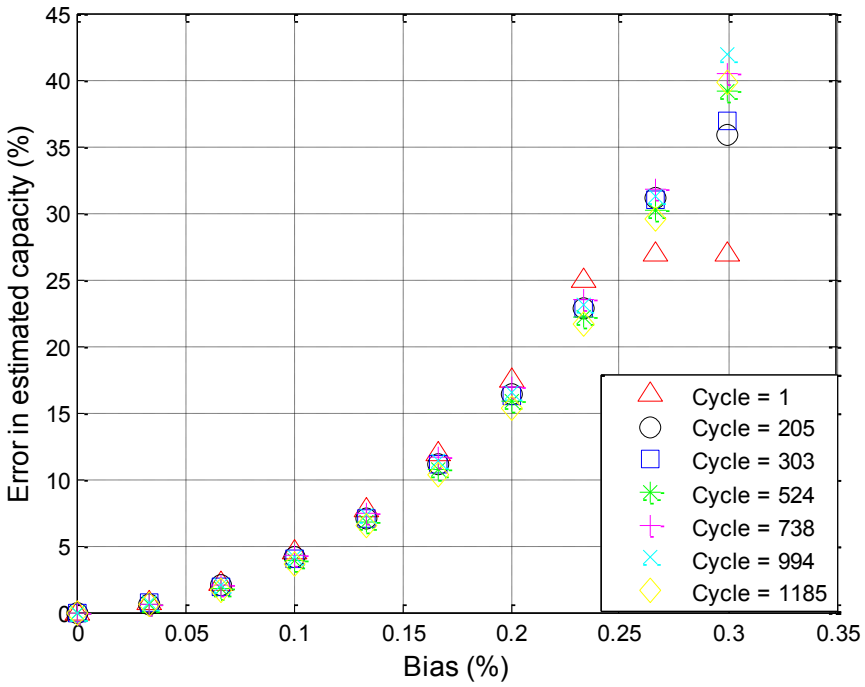

Figure 55: Percentage error in estimated capacity vs. bias in voltage sensor for a number of different aging cycles

Consider a voltage sensor with full scale range of 5 V corresponding to a resolution of 4.9 mV (0.11% bias) on a 10 bit converter. Looking at Figure 55, we can say that the algorithm is fairly insensitive to bias in voltage sensor because the sensor will be unaffected by any bias in voltage sensor less than 0.11%.

4.2.2 Error in current sensor

4.2.2.1 Effect of noise

In this section, sensitivity of the algorithm against noise in current sensor is analyzed. This is done by generating an array of normally distributed random numbers with zero mean and different standard deviations. This noise is added to the actual measured current

obtained from the experimental data. A number of different standard deviations are chosen such that the maximum standard deviation equals 3% of the maximum current for the battery cell. This maximum current can be different depending on the type of profile engineered. For the experiment considered in this study, this maximum current was observed to be around 160 A. Hence, a maximum standard deviation of 4.82 A is chosen. Percentage change in capacity is calculated with respect to the capacity estimated without any noise. This is done for a number of different cycles. In figure below, the percentage change in estimated capacity is plotted against the standard deviation of the injected noise. It can be observed from Figure 56, that the algorithm is almost insensitive to any noise in the current sensor. Even for noise with standard deviation of 3% (corresponds to 4.82 A), the percentage change in estimated capacity is about 0.5%. This is because the capacity is estimated using a wide scope of data. Hence, any positive and negative effects of noise in current sensor get cancelled out and the end effect is almost void.

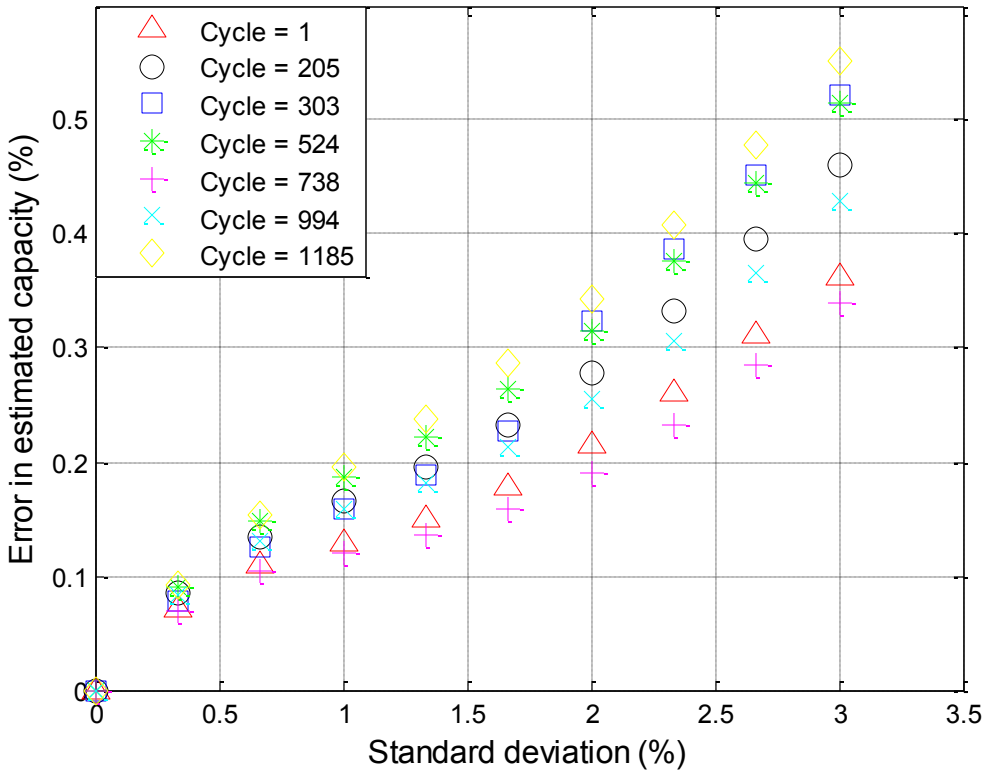

Figure 56: Percentage error in estimated capacity vs. standard deviation in current sensor for a number of different aging cycles

4.2.2.2 Effect of bias

In this section, sensitivity of the algorithm against a bias in current sensor is analyzed. A constant bias of different magnitudes is added to the actual measured voltage from the experimental data. The magnitudes are so chosen such that the maximum magnitude equals 0.3% of the maximum current. Hence, a maximum bias of 0.48 A is chosen. As before, percentage change in capacity is calculated with respect to the capacity estimated without any bias. This is done for a number of different cycles. In Figure 57, the percentage change in estimated capacity is plotted against the bias.

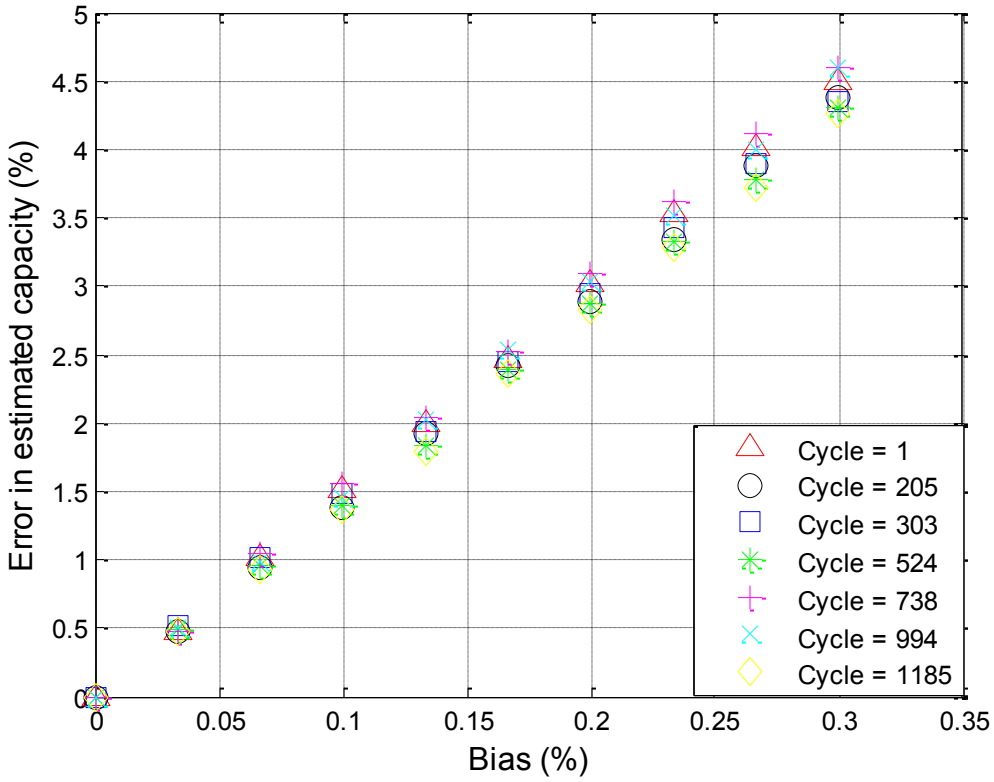

Figure 57: Percentage error in estimated capacity vs. bias in current sensor for a number of different aging cycles

It can be observed that the algorithm is not as sensitive to a bias in current sensor as it is to a bias in voltage sensor. However, it is still sensitive because a 0.48 A of bias in the current sensor gives an error of around 4.5 % in the estimated capacity.

4.2.3 Error in temperature sensor

4.2.3.1 Effect of noise

In this section, sensitivity of the algorithm against noise in the temperature sensor is analyzed. This is done by generating an array of normally distributed random numbers with

zero mean and different standard deviations. This noise is added to the actual measured temperature obtained from the experimental data. A number of different standard deviations are chosen such that the maximum standard deviation equals 3 °C. Note that for the experiment considered, the temperature is constant at 30 °C. So, 3 °C corresponds to a standard deviation of around 10%. Percentage change in capacity is calculated with respect to the capacity estimated without any noise. This is done for a number of different cycles. In figure below, the percentage change in estimated capacity is plotted against the standard deviation of the injected noise.

It can be observed from Figure 58, that the algorithm is almost insensitive to any noise in the temperature sensor. Also, the behavior is similar to that seen in the presence of noise in the current sensor. Even for noise with standard deviation of 10% (corresponds to 3 °C), the percentage change in estimated capacity is about 1.5%. However, it is assumed that the thermal management system in a BMS ensures that the measured temperature is accurate.

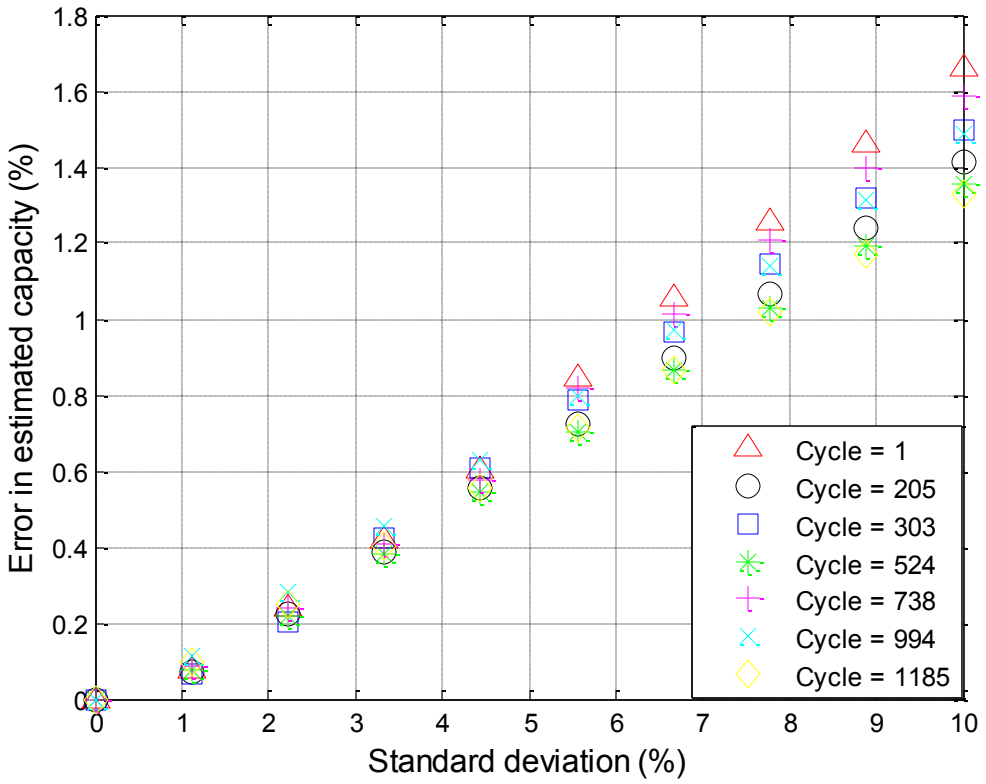

Figure 58: Percentage error in estimated capacity vs. standard deviation in temperature sensor for a number of different aging cycles

4.2.3.2 Effect of bias

In this section, sensitivity of the algorithm against a bias in temperature sensor is analyzed. A constant bias of different magnitudes is added to the actual measured voltage from the experimental data. The magnitudes are so chosen such that the maximum magnitude equals 10% of the maximum temperature. Hence, a maximum bias of 3 °C is chosen. As before, percentage change in capacity is calculated with respect to the capacity estimated without any bias. This is done for a number of different cycles. In Figure 59, the percentage change in estimated capacity is plotted against the bias.

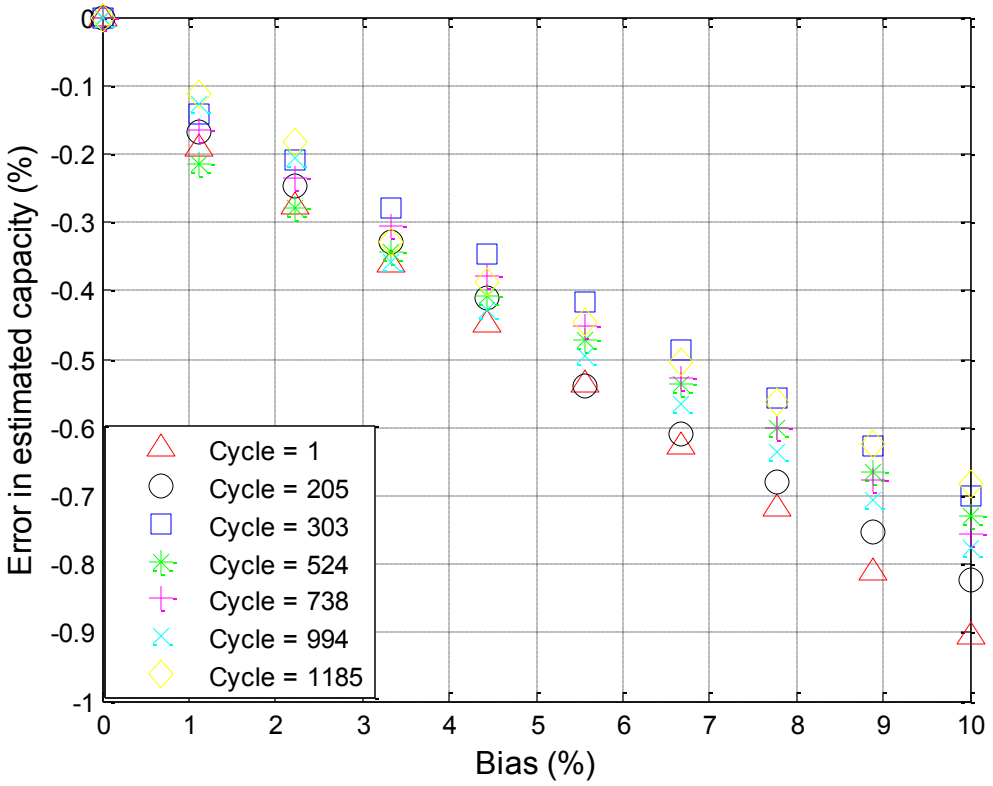

Figure 59: Percentage error in estimated capacity vs. bias in temperature sensor for a number of different aging cycles

It can be observed that the algorithm is not as sensitive to a bias in temperature sensor as it is to a bias in voltage sensor. Infact, it is least sensitive to a bias as compared to bias in current and voltage sensors. A 10% standard deviation which is a lot, results in an error of 1% in the estimated capacity.

4.3 Sensitivity Analysis: A Summary

The following points are worth noting in-order to summarize the sensitivity analysis conducted in this chapter:

1) The algorithm is insensitive to any errors in the initial state of charge estimation method. When the battery is in a completely relaxed state the OCV map can provide an accurate estimate of the SoC_0 value and for applications in the filed it is assumed that the BMS has an imbedded algorithm for state of charge estimation that is reasonable accurate.
2) The algorithm is insensitive towards scope of data as long as the battery is not used with very shallow depth of discharge like around 10-15%. Beyond that, the results obtained are very similar in nature and provide reliable estimates. It is also interesting to note that, in case of data drop because of very shallow discharge, the algorithm can be implemented on the next event without any knowledge of the previous events.
3) The algorithm is also insensitive to the rate at which data is acquired and hence it's best to utilize down sampled data in-order to reduce computation time for real time implementation.
4) The algorithm is very robust in terms of model parameters as seen in the sensitivity analysis against internal resistance of the battery model. This is again attributed to the fact that a wide scope of data is utilized for error calculations and minimization resulting in the cancelation of point wise errors.

5) Since, the algorithm does rely on conventional sensor measurements, it's bound to be somewhat sensitive to errors in sensors. However, due to the nature of the algorithm, these errors mostly get cancelled over a wide scope of data resulting in fairly little sensitivity towards current, voltage and temperature sensors.

Chapter 5: Sample Results and Post-Processing

In the previous chapters namely 3 and 4, the algorithm was presented and sensitivity analysis was carried out. However, this was done only for a few aging events without implementing the algorithm for all the events for any given aging protocol. The algorithm presented was implemented on all the aging protocols described in the aging campaign in section 2, chapter 2. In this chapter, the complete capacity estimation results will be presented for a particular aging protocol. After obtaining raw results from the capacity estimator, three major steps will be carried out to post-process the raw results. These include: outlier rejection, gap filling and filtering and normalizing. The algorithm results relies on experimental measurements made in the laboratory, which are prone to errors due to equipment malfunctioning. Hence, the raw results need to be checked for outliers resulting from incorrect measurements made in the laboratory. As a result of outlier rejection, there will be gaps that need to be filled in-order to maintain a continuous stream of capacity estimates. It can be recalled from section 2, chapter 2 on aging campaign description that assessment tests were conducted at regular intervals throughout the aging campaign to obtain baseline energy and power measurements. These assessment tests are intrusive and rely on data which is never available in the field. As a result of these tests, it was observed that the behavior of battery changed at each of those points in the life of cell when an assessment test occurred. Consequently, the capacity estimation results need to be

filtered and smoothed to represent actual aging occurring in the field. The EOL criteria for batteries used in vehicles is set according to the percentage degradation with respect to a new cell. The algorithm gives an estimate of the remaining capacity in terms of ampere hour and hence a method to normalize the estimate and obtain capacity degradation has to be established. The following sections will address all of the post-processing steps mentioned above.

5.1 Raw Results

In this section, raw results on event basis as obtained from the algorithm are shown. Experiment number 4 in Table 2, chapter 2 (Level 2 Charging, CD to 45% SoC) is chosen as an example aging protocol to represent the raw results. Capacity estimated from the algorithm at each aging event is plotted against the ampere hour throughput at the end of that aging event in Figure 60. The figure also shows the results for capacity measurements made through assessment tests conducted in the lab. For the particular experiment considered, the total ampere hour throughput was found to be 24,555 Ah. This corresponded to a total of 1319 aging cycles. The capacity at the beginning of life was estimated to be at 14.17 Ah and that at the end of experiment was found to be at 12.58 Ah. Note that due to time constraints, the end of experiment didn't correspond to EOL for this case.

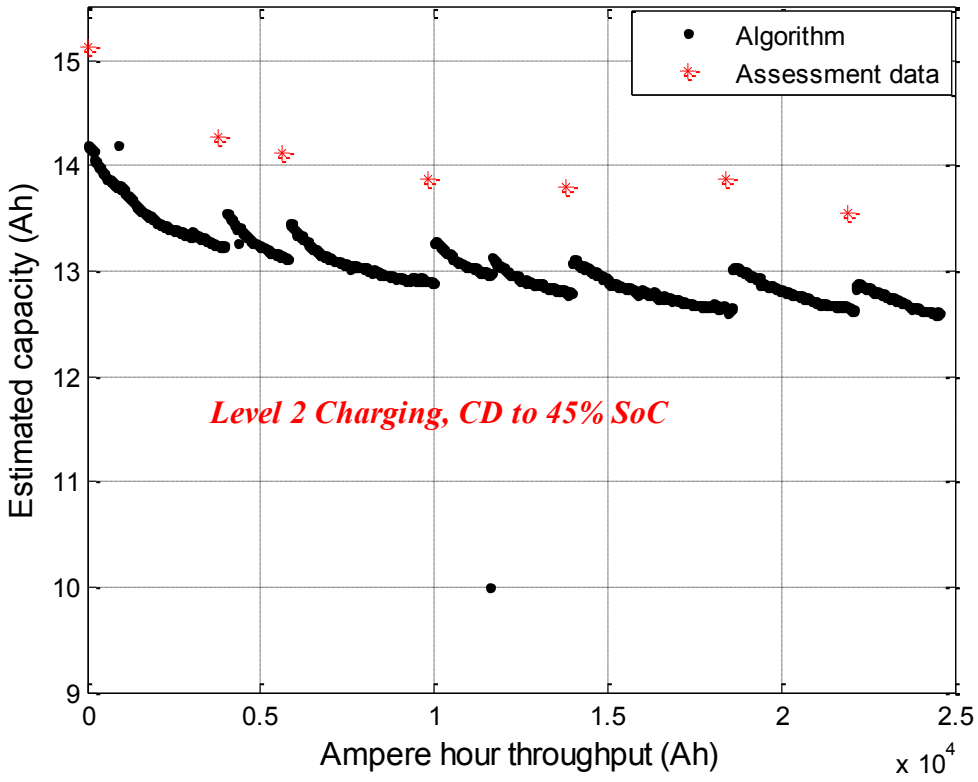

Figure 60: Estimated capacity vs. ampere-hour throughput for an example aging protocol

It can be observed from the results that, estimated capacity is always lower than the capacity measured through assessment tests conducted in the lab. This should not be a concern because battery aging is always characterized in terms of capacity degradation and not absolute capacity in ampere-hour. Although, absolute numbers vary it is interesting to note that the capacity estimator does capture the overall trend as the cell ages. A key advantage offered by the capacity estimation algorithm over assessment tests is the rich data density. While, the assessment tests are intrusive and yield only around 7-8 estimates throughout the life of cell, the capacity estimation algorithm yields a large number of

estimates (total of 1319 estimates for this particular experiment). It can also be observed, that for cycle number 619^{th}, the estimated capacity is way low at 10 Ah. This necessitates the need for outlier rejection and the same will be addressed in the upcoming section on post-processing.

5.2 Post Processing

Raw results from the capacity estimation algorithm cannot be used to deduce any vital information about the battery state of health. These results need to be post processed in order to be used for various other diagnosis and prognosis purposes. Post processing is also done in order to filter out the noise and obtain a smooth aging model in terms of capacity degradation. For the algorithm presented in this thesis, these post processing techniques will involve outlier rejection, gap filling and filtering. Outlier rejection will be done to discard certain aging events, gap filling will be done to fill the voids created by the events being discarded and filtering will be done to remove the noise in the results and obtain a smooth degradation curve. For all the post processing done in this section, raw results shown in Figure 1 will be used.

5.2.1 Outlier rejection

The capacity estimation algorithm relies on measurements made by current, voltage and sensors. In an actual vehicle, these sensors can read incorrect numbers due to various reasons. If the capacity estimation is done using these wrong sensor measurements, than the estimated capacity value should be discarded. Also, it was observed in the earlier chapter on sensitivity analysis, that the capacity estimation becomes quite inaccurate when the scope of data used for capacity estimation is made shorter. Hence, a threshold should

be set on the minimum ampere hour throughput required for the aging event to be considered viable for capacity estimation.

In order to account for incorrect sensor measurements, those aging events are discarded when the measured voltage at the end of CV charging period exceeds the maximum charging voltage as listed by the manufacturer or the measured voltage at the end of charge depleting event is lower than the minimum discharging voltage as listed by the manufacturer . For the cells under consideration, this maximum voltage is 4.15 V and the minimum voltage is 2.8 V. However, in order to account for any noise in the measurements made in the lab the maximum and minimum voltages used for outlier rejection in the work described in this thesis are set as 4.17 V and 2.78 V respectively. To ensure a significantly long scope of aging data is used for capacity estimation, 50% of the nominal capacity is chosen as the minimum ampere hour throughput per aging cycle required for the cycle to be considered for capacity estimation. For the cell under consideration this value is calculated to be 7.5 Ah. The value of 7.5 Ah is chosen after looking at the results of the sensitivity analysis obtained in chapter 3. A constant current discharge of 7.5 Ah on a fully charged cell corresponds to a SoC range of 50% and for this SoC range the results obtained from sensitivity analysis were consistent. Although the PHEV like profile is not a constant current profile this approximation was assumed to be a suitable one. The ampere hour throughput for each aging cycle can be calculated using the known measurements of time and current. Hence, whenever the ampere hour throughput per cycle is lower than 7.5 Ah, the particular cycle is discarded. Note, the capacity estimation algorithm can still be run if the cycle is rejected based on the above criteria. However, it will be removed and the voids

thus created will be filled using suitable techniques described in later sections of this chapter. It was also observed from the results of other experiments, that when ampere hour throughput was insufficient for a particular cycle, a couple of cycles following that yielded noisy capacity estimates. This could be attributed to errors in executing the experiments in laboratory. Hence, whenever there is an outlier rejection not just that particular cycle but 2 cycles following that are rejected as well. Considering a cell takes a couple of thousand cycles to reach the EOL criteria depending on the severity of aging protocol, discarding a couple of cycles would not have any impact.

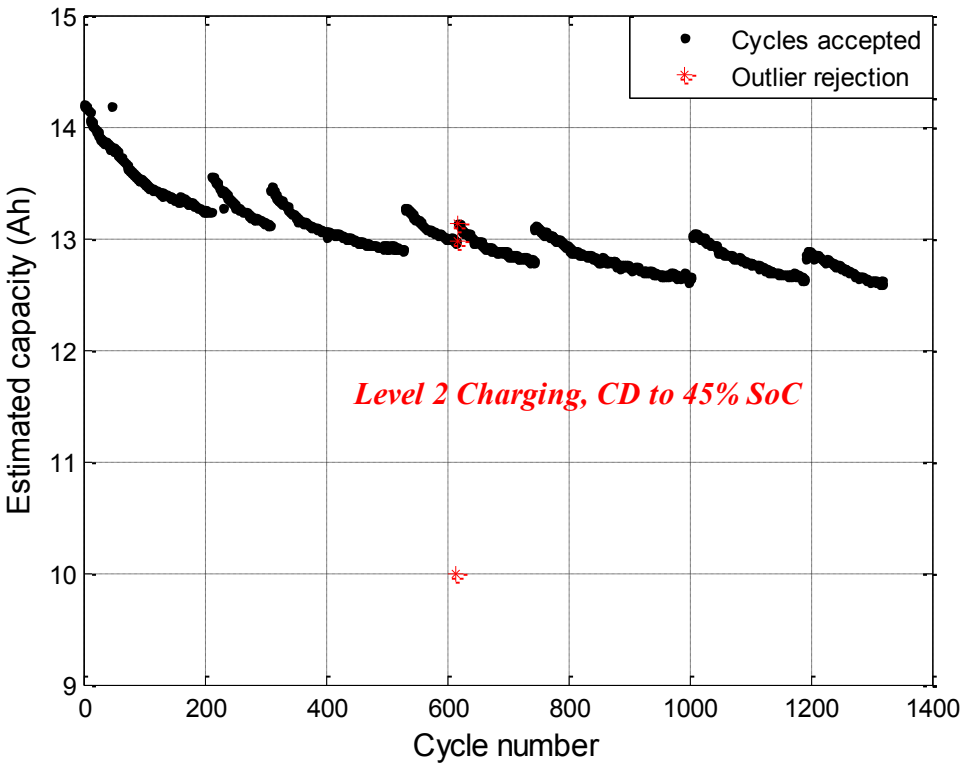

Figure 61: Results depicting outlier rejection based on set criteria for an example aging protocol

In Figure 61, the estimated capacity is plotted against corresponding cycle number for a sample aging protocol. The black dots represent cycles which are accepted and the red stars indicate those that have been removed based on the set criteria. In particular, cycle number 619 was rejected because the ampere-hour throughput was too low implying the aging protocol wasn't followed in the laboratory. Consequently, as per the set criteria a couple of cycles preceding the discarded cycle (619) were discarded as well. As a result of this, gaps were created and the same will be filled using suitable techniques.

5.2.2 Gap filling and filtering

It was seen earlier that certain cycles had to be rejected because of the estimation results being completely off. In order to maintain a continuous stream of capacity estimates, the gaps thus created needed to be filled using a suitable technique. Looking at the sample results, it can be observed that capacity degradation over a local aging period is almost linear. Hence, it was assumed reasonable to fill in the gaps by doing a linear curve fit of capacity estimates over a local window, prior to the cycle pertaining to the gap. The local slope was then used to calculate the next capacity estimate or in other words, fill the gap. Different window lengths could be used for this purpose. A longer window length assured better averaging and a shorter window length assured that the local effects were not completely ignored. The capacity estimation algorithm was to be implemented on a number of different experiments each with different number of aging cycles at the end of aging campaign. Considering this, a window length of 150 cycles was chosen to fill the gaps. It should also be noted that while filling the gaps, if the local slope calculated using a linear-

fit was found out to be positive the gap was filled by using the same value as the previous capacity estimate. This was done to ensure that the estimated cell capacity always decreased as the cell aged. The procedure to fill in the gaps based on linear-fit over different window lengths is depicted in Figure 62 and Figure 63.

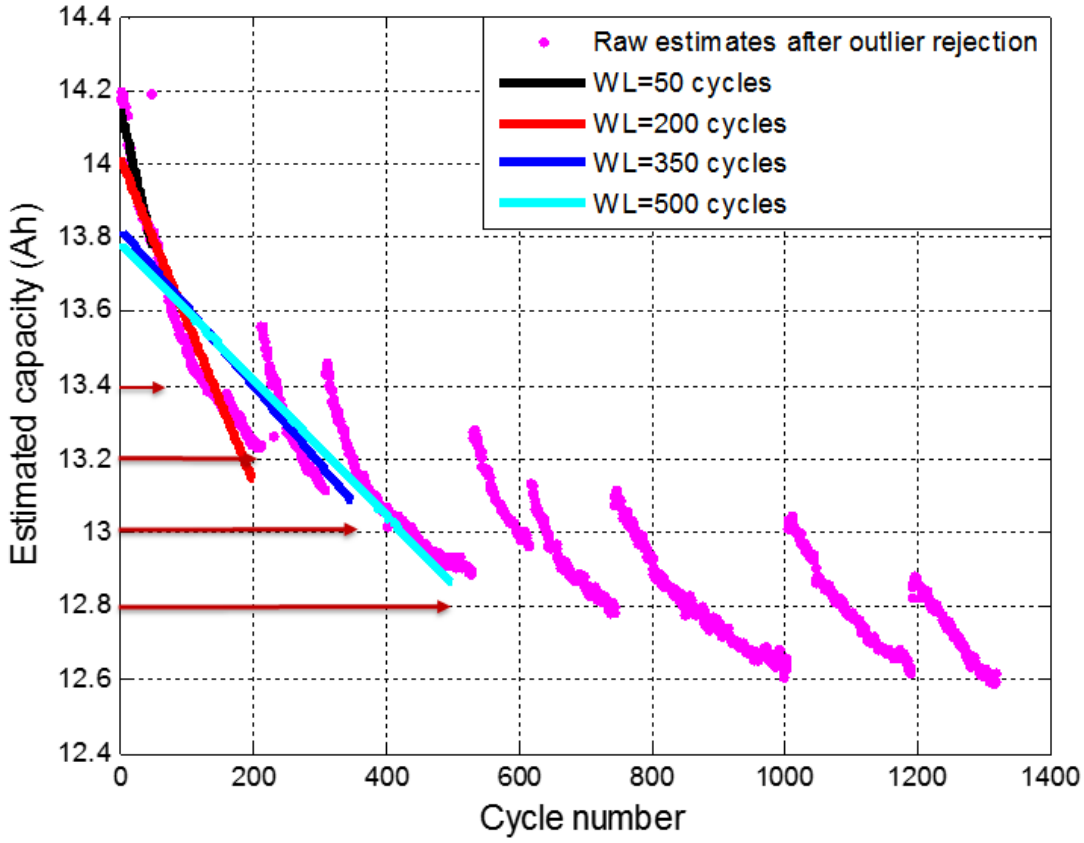

Figure 62: Technique depicting gap filling and filtering using different window lengths

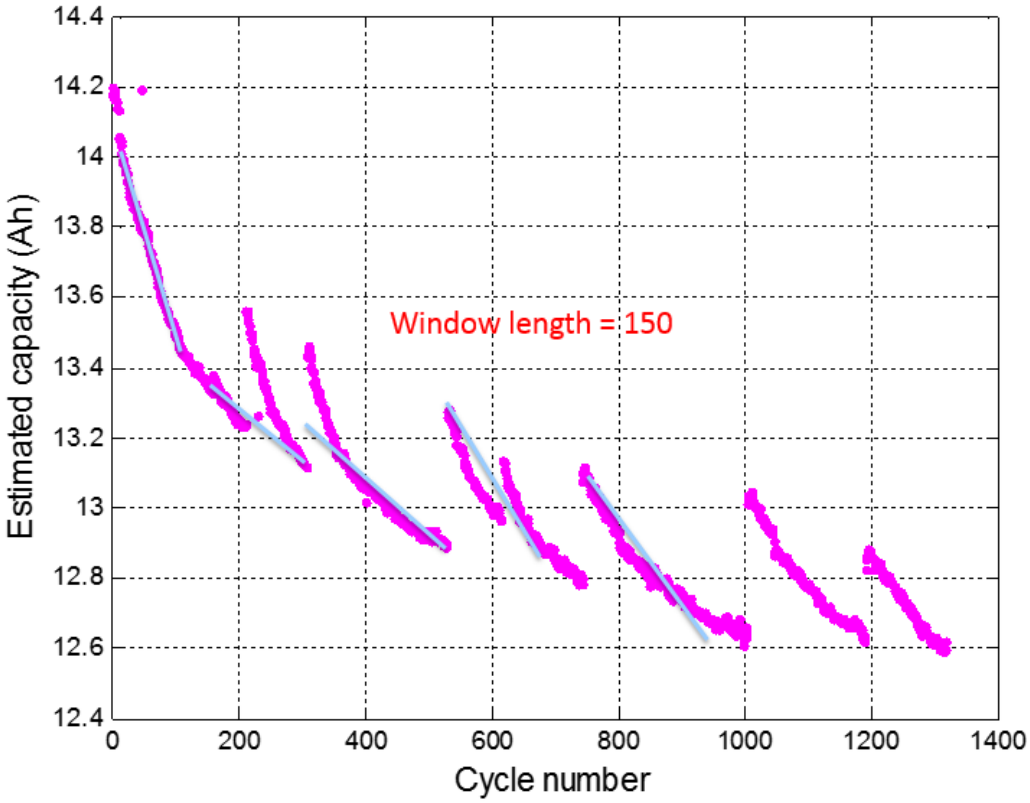

Figure 63: Gap filling using a recommended window length of 150 cycles

After filling the gaps and obtaining a continuous stream of capacity estimates, the next step is to filter the estimates and obtain a smooth degradation curve. This would also help get rid of the rejuvenation experienced by the cells when there was an assessment test conducted in the laboratory. Filtering was done in the same way as gap filling. A linear curve fit was done of capacity estimates prior to the estimate being filtered and the local slope was used to calculate the next filtered estimate. Initialization was done by assuming the first filtered estimate to be equal to the raw estimate. Beyond that different window lengths were used to achieve the filtering process. Note that for cycles until the window length value, filtering was done by doing curve fit over all the cycles up to that cycle

number. Again care was taken in order to ensure that the cell capacity didn't increase at any point in life. For this whenever the local slope calculated was positive, the previous filtered estimate was held constant. Figure 64 shows the filtered capacity estimates for a few different window lengths.

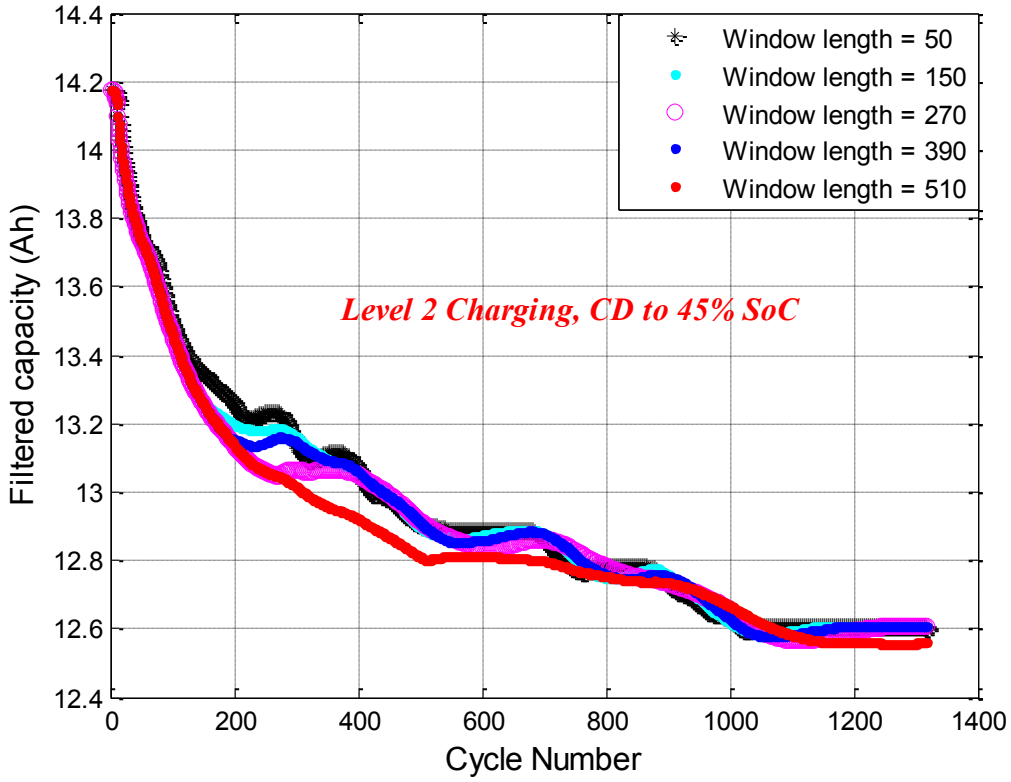

Figure 64: Filtering the capacity estiamtes using different window lengths

It can be observed that, a shorter window length yields degradation with local effects more pronounced and a longer window length captures the overall trend better. Though, the nature and magnitude of degradation depends a lot on the severity of aging, in general it

can be concluded that beyond a certain number of aging cycles, the window length doesn't have a pronounced effect. Though not relevant from the capacity estimation algorithm point of view, selecting the right window length becomes critical if the results of algorithm are used for life estimation purposes. Because some of the experiments considered in this project could not be aged significantly, a window length of 150 cycles will be used for filtering purposes in the work presented in this thesis.

5.2.3 Normalizing

Because absolute capacity in ampere-hours doesn't tell much about battery state of health, normalizing is done to obtain capacity degradation with respect to a new cell. It was also observed from the raw results, that the algorithm always under predicted the cell capacity. This further necessitated the need for normalizing to check if the percentage degradation was same as that observed from assessment tests. The capacity estimates are normalized using the first estimated capacity and can be calculated as shown in equation 5.1 below. This can be done on the raw estimates (after outlier rejection) as well as on the filtered estimates. The capacity degradation results are shown in Figure 65.

$$Q_{loss} = \frac{Q_{est_1} - Q_{est}}{Q_{est_1}} * 100 \quad (5.1)$$

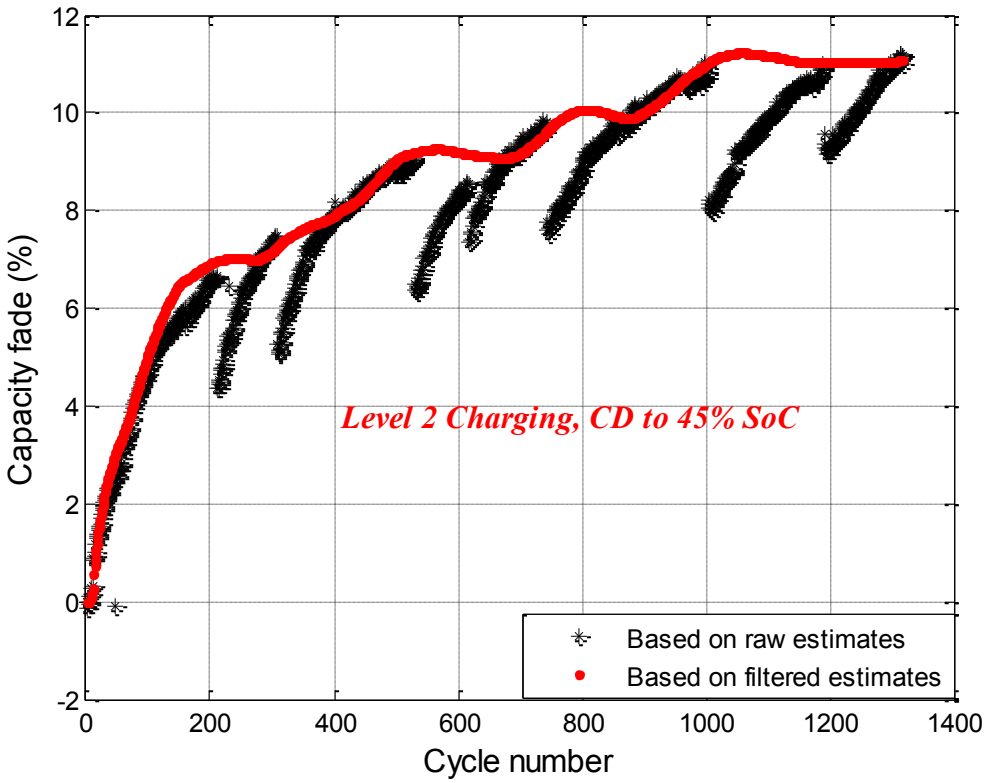

Figure 65: Normalizing the estimated capacity to obtain percentage degradation

Chapter 6: Resistance Estimation and Combined Framework

6.1 Need for Resistance Estimation

It can be recalled from Section 2 of Chapter 1 on literature review, that battery state of health is very closely associated with capacity fade and internal resistance growth at the cell level. In the previous chapters, a framework was established to track the cell capacity loss as it ages. However, it is equally important to develop an algorithm that can estimate the cell internal resistance. Growth in cell internal resistance directly affects its ability to deliver power implying poor performance in a HEV, PHEV or BEV. While capacity degradation is more critical for batteries used in PHEVs and BEVs, internal resistance growth is important in case of batteries used in HEVs. For the capacity estimation algorithm presented in chapter 3, this internal resistance was accounted for by the battery model. However, the internal resistance of the model was only a function of battery temperature and current direction. It wasn't a function of the age of the battery cell. A constant internal resistance was used to estimate the cell capacity throughout the life of the cell. This is not ideal because in an actual vehicle the cell internal resistance is a dynamic parameter. Hence, in order to obtain a complete picture of the battery state of health it is critical to develop a suitable algorithm to track the cell internal resistance as well. One such algorithm very similar to the capacity estimation algorithm developed in chapter 3 is presented in this chapter.

6.2 Commonly Adopted Technique

Alexander K Suttman, a former graduate student at The Ohio State University established a method to track the cell internal resistance in [39]. In his research, he used a zeroth order equivalent circuit battery model to estimate the cell internal resistance. A zeroth order equivalent circuit is typically modeled as a voltage source and a resistor. The terminal voltage for such a model can hence be represented as in equation below. Alexander also makes an assumption that the cell open circuit voltage is mostly just the function of SoC and temperature hence for small changes in SoC at a given temperature, it could be assumed to be constant. With such an assumption, the battery model would take the form as in equation below for small transients in the input current. The internal resistance at these transient points can thus be calculated as shown in equation below. Alexander K Suttman used these resistance estimates to make EOL predictions at various operating conditions.

$$V = E_0 - IR_0 \tag{6.1}$$

$$\Delta V = \Delta I R_0 \tag{6.2}$$

$$R_0 = \frac{\Delta V}{\Delta I} \tag{6.3}$$

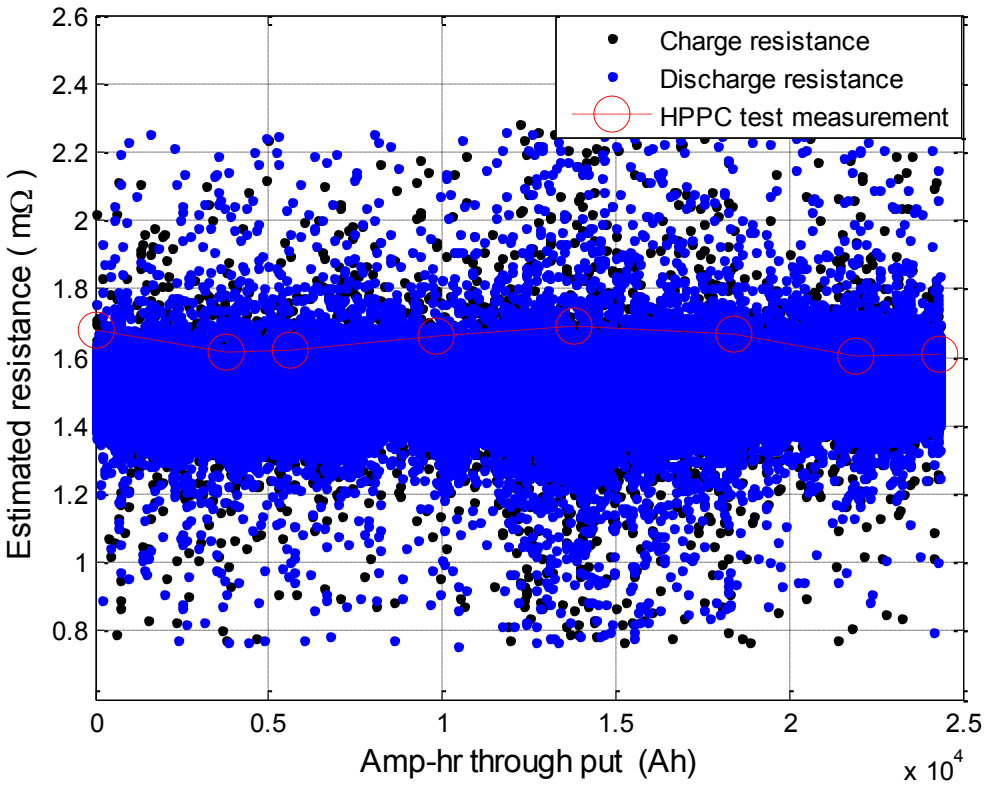

Figure 66: Resistance estimation using ohm's law

Using a similar approach, the resistance calculations were made for all the experiments described in the aging campaign in chapter 2. Results for one of the experiments are shown in Figure 66 where, the estimated resistance is plotted against the ampere hour throughput. It is interesting to note that, if a straight line was used to fit all the resistance estimates calculated (after some outlier rejection), the cell internal resistance would remain nearly constant. This could be because the cell was used in charge depleting mode representative of a PHEV like power profile and the mechanisms responsible for cell capacity fade were more dominant than those responsible for internal resistance growth. The same is indicated

by HPPC test implying that the technique does yield reliable estimates. The biggest advantage of this method is its very cheap computationally and can be easily coded into a microprocessor and embedded onboard a vehicle. It also doesn't require a special battery model and hence requires very little calibration effort. It relies on the measured voltage and current, which are readily available through the BMS in a hybrid or an electric vehicle. Consequently, this technique is universal and can be applied to any battery chemistry. However, it can be seen from the figure above that, the resistance estimation process leads to very noisy estimates. While, the measurements made through HPPC test yield a nearly constant resistance estimate of 1.6 mΩ, the earlier described technique yields results in the range of 0.8 to 2.5 mΩ. This is expected because the technique relies on instantaneous measurements of current and voltage which are bound to contain some noise. It should also be noted that, the estimates obtained above are from the data that was recorded in an aging laboratory which are relatively clean. Hence, it can be assumed that measurements coming from an actual vehicle might lead to noisier measurements. Consequently, the technique would require a lot of post- processing to be done on the raw estimates, to get useful information about state of health or EOL predictions. It can be concluded that though the resistance estimation technique proposed by Alexander K Suttman can provide reliable estimates, it requires a lot of post-processing and filtering to be practically implementable for state of health assessment. The needs and wants of an ideal resistance estimator are very similar to those outlined for an ideal capacity estimator and can be recalled here as follows:

1) It shouldn't be affected by normal vehicle operation wherein the current, voltage and sometimes temperature are dynamic variables.
2) Cheap from a computation stand point so that it can be imbedded in a microprocessor.
3) It should not require the battery to be charged fully or discharged below its normal SoC limits, to avoid shortening of battery lifespan through overcharging and over discharging.
4) Robust enough to provide relatively accurate estimates in the presence of sensor noise.
5) Adaptable to various lithium ion chemistries.

In addition to the above traits it is also desirable for the capacity and resistance estimation algorithms to be able to function independently such that both the parameters can be tracked individually. Such an algorithm, which has the traits listed above and where in the resistance growth can be tracked individually is developed in the next section. In the final section of this chapter, a framework is developed to track the resistance growth and the capacity fade simultaneously. This is highly desirable of a state of health estimator because it facilitates understanding of scenarios in which one is more dominant over the other and vice-versa.

6.3 Algorithm Presented in this Thesis

6.3.1 Flowchart and description of the algorithm

The algorithm for resistance estimation is very similar in concept to the algorithm presented for capacity estimation in chapter 3. Inputs to the algorithm are the measured quantities of

current, voltage and temperature, battery model parameters, initial state of charge and a target vector of battery cell internal resistance. An estimate of the cell internal resistance is obtained at the end of each event starting from the BOL until the EOL criteria is met. In this way, the cell internal resistance can be continuously tracked as it ages.

The algorithm relies on measurements made by current, voltage and temperature sensors and also requires a battery model that can estimate the cell dynamic voltage. The same first order equivalent circuit model employed in capacity estimation algorithm is used here as well. The dynamic voltage when added to open circuit voltage will give an estimate of the terminal voltage. In the resistance estimation algorithm, the open circuit voltage is determined by using the known cell capacity, initial state of charge and the OCV vs SoC map. Using the input current profile and the initial state of charge value, the SoC can be tracked using coulomb counting. Once, the SoC is known the OCV vs SoC map can be interpolated to get the corresponding OCV at each instant during the aging cycle. The cell dynamic voltage is determined using the measured current, temperature and battery model parameters. It is to be noted that, the internal resistance parameter in the battery model is replaced by a target internal resistance value. This is done for all the values in the target internal resistance vector and hence a matrix of dynamic voltage values are obtained. When the OCV calculated earlier is added to this dynamic voltage matrix, a matrix of estimated terminal voltage values are obtained. The actual measured voltage can be used to compute the error for each of those target resistance values and hence an error vector with the same length as the target resistance vector is obtained. As in the case of capacity estimation, error

minimization techniques can then be used to obtain an estimate of the cell internal resistance that yields minimum error.

A flowchart showing the resistance estimation algorithm is shown in Figure 67. The same convention as used earlier in the description of capacity estimation algorithm for differentiating vectors, matrices and scalars is used in the flowchart described in figure below. It should also be noted that, the resistance estimator functions only when the vehicle is in operation and the battery is being used in charge depleting mode. Hence, the time duration when the measured inputs of current, voltage and temperature are used is from the beginning of a charge depleting driving event to the end of it.

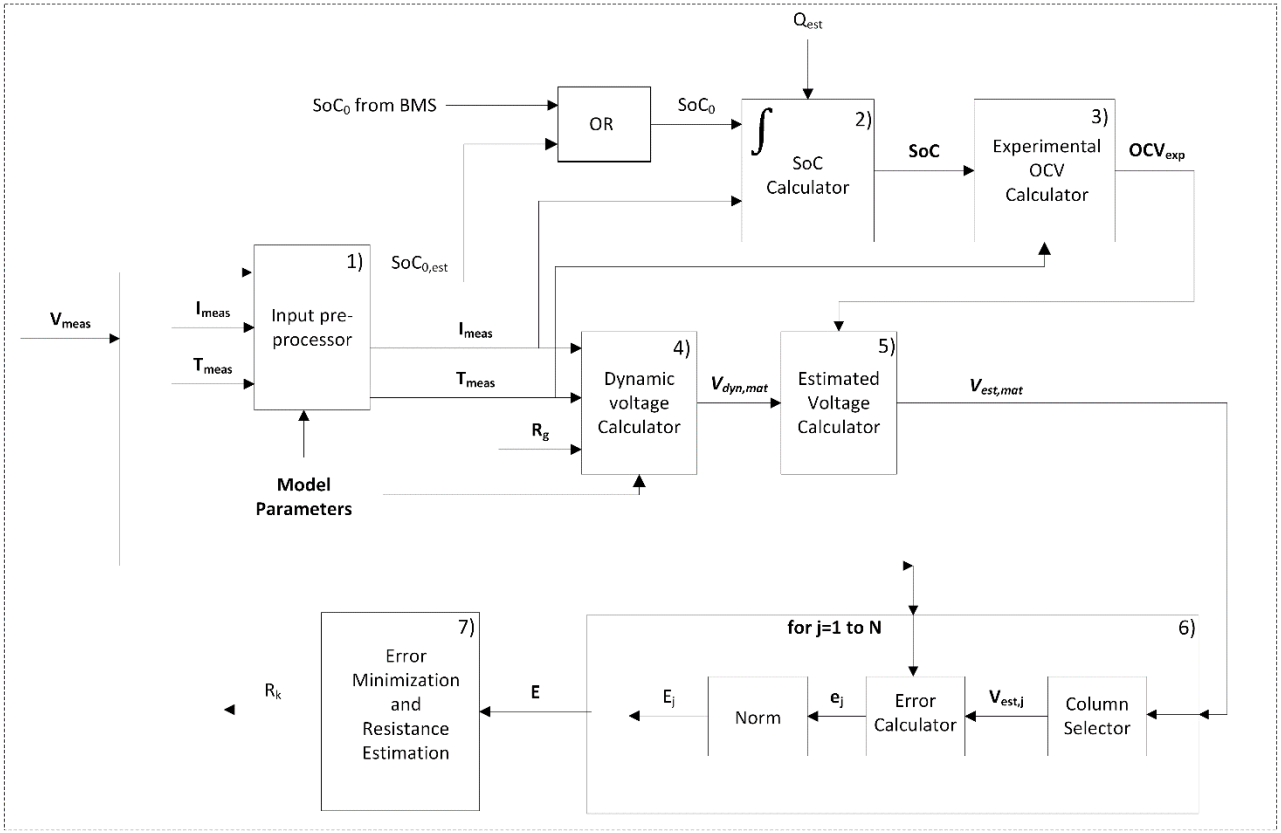

Figure 67: Detailed flowchart depicting the resistance estimation algorithm

All the steps of the resistance estimation algorithm can be briefly described below:

1) Estimate the initial state of charge value using the input measurements of current, voltage and temperature in the same manner as described in step 1 of the capacity estimation algorithm described in section 3,chapter 3.
2) Using the input current, a known initial state of charge value and a known capacity value, track the state of charge value by doing coulomb counting.

$$SoC_j(t) = SoC_0 - \int_{t_o}^{t} \frac{I_{meas}(\Gamma)d\Gamma}{Q_{est}} \quad (6.4)$$

A parameter that can be varied in this step is the value of capacity used to calculate the state of charge. A known and fixed initial capacity can be used as recommended by the manufacturer or the output of the capacity estimation algorithm from the previous event can be used. Both these options are explored in this thesis and sample results obtained are discussed in the next section.

3) Interpolate the experimentally established OCV vs. SoC map to calculate the OCV_{exp} value.
4) Equivalent circuit battery model described in chapter 2 is implemented to get an estimate of the cell dynamic voltage. Note that the resistance parameter is not the one calibrated for the battery model, but a value from the target resistance vector. This step is repeated N times, where N is the number of target resistance values considered. The result is a vector of dynamic voltage value for each target resistance and hence a matrix of dynamic voltage values for all the N target resistance values considered.

5) The forward battery model is implemented by adding OCV_{exp} vector calculated in step 3 to the dynamic voltage vectors calculated in step 4, for each of the N target resistance values considered, resulting in a matrix of estimated voltage values.
6) A vector of error values between the measured and estimated voltage is generated for a particular target resistance value. Using a suitable norm the calculated error vector can be reduced to a single number. This is repeated for all the target resistance values resulting in an error vector with the same length as the target resistance vector.
7) Error minimization techniques similar to those employed in the capacity estimation algorithm are used to obtain an estimate of the cell internal resistance.

6.3.2 Sample results and post-processing

6.3.2.1 Sample results

In this section, results obtained from the algorithm presented above are shown for an example experiment. In particular experiment number 4 from the summary of experiments described in Table 2 of chapter 2, section 3 is chosen. The particular aging protocol was medium charging and charge depleting operation to a minimum of 45% SoC at 30 °C. One of the inputs to the resistance estimation algorithm is the cell capacity. As noted earlier in the previous section on algorithm description, this capacity can be a fixed initial value as obtained from initial characterization tests in the laboratory. In such a case, the resistance estimation algorithm will function independent of the capacity estimation algorithm. However, since the capacity estimation algorithm has already been developed, the estimated cell capacity from previous cycle can be extracted from the results of the capacity

estimator and used as an input to the resistance estimation algorithm. This way the capacity can be updated at each cycle resulting in a more practical implementation. The figure shown below showcases results for both the implementation methods.

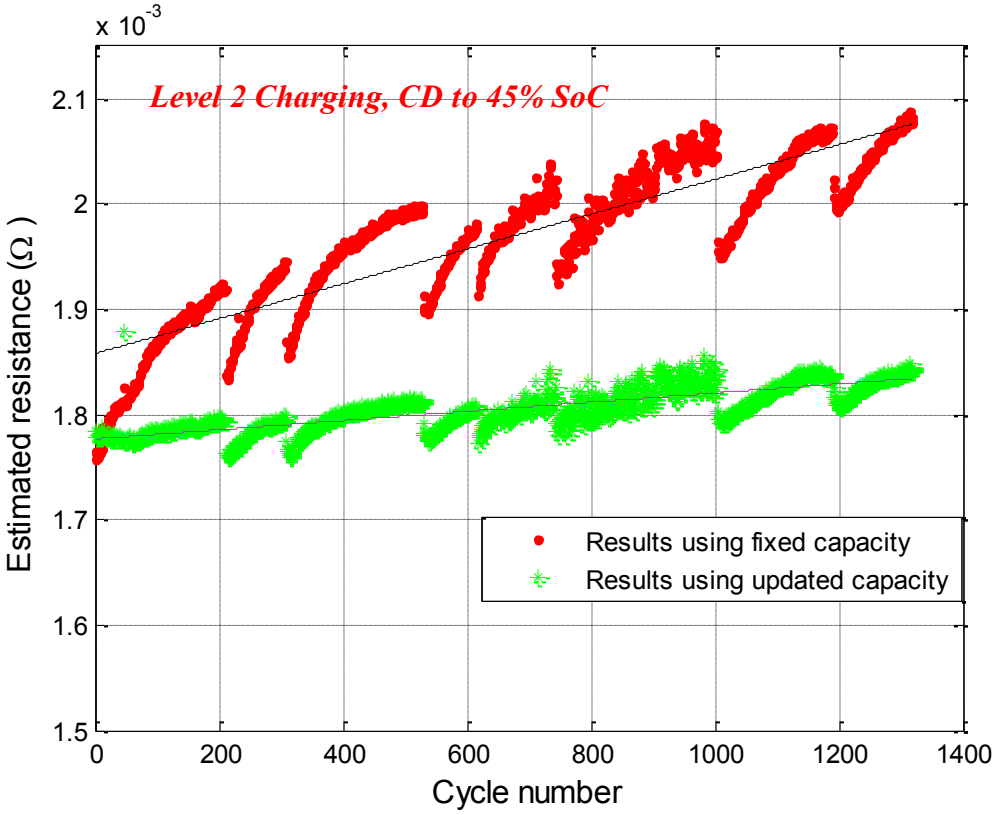

Figure 68: Estimated resistance vs. cycle number for an example aging protocol

The results obtained using a fixed capacity are very similar in nature to the capacity estimation results obtained using a fixed internal resistance. This could be attributed to the fact that because the cell capacity is assumed constant, the entire effect of battery aging is encapsulated in the increased cell internal resistance. Contrasting the results obtained using

fixed capacity with that obtained using updated capacity from previous cycle, we can conclude that the algorithm can work independently as well as in conjunction with the capacity estimation algorithm. This is advantageous because in practicality, both resistance as well as capacity are dynamic variables and neither can be assumed to be constant. It is also interesting to note that, when the estimated capacity from previous cycle is used as an input to the resistance estimation algorithm, the resistance growth is really small as compared to when the capacity is assumed constant. In the results shown in figure above, when updated capacity is used for resistance estimation, the resistance grows from a value of 1.77 mΩ to 1.85 mΩ. On the contrary, when a fixed capacity is used the resistance grows from a value of 1.75 mΩ to 2.1 mΩ. This goes to show that, both the effects of capacity fade and resistance growth are being accounted for if the resistance estimation algorithm uses the estimated capacity from previous cycle. A similar observation regarding the resistance growth was also made through HPPC tests conducted in the laboratory where in the resistance for most of the aging protocols described in chapter 2 did not increase much.

6.3.2.2 Post processing

Post processing the resistance estimates included the same steps, undertaken for post processing the capacity estimation results. These were outlier rejection, gap filling, filtering and normalizing. Outlier rejection was done by removing the cycles for which the ampere-hour throughput was below the threshold value of half of the nominal capacity i.e. 15. In addition it was also noted in the post processing described in chapter 5, that due to experimental errors three cycles were removed whenever there was an outlier rejection. The gaps created as a result of outlier rejection were filled by doing a linear fit locally, over

a sliding window length of 100 cycles and adding the slope of fitted line to the previous raw estimate. For instance, a gap at cycle number 150 was filed by doing a linear fit of raw estimates obtained for cycle 50 to 149 and adding the slope of that fit to the raw resistance estimated for 149^{th} cycle. If the gap to be filled occurred before the numerical value of window length (100 in this case), all the available estimates prior to the gap were utilized for curve fitting. The cell internal resistance is expected to increase throughout its life and to be consistent with that notion, the previous resistance was held constant whenever the slope of fitted line was negative. Filtering of the resistance estimates was performed in the same manner as gap filling. The difference being the calculated slope over a local window was added to the previous filtered estimate in order to get the filtered estimate for the current cycle. An example of post processed results are shown in Figure 69. The resistance estimates obtained using a fixed initial capacity for the same experiment considered in the results section above (medium charging and charge depleting operation to a minimum of 45% SoC at 30 °C) are used for post processing.

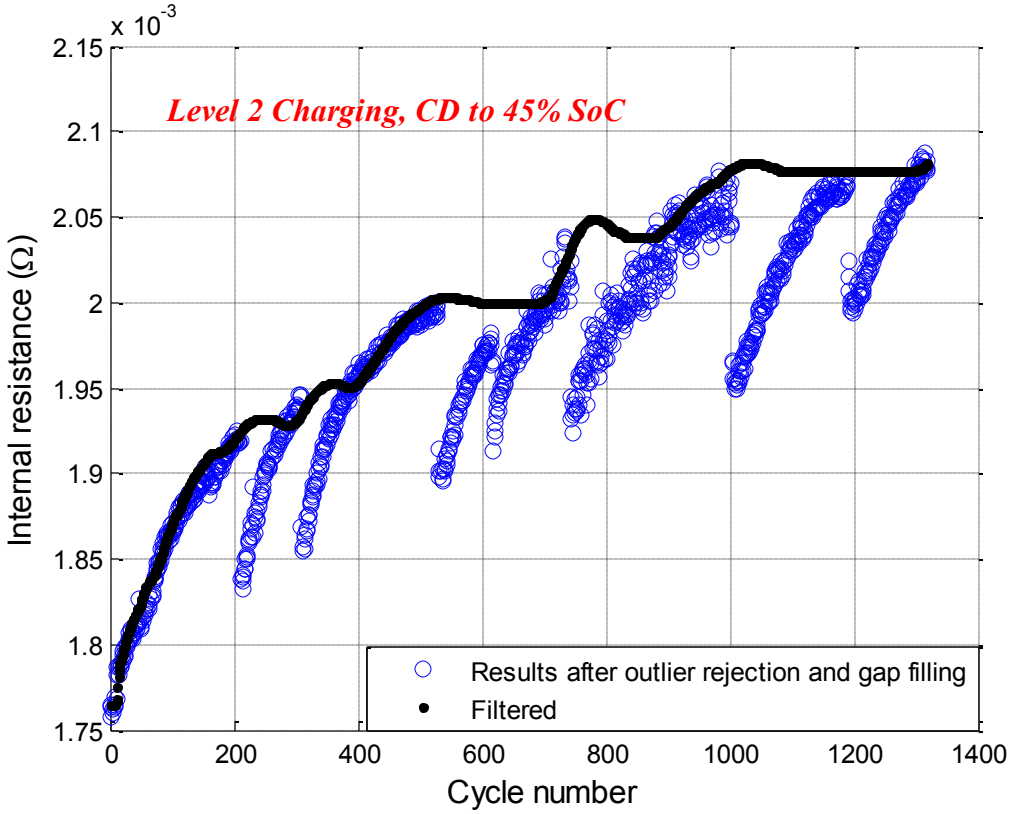

Figure 69: Filtering of estimated resistance using a window length of 150 cycles

Raw resistance values cannot provide much indication about the battery state of health and hence, the filtered resistance estimates need to be normalized to obtain percentage resistance growth. This is achieved via the same technique employed for normalizing the capacity estimates and was described in section 3 of chapter 5. Sample results for the experiment considered earlier are shown in Figure 70, where the percentage resistance growth is plotted against cycle number.

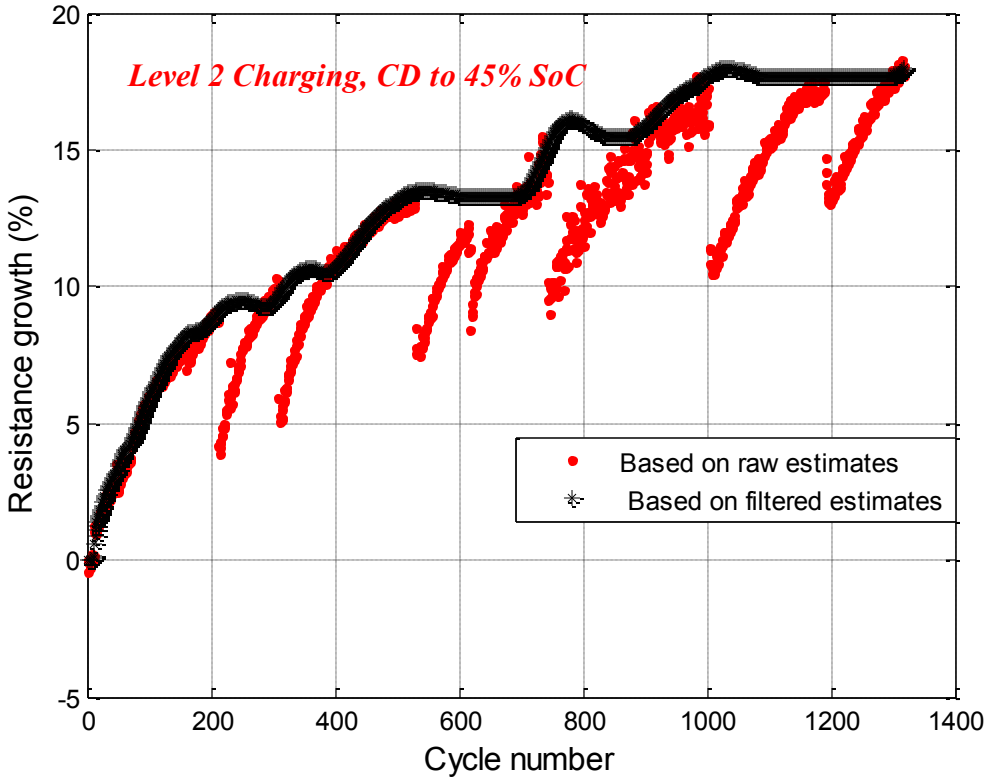

Figure 70: Normalizing the estimated resistance to obtain percentage resistance growth

It is interesting to note that, the capacity estimates used to feed into the resistance estimation algorithm were still obtained using a fixed internal resistance. Hence, the next step should be to develop a framework where in both the resistance and capacity are estimated at each cycle and the output of one algorithm is used as an input to the other and so on until the end of life criteria is met. Such a framework will enable continuous tracking of both the parameters and is presented in the next section.

6.4 Capacity and Resistance Estimation: A Combined Framework

So far in this thesis, capacity and resistance estimation algorithms have been developed to function independent of each other. However, in an actual vehicle both these parameters change simultaneously and hence it would be best to develop a framework such that both these parameters are interactively estimated at each event. Such a framework can capture the effect of change in one parameter on the other and vice-versa. The desirable traits of such an algorithm still remain the same as those outlined for capacity and resistance estimation algorithms. The only extra requirement would be to have both capacity and resistance estimate outputs at each event.

6.4.1 Framework

The framework for simultaneous estimation of capacity and resistance is shown in Figure 71. Note that inputs to both the capacity and resistance estimation algorithms contained in the combined framework are the same as those described in their independent operation in chapters 3 and 6. A unique advantage the combined framework offers is the capability to estimate both the parameters simultaneously by toggling between each other. Initialization of this combined algorithm is achieved by using the known resistance calibrated by the battery model and estimating the capacity at beginning of life. However, it can also be done by using the known capacity from initial characterization tests and starting the algorithm with resistance estimation at the beginning of life. The former initialization technique is chosen because the capacity estimation algorithm was observed to be insensitive to resistance in chapter 4 on sensitivity analysis. Hence, any initialization errors would not affect the long term results of the algorithm. The estimated capacity and resistance at every

event were filtered using the same techniques described in post processing in chapter 5. This ensured that the noise from one estimation technique did not affect the output of the other and vice-versa. This combined algorithm is run from the beginning of life until the end of life criteria is met.

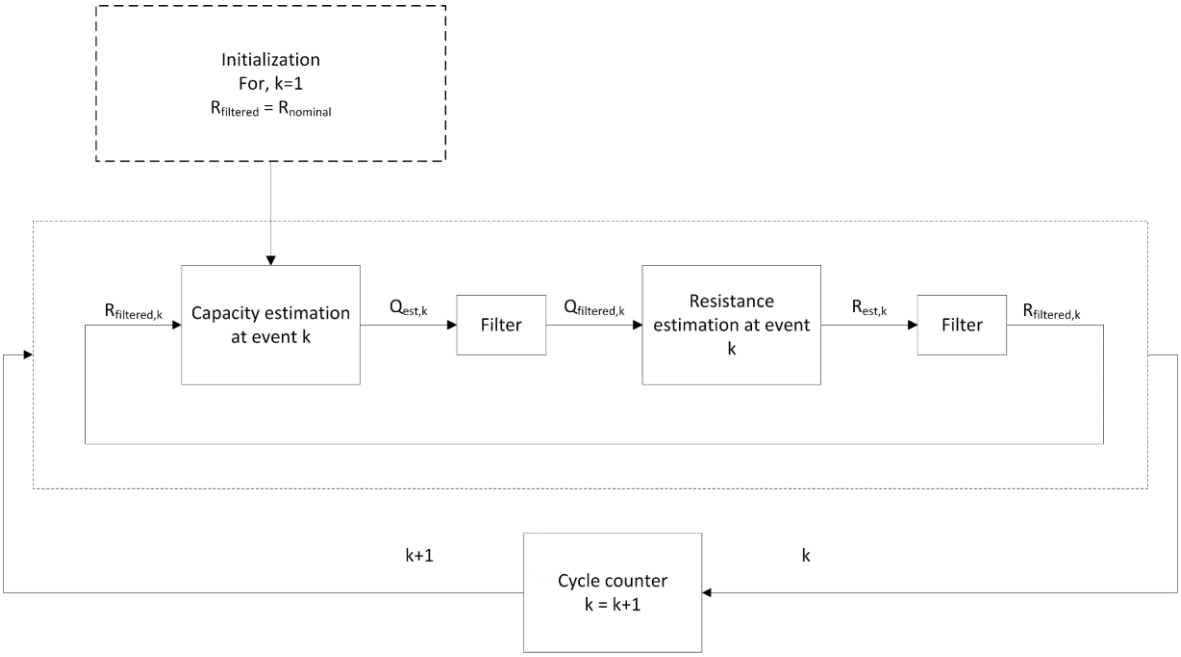

Figure 71: Flowchart depicting combined framework to estimate capacity and resistance at every event

6.4.2 Sample results

The combined framework presented above in previous section can be used to estimate the capacity and resistance for any of the aging protocols summarized in section 2 of chapter 2. As an example, experiment 10 from Table 4 is chosen to show some results. The particular aging protocol was medium charging and charge depleting operation to 35% SoC at 45 °C. Because the aging occurred at a higher temperature, the experiment met EOL

criteria with only 15000 ampere-hour throughput. Capacity and resistance estimation results are shown in Figure 72 and Figure 73.

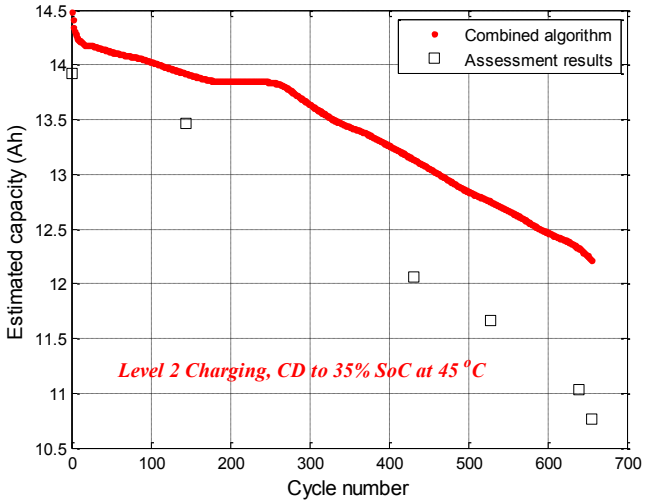

Figure 72: Estimated capacity using the combined framework for an example aging protocol

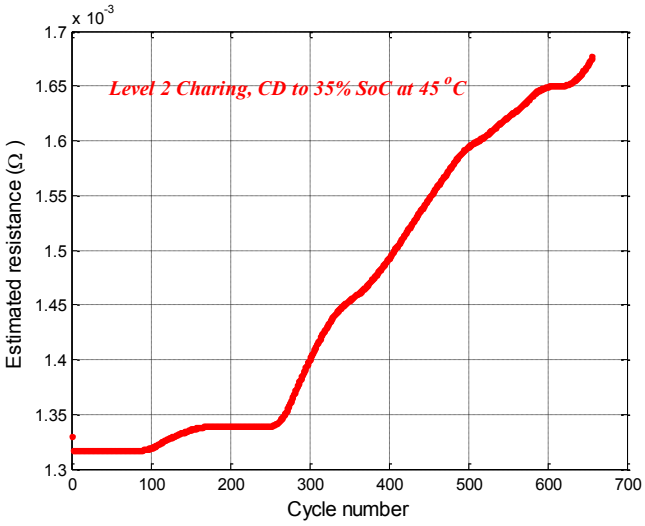

Figure 73: Estimated resistance using the combined framework for an example aging protocol

The results shown in figures above, support the fact that lithium-ion batteries undergo fast aging at higher temperatures. According to the assessment tests conducted in laboratory, the capacity faded by about 22% at the end of around 650 aging cycles while, according to the combined framework, the capacity faded by about 16%. Though the magnitudes aren't equal, the algorithm does capture the overall trend for both capacity as well as resistance estimation. In the resistance estimation results shown above, there are several instances when the estimated resistance remains constant like near the BOL. This is attributed to the way the raw resistance estimates are filtered. In particular, when the slope of the fitted line was negative the resistance was held constant to the previous value in order to be consistent with the notion that resistance cannot decrease with increased aging.

6.5 Objectives Achieved

It can be recalled from section 4, chapter 2 that a number of objectives were set for the development of capacity and resistance estimation techniques. Through the work described in chapters 3, 4, 5, and 6 the following objectives have been achieved:

1) Large amount of data was collected across 18 experiments in total, to gain insight into battery aging phenomenon. These experiments investigated battery aging in different operating conditions by considering four severity factors for the DOE.
2) Algorithms for capacity and resistance estimation were developed and tested on different aging protocols. These algorithms fulfilled the needs and wants of an ideal state of health estimator listed in section 3, chapter 2.

3) Sensitivity analysis was conducted to analyze the performance of capacity estimation algorithm in presence of sensor errors and variation in parameters governing the algorithm. Results from the sensitivity analysis suggested that the algorithm is fairly insensitive to most of the factors considered.
4) Suitable post processing techniques were developed to remove outliers, fill the gaps, remove noise from raw estimates and convert the estimated parameters into percentage fade/growth. The results from both the algorithms developed in this thesis can be used to feed into a state of health estimator and possibly make EOL predictions. This is a part of the proposed future work and will be addressed in the concluding chapter.

Chapter 7: Summary of Results

Capacity and resistance estimation algorithms and the combined framework for estimating both the parameters simultaneously were implemented on all the aging protocols described in Table 4 (a total of 18 experiments). The aging protocols covered different aging severity factors like minimum state of charge, charging level, mode of operation and temperature. In this chapter, capacity and resistance estimation results for a few example cases are presented. In particular the following cases are chosen, to cover different aging severity factors and demonstrate the capability of the algorithms:

1) Example 1: Level 3 Charging, CD to 25% SoC at 30 °C.
2) Example 2: Level 1 Charging, CD to 45% SoC at 30 °C.
3) Example 3: CD-CS (1:1) blend mode of operation at 10 °C.
4) Example 4: Level 2 Charging, CD to 35% SoC at 45 °C.
5) Example 5: Level 2 Charging, CD to 25% SoC at 30 °C.
6) Example 6: Level 2 Charging, CD to 35% SoC at 55 °C.

7.1 Capacity Estimation Results

7.1.1 Example 1: Level 3 charging, CD to 25% SoC at 30 °C

The level 3 charging and charge depleting at 25% SoC aging protocol is an example of accelerated aging owing to fast charging. As a result, the cell aged under this particular protocol underwent a total ampere hour throughput of around 30,000 Ah. The capacity

estimated at BOL as around 14.5 Ah and that at the end of experiment was around 13 Ah. This indicated a loss of around 10% in the estimated capacity, a number very close to the results of assessment tests conducted for this experiment, which indicated a loss of 11.5% at the end of experiment. The estimated capacity as a function of ampere hour throughput are shown in Figure 74.

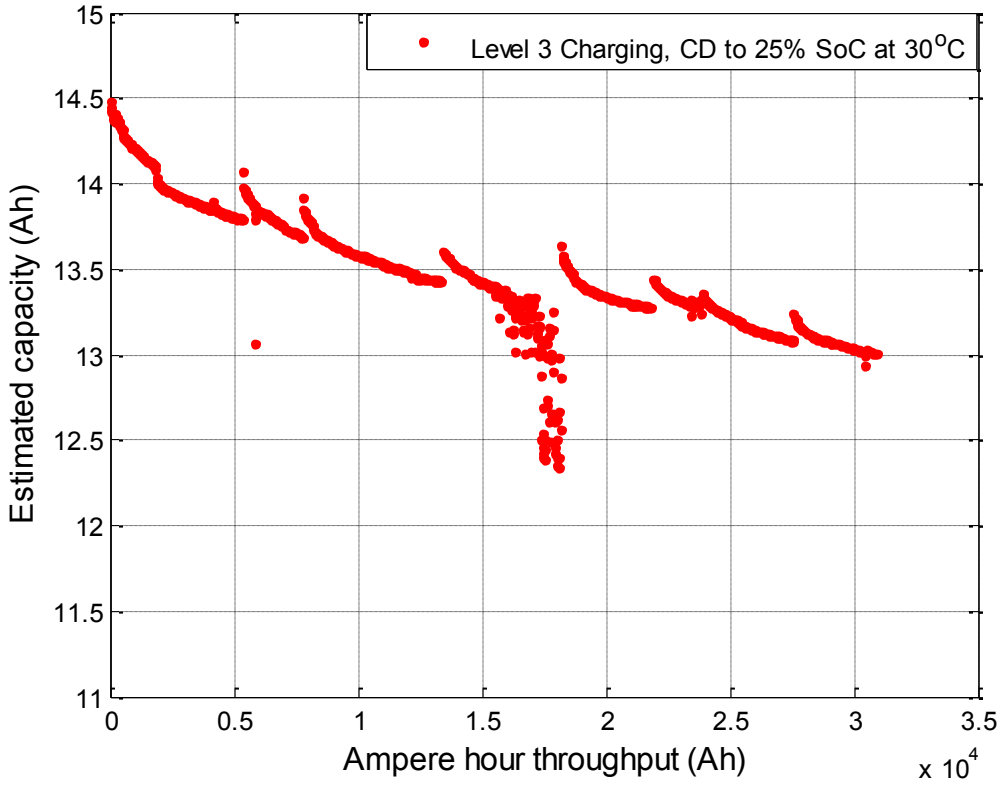

Figure 74: Estimated capacity vs. ampere hour throughput for Level 3 Charging, CD to 25% SoC at 30 °C

Due to issues in executing the experiment, the aging protocol wasn't correctly followed for a number of cycles in between 15,000 and 20,000 Ah. The result was the ampere hour

throughput for some of those cycles was lower than the nominal ampere hour throughput for that particular aging protocol. Owing to this reduced scope of data available for capacity estimation, the capacity estimated from the algorithm was slightly lower and the same was observed in the sensitivity analysis on scope of data used (Figure 48). However, it should be noted that the overall aging trend is well captured and the percentage capacity loss obtained is almost same as that obtained from assessment tests.

7.1.2 Example 2: Level 1 charging, CD to 45% SoC at 30 °C

The level 1 charging and charge depleting at 45% SoC aging protocol is an example of relatively slow aging owing to slow charging. As a result, the cell aged under this particular protocol underwent a total ampere hour throughput of only around 12,000 Ah. The capacity estimated at BOL as around 14 Ah and that at the end of experiment was around 12.8 Ah. This indicated a loss of around 8.5% in the estimated capacity, a number very close to the results of assessment tests conducted for this experiment, which indicated a loss of 6.5% at the end of experiment. The estimated capacity as a function of ampere hour throughput are shown in Figure 75. It can be observed from the figure that, apart from a few values that are slightly off the overall aging trend is very well captured.

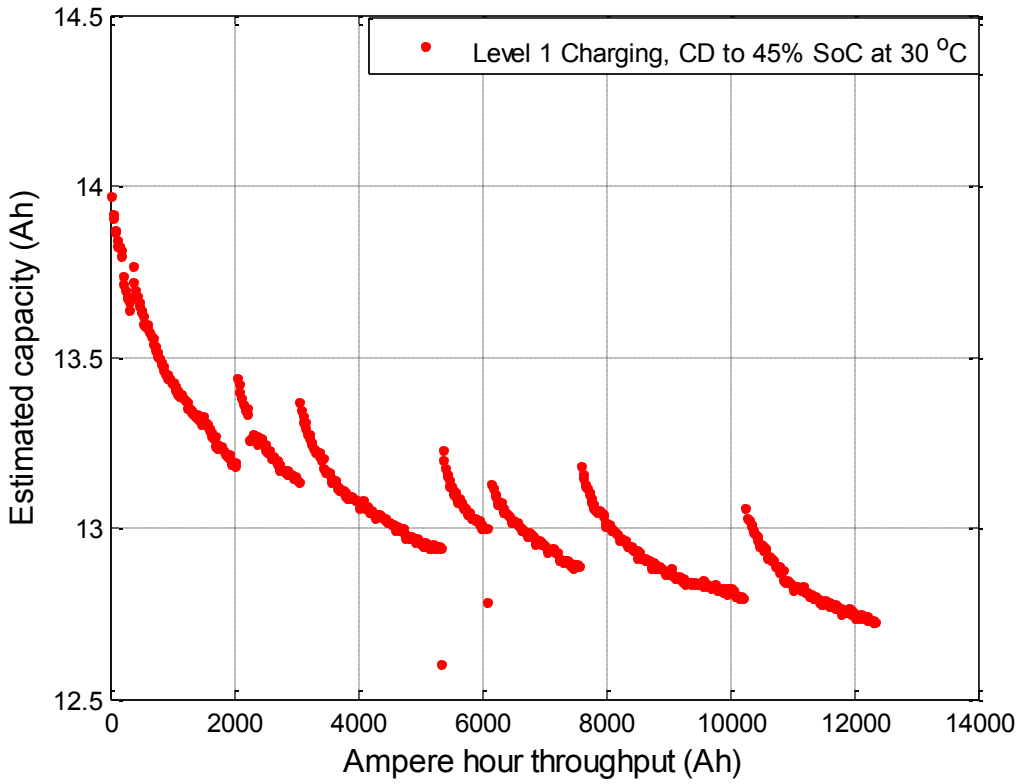

Figure 75: Estimated capacity vs. ampere hour throughput for level 1 charging, CD to 45% SoC at 30 °C

7.1.3 Example 3: CD-CS (1:1) to 35% SoC at 10 °C

The CD-CS (1:1) aging protocol is representative of a range extender vehicle wherein, the vehicle runs on power from the battery until the battery SoC reaches a pre-defined threshold limit. Beyond this the battery state of charge remains nearly constant and the main source of power is either the internal combustion engine or an electric generator depending on the system powertrain architecture. Since, the algorithm relies on error minimization over a broad state of charge region, the algorithm can be implemented by either utilizing the entire driving data (CD+CS) or by utilizing just the CD portion of data.

For the results presented in Figure 76, only the CD portion of data is utilized for capacity estimation.

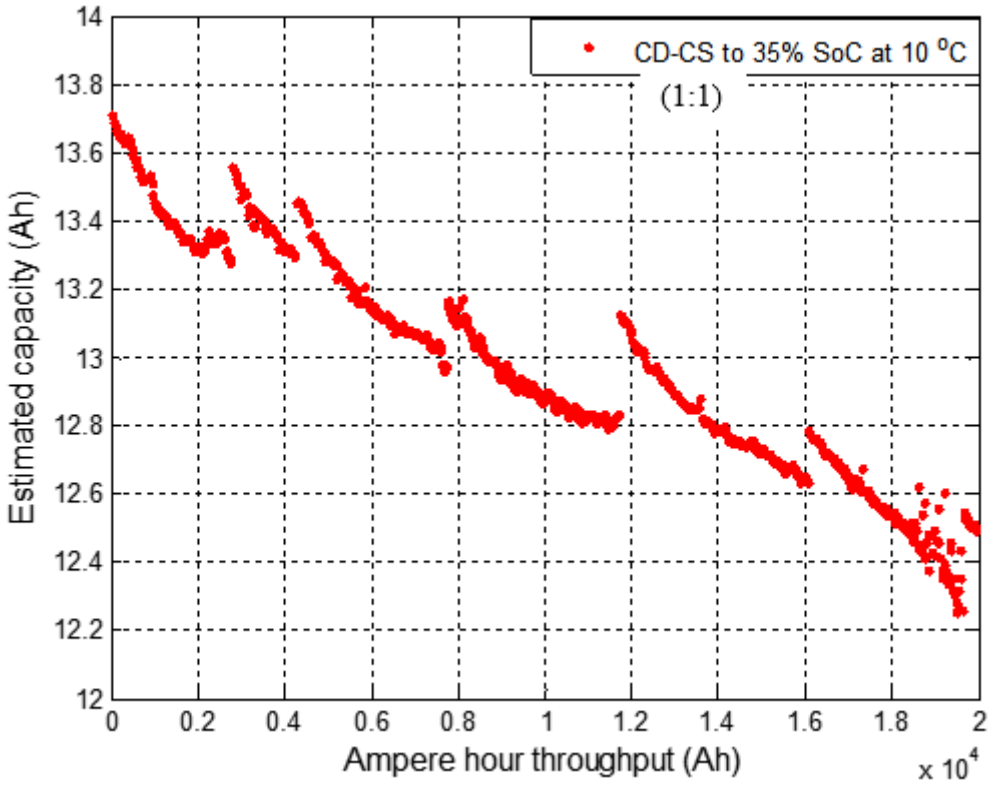

Figure 76: Estimated capacity vs. ampere hour throughput for CD-CS (1:1) to 35% SoC at 10 ° C

The capacity estimated at BOL is around 13.7 Ah and that at the end of experiment is around 12.3 Ah. This indicated a loss of around 10% in the estimated capacity, a number very close to the results of assessment tests conducted for this experiment, which indicated a loss of 10.6% at the end of experiment.

7.1.4 Example 4: Level 2 charging, CD to 35% SoC at 45 °C

The initial design of experiments didn't account for the impact of elevated temperatures on lithium-ion battery aging. However, at a later stage two additional aging experiments were started with aging at higher temperatures. These were level 2 charging, CD to 35% SoC at 45 °C and level 2 charging, CD to 35% SoC at 55 °C. Results for one of these experiments are shown in Figure 77.

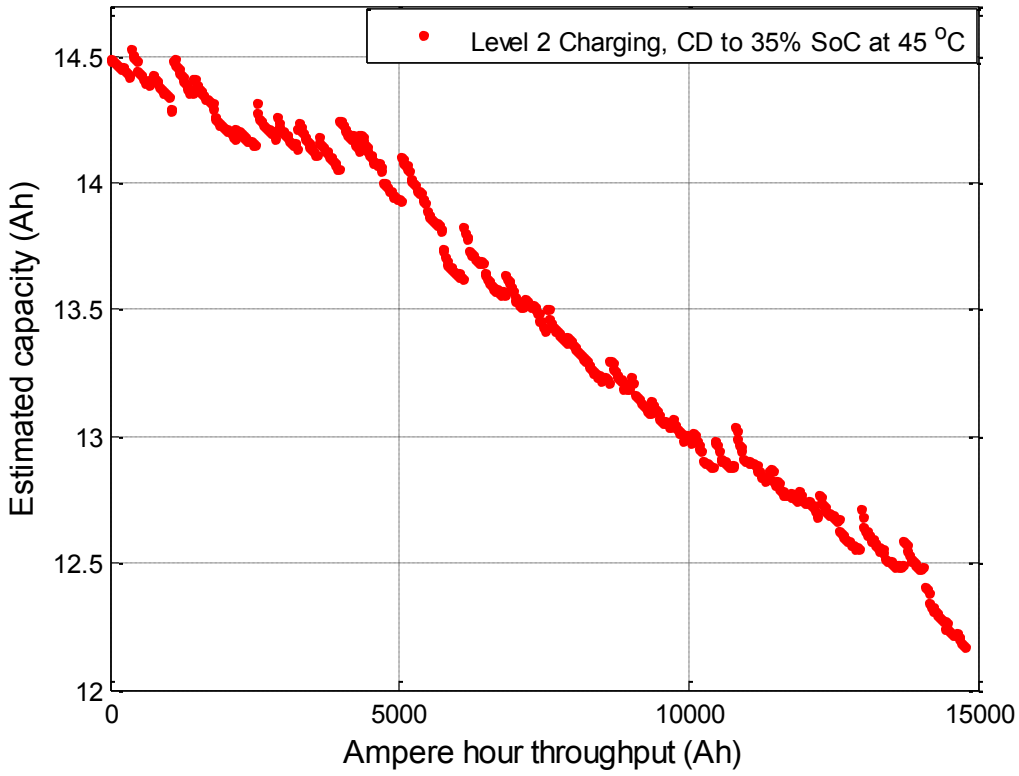

Figure 77: Estimated capacity vs. ampere hour throughput for level 2 charging, CD to 35% SoC at 45 °C

It can be seen from the figure that, high temperatures can lead to degradation in lithium-ion batteries very fast. In particular, the estimated capacity drops from 14.5 Ah at the BOL

to 12.2 Ah within an ampere hour throughput of 15,000 Ah. This amounts to almost 20% degradation in battery capacity implying EOL criteria for the cell under aging. From the results of Figure 77, it can be concluded that the algorithm does succeed in capturing the effects of high temperatures on lithium-ion battery aging.

7.2 Resistance Estimation Results

7.2.1 Example 5: Level 2 charging, CD to 25% SoC at 30 °C

It can be recalled from earlier chapter that, capacity was used as an input to the resistance estimation algorithm. As a result, the algorithm could be implemented in two different ways: using a fixed capacity or using an updated capacity at each cycle. Results from both the implementation methods are shown in Figure 78. The results obtained using a fixed capacity are very similar in nature to the capacity estimation results obtained using a fixed internal resistance. This could be attributed to the fact that because the cell capacity is assumed constant, the entire effect of battery aging is encapsulated in the increased cell internal resistance. Contrasting the results obtained using fixed capacity with that obtained using updated capacity from previous cycle, we can conclude that the algorithm can work independently as well as in conjunction with the capacity estimation algorithm. This is advantageous because in practicality, both resistance as well as capacity are dynamic variables and neither can be assumed to be constant. It is also interesting to note that, when the estimated capacity from previous cycle is used as an input to the resistance estimation algorithm, the resistance growth is really small as compared to when the capacity is assumed constant. In the results, when updated capacity is used for resistance estimation, the resistance seems to decrease initially. On the contrary, when a fixed capacity is used

the resistance grows from a value of 1.65 mΩ to 2.1 mΩ. This goes to show that, both the effects of capacity fade and resistance growth are being accounted for if the resistance estimation algorithm uses the estimated capacity from previous cycle. A similar observation regarding the resistance growth was also made through HPPC tests conducted in the laboratory where in, the resistance for most of the aging protocols described in Table 4 did not increase much.

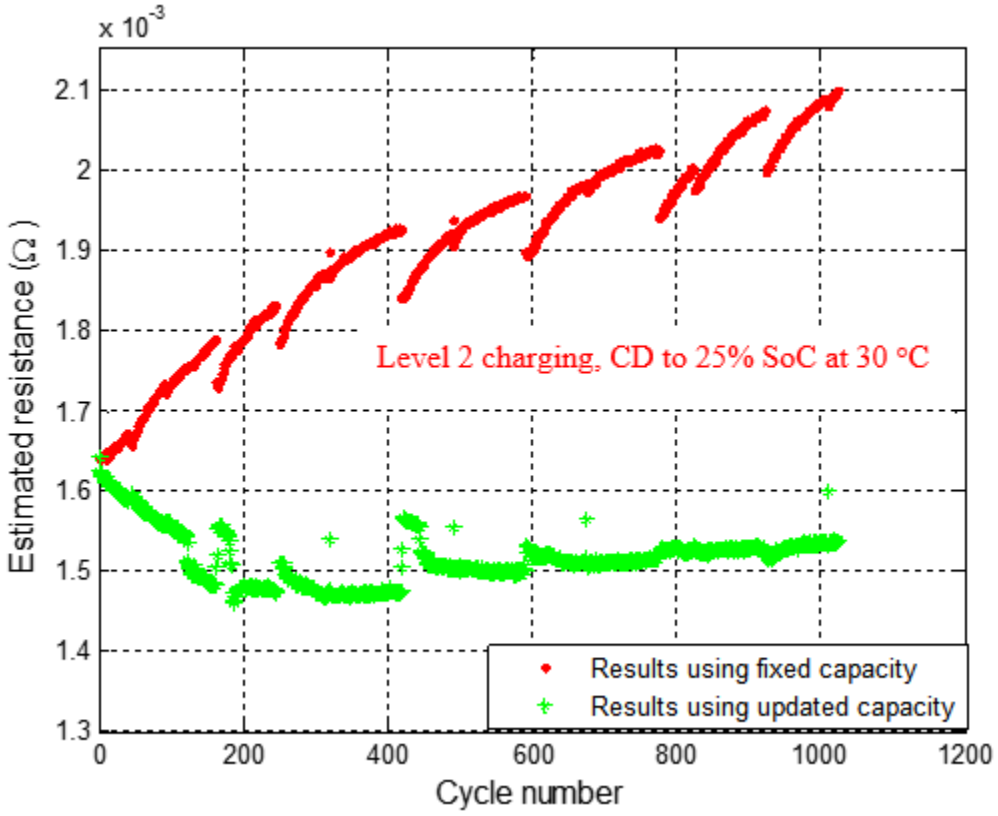

Figure 78: Estimated resistance vs. cycle number for level 2 charging, CD to 25% SoC at 30 °C

7.2.2 Example 6: Level 2 charging, CD to 35% SoC at 55 °C

It was noted earlier, that the capacity estimation algorithm was able to capture the effects of elevated temperatures on battery aging. However, higher temperatures not only cause the cell capacity to fade fast, it also causes the internal resistance to increase faster. The results shown in Figure 79 support the known facts about impact of higher temperatures on lithium-ion battery aging.

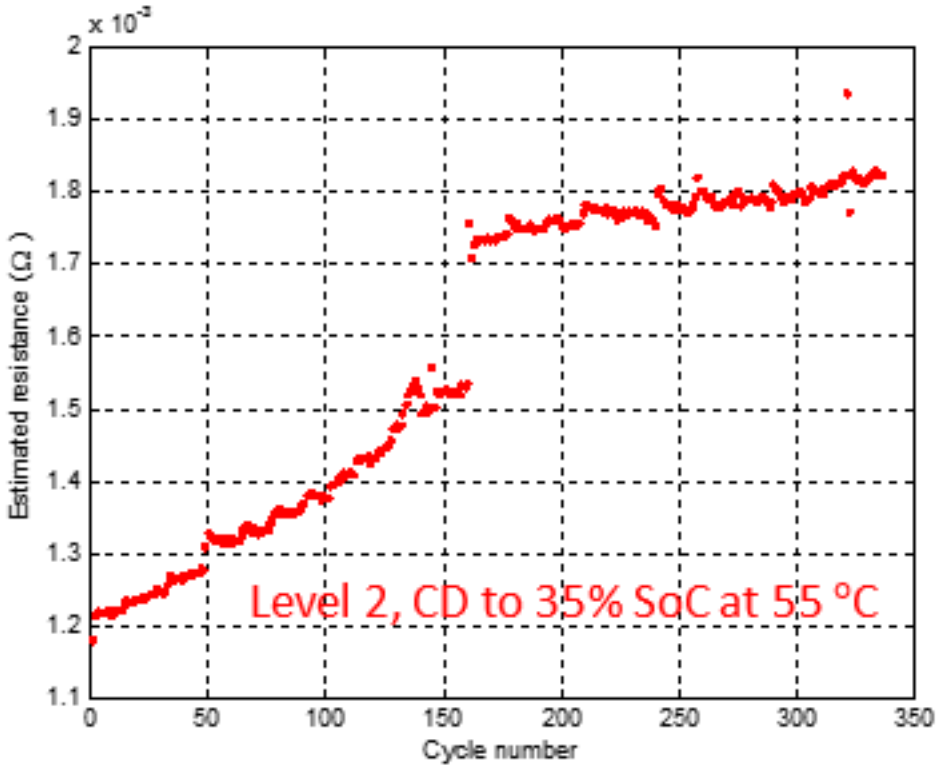

Figure 79: Estimated resistance vs. cycle number for level 2 charging, CD to 25% SoC at 55 ° C

Note that there is a discontinuity in the estimation algorithm around 160^{th} cycle. This was because the temperature in the laboratory wasn't controlled properly and it increased to a higher value from 160^{th} cycle onwards.

Chapter 8: Conclusions and Recommendations

In this work algorithms capable of *in-situ* estimation of capacity and internal resistance of lithium-ion batteries used in HEVs, PHEVs and BEVs were developed. Motivation behind the proposed approach was to utilize a unique property of self-similarity observed in the voltage response curves as a function of SoC for lithium-ion batteries regardless of age and mode of aging. The challenge was to incorporate a technique that could effectively utilize this property under dynamic conditions experienced in an actual vehicle. The estimation algorithms were implemented on a wide variety of data collected at the Center for Automotive Research Battery Aging Laboratory. This wide gamut of data tested battery operation under variety of aging protocols.

The algorithms rely on dynamic measurements made in an actual vehicle and do not incorporate any additional sensors or advanced techniques. As a result, they can be implemented without interfering with normal vehicle operation, something highly desirable of an *in-situ* capacity/resistance estimator. Because the algorithms rely on simple mathematical computations, they can be imbedded in a micro-processor on-board an actual vehicle and hence implemented in real time with very little computing power or memory requirements. The algorithms were implemented on event/cycle basis with an event being defined as the time period when the battery is used in charge depleting mode of operation. Consequently, the algorithms do not require full charging or discharging of the battery and

hence resulting in a non-intrusive implementation method. The self-similarity property that forms a basis of the proposed technique has been observed for a number of lithium-ion chemistries. Some of these might have the voltage curves self-similar only across a certain state of charge region while, others might be self-similar across the entire state of charge range. Nonetheless, this algorithm can still be implemented because it does not rely on point wise measurements. The algorithms are model based but do not require sophisticated models for implementation. They only require battery models that can predict cell dynamics with reasonable accuracy. The work presented in this thesis utilizes a simple first order equivalent circuit battery model and hence it requires very little calibration effort.

The algorithms inherently rely on error minimization over a wide scope of data during the entire event and hence are robust enough to provide reliable estimates in the presence of modeling errors, parameter variations and sensor errors. These observations were justified by conducting sensitivity analysis wherein, it was concluded that the algorithms were fairly robust and insensitive to various errors. Aging experiments conducted in the laboratory incorporated a number of reference performance tests throughout the aging campaign. It has been observed that these reference performance tests cause some rejuvenation at the micro level due to which the cell capacity increases slightly after being subjected to any such test. Furthermore, these tests are intrusive and never occur in the field. Hence, relevant post-processing techniques were established to ignore the rejuvenation experienced as a result of the above mentioned tests and depict battery aging in a more practical manner.

It is widely known that battery aging can result in capacity fade and/or resistance growth. Independent implementation of the capacity estimation algorithm relied on the knowledge

of battery model resistance and independent implementation of the resistance estimation algorithm relied on the knowledge of battery capacity. However, to estimate both the parameters simultaneously, a framework was developed wherein, both capacity and resistance estimates were obtained and updated at each cycle resulting in a more practical implementation, which tracks both the parameters simultaneously and yields either results while automatically adapting the model as the battery ages.

Aging experiments in the Battery Aging Laboratory were conducted at constant temperatures, hence as part of the future work, the algorithms need to be implemented on variable temperature data, both changing between events and intra-event. The self-similarity property utilized in this work has been observed for a number of lithium-ion chemistries. The algorithms presented should be implemented on a different lithium-ion chemistry in the future. Though, the aging protocols engineered in laboratory were representative of actual PHEV like aging profiles, it is essential to validate the algorithms on data collected from an actual vehicle. Most of the aging models utilize capacity and resistance information gathered through aging campaigns run in the laboratory. These are open loop estimation techniques and do not incorporate a feedback correction path for tracking battery aging. A very important capability of the algorithm is to be able to provide a rich stream of capacity and resistance estimates based on dynamic measurements throughout the life. Consequently, these estimates can be used to form a feedback path for various prognosis and diagnosis purposes (Figure 80). Realizing the powerful and novel capabilities of the algorithms developed in this work, an invention disclosure titled "Method for determining Li-ion Battery Capacity in Application(s)" was made (Tech ID #

2014-024) with The Ohio State University Technology Commercialization Office (TCO). Consequently, a provisional patent has been filed in June 2014 (Application Number: 62/010, 671), to protect the intellectual property resulting from work done in this project.

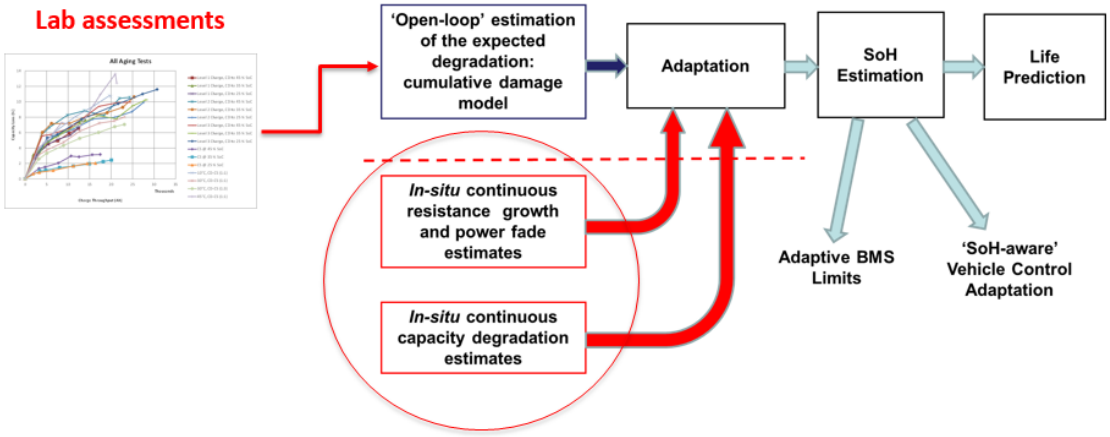

Figure 80: Adaptive battery aging model for state of health estimation and life prediction

In summary, it can be concluded that capacity and resistance estimation algorithms were developed and tested on a wide gamut of data that, tested battery operation in different operating conditions. These algorithms satisfied the needs and wants of an ideal state of health estimator and hence can be imbedded in a micro-processor on-board an actual vehicle.

References

1. "Tires and Passenger Vehicle Fuel Economy". Transportation Research Board (2006). Web. http://onlinepubs.trb.org/onlinepubs/sr/sr286.pdf.
2. Chiara, F., Canova, M., and Rizzoni, G. "Future mobility challenges, Where Will We Find Fuel Efficient Solutions?" (April 24, 2012).
3. Atabani, A.E., Badruddin, I.A., Mekhilef, S., and Silitonga, A.S. "A Review on Global Fuel Economy Standards, Labels and Technologies in the Transportation Sector". Renewable and Sustainable Energy Reviews 15 (2011). Pg. 4586– 4610.
4. "Energy Consumption by Sector". U.S. Energy Information administration (2010). Web. http://www.eia.gov/emeu/aer/pdf/pages/sec2.pdf.
5. "BP Statistical Review of World Energy" (June 2013). Web. http://www.bp.com/statisticalreview.
6. "CO_2 Emissions from Fuel Combustion". International Energy Agency (IEA - 2010). Web. http://www.iea.org/co2highlights/co2highlights.pdf
7. "CO_2 Emissions from the Japanese Transport Sector Already Decreasing". Japan for Sustainability (JFS - 2010). Web. http://www.japanfs.org/en/mailmagazine/newsletter/pages/030151.html

8. Pollet, B.G., Staffell, I., and Shang, J.L. “Current Status of Hybrid, Battery and Fuel Cell Electric Vehicles: From Electrochemistry to Market Prospects”. Electrochimica Acta 84 (2012). Pg. 235– 249.
9. Nazri, G.A., and Pistaoie, G. “Li-Ion Batteries for EV, HEV and Other Industrial Applications”. Lithium Batteries, Science and Technology, Kluwer Academic Publishers (2004), Chapter 21.
10. Viswanathan, V.V., Choi, D., Wang, D., Xu, W., Towne, S., Williford, R.E., Zhang, J.G., Liu, J., and Yang, Z. “Effect of Entropy Change of Lithium Intercalation in Cathodes and Anodes on Li-ion Battery Thermal Management”. Journal of Power Sources, vol. 195, no. 11 (2010). Pg. 3720-3729.
11. Contestabile, M., Offer, G.J., Slade, R., Jaeger, F., and Thoennes, M. Energy & Environmental Science 4 (2011). Pg. 3754.
12. McKinsey & Company. “Beitrag der Elektromobilität zu langfristigen Klimaschutzzielen und Implikationen für die Automobilindustrie, Studie imAuftrag des Bundesministerium für Umwelt, Naturschutz und Reaktorsicherheit” (2010). Web. http://www.bmu.de/files/pdfs/allgemein/application/pdf/elektromobilitaet_klimaschutz.pdf.
13. Karden, E., Ploumen, S., Fricke, B., Miller, T., and Snyder, K. “Energy Storage Devices for Future Hybrid Electric Vehicles”. Journal of Power Sources 168 (2007). Pg. 2–11.
14. Fuhs, A.E. “Hybrid Vehicles and the Future of Personal Transportation”. CRC Press, USA (2009).

15. “Investigation into the Scope for the Transport Sector to Switch to Electric Vehicles and Plug-in Hybrid Vehicles”. BERR & Department for Transport (2008).
16. Sammes, N. “Fuel Cell Technology: Reaching Towards Commercialization”. Springer-Verlag, London (2006).
17. Hermann, A., Chaudhuri, T., and Spagnol, P. International Journal of Hydrogen Energy 30 (2005). Pg. 1297.
18. Meissner, E., and Richter, G. “The Challenge to the Automotive Battery Industry: The Battery has to become an Increasingly Integrated Component within the Vehicle Electric Power System”. Journal of Power Sources 144 (2005). Pg. 438–460.
19. Nagpure, S.C. “Multi-scale Characterization Studies of Aged Li-ion Battery Materials for Improved Performance”.
20. Chan C.C., and Wong, Y.S. “Electric Vehicles Charge Forward”. IEEE Power and Energy Magazine (2004). Pg.24–33.
21. Chau, K.T., Wong, Y.S., and Chan, C.C. “An Overview of Energy Sources for Electric Vehicle”. Energy Conversion & Management, Elsevier (1999). Pg. 1953–1968.
22. Tie, S.F., and Tan, C.W. “A Review of Energy Sources and Energy Management System in Electric Vehicles”. Renewable and Sustainable Energy Reviews 20 (2013). Pg. 82–102.
23. Sun, L., Ruchuan, C., Liang, C., Wang, C., and Qingcai. “State-of-Art of Energy System for New Energy Vehicles”. IEEE Vehicle Power and Propulsion Conference, VPPC (3–5 September, 2008). Pg. 1–8.

24. Khaligh, A., and Li, Z. “Battery, Ultra-capacitor, Fuel Cell, and Hybrid Energy Storage Systems for Electric, Hybrid Electric, Fuel Cell, and Plug-In Hybrid Electric Vehicles: State of the Art”. IEEE Transactions on Vehicular Technology 59 (2010). Pg. 2806–2814.
25. Whittingham, M. S. “History, Evolution, and Future Status of Energy Storage”. Proceedings of the IEEE, volume 100 (2012). Pg. 1518–34.
26. Ribeiro, P.F., Johnson,B.K., Crow,M.L., Arsoy,A., and Liu,Y. “Energy Storage Systems for Advanced Power Applications”. Proceedings of the IEEE (2001). Pg. 1744–1756.
27. Lukic S. “Charging Ahead”. IEEE Industrial Electronics Magazine, 2 (4), (2008). Pg. 22–31.
28. Tarascon, J.M., and Armand, M. Nature, 414 (2001). Pg. 359.
29. Yoshino, A. “Development of the Lithium-Ion Battery and Recent Technological Trends”. Lithium-Ion Batteries, Advances and Applications (2014).
30. Orecchini,F., Santiangeli, A., and Dell’Era., A “EVs and HEVs Using Lithium-Ion Batteries”. Lithium-Ion Batteries, Advances and Applications (2014).
31. Axsen, J., Burke, A., and Kurani, K.S. “Batteries for Plug-in Hybrid Electric Vehicles (PHEVs): Goals and the State of Technology circa 2008”. Institute of Transportation Studies, University of California, Davis, Research Report UCD-ITS-RR-08-14.
32. Zhang, Z.J., Ramadass, P., and Fang, W. “Safety of Lithium-Ion Batteries”. Lithium-Ion Batteries, Advances and Applications (2014).

33. “Dell Recalls Lithium Batteries”. Chem. Eng. News: American Chem. Soc. (August 21, 2006).
34. “A123 Systems to Recall Electric-Car Battery Packs for Fisker, others”. News article from http://www.greencarreports.com (March 26, 2012).
35. Masato, O., Miyamoto, T., Horie, H., and Katayama, K. “Development of a Lithium-ion Battery System for EVs”. SAE International, SAE Digital Library (1997).
36. Stamp, A., and Widmer, R. “E-Mobility: Prospective Environmental Assessments”. (02.03.2011)
37. Gaines, L., and Dunn, J. “Lithium-Ion Battery Environmental Impacts”. Lithium-Ion Batteries, Advances and Applications (2014).
38. Y, L.B., and Dubarry, M. "From Driving Cycle Analysis to Understanding Battery Performance in Real-life Electric Hybrid Vehicle Operation." Journal of Power Sources 175.1 (2007). Pg. 76-88.
39. Suttman, A. “Lithium Ion Battery Aging Experiments and Algorithm Development for Life Estimation”.
40. Dees, D., Battaglia, V., and Bélanger, A. “Electrochemical Modeling of Lithium Polymer Batteries”.
41. Sabatier, J., Merveillaut, M., Francisco, J.M., Guillemard, F., and Porcelatto, D. “Lithium-Ion Batteries Modeling Involving Fractional Differentiation”.
42. Tobishima, S., Takei, K., Sakurai, Y., and Yamaki, J.I. Journal of Power Sources 90 (2000). Pg. 188-195.

43. Chiu, K., Lin, C., Yeh, S., Lin, Y., and Chen, K. “An Electrochemical Modeling of Lithium-Ion Battery Nail Penetration”.

44. Cho, S., Jeong, H., Han, C., Jin, S., Lim, J., Oh, J. “State-of-Charge Estimation for Lithium-Ion Batteries under Various Operating Conditions using an Equivalent Circuit Model.”

45. Chiang, Y., Sean, W., and Ke, J. “Online Estimation of Internal Resistance and Open-Circuit Voltage of Lithium-Ion Batteries in Electric Vehicles”.

46. Guy, S., Blanchard, P., and Broussely, M. "Aging of Lithium-ion Batteries." Journal of Power Sources 127.1-2 (2004): Pg. 65-71.

47. Broussely, M., Biensan, P., Bonhomme, F., Blanchard, P., Herreyre, S., Nechev, K., and Staniewicz, R. "Main Aging Mechanisms in Li-ion Batteries." Journal of Power Sources 146.1-2 (2005). Pg. 90-96.

48. Peled, E. Journal of Electrochemical Society 126 (1979). Pg. 2047.

49. Barré, A., Deguilhem, B., Grolleau, S., Gérard, M., Suard, F., and Riu, D. “A Review on Lithium-Ion Battery Ageing Mechanisms and Estimations for Automotive Applications”.

50. Vetter, J., Novak, P., Wagner, M., Veit, C., Moller, K., Besenhard, J., Winter, M., Wohlfahrt-Mehrens, M., Vogler, C., and Hammouche, A. "Ageing Mechanisms in Lithium-ion Batteries." Journal of Power Sources 147.1-2 (2005): Pg. 269-81.

51. Lu, L., Han, X., Li, J., Hua, J., and Ouyang, M. “A Review on the Key Issues for Lithium-Ion Battery Management in Electric Vehicles.”

52. Schwunk, S., Armbruster, N., Straub, S., Kehl, J., Vetter, M. “Particle Filter for State of Charge and State of Health Estimation for Lithium Iron Phosphate Batteries”.
53. Plett, G. “Battery Management System Algorithms for HEV Battery State-of-Charge and State-of-Health Estimation”.
54. Weng, C., Cui, Y., Sun, J., Peng, H. “On-Board State of Health Monitoring of Lithium-Ion Batteries using Incremental Capacity Analysis with Support Vector Regression.”
55. Le, D., and Tang, X. “Lithium-Ion Battery State of Health Estimation Using Ah-V Characterization.”
56. Tang, X., Mao, X., Lin, J., and Koch, B. “Capacity Estimation for Li-ion Batteries”.
57. Liaw, B., Jungst, R., Nagasubramanian, G., Case, H., and Doughty, D. “Modeling Capacity Fade in Lithium-Ion Cells,” Journal of Power Sources, vol. 140, (2005). Pg. 157–161.
58. Bhangu, B., Bentley, P., Stone, D., and Bingham, M. “Nonlinear Observers for Predicting State-of-Charge and State-of-Health of Lead-Acid Batteries for Hybrid-Electric Vehicles”. IEEE Transactions on Vehicular Technology, vol. 54, (2005). Pg. 783–794.
59. Stamps, A., Holland, C., White, R and Gatzke, E. “Analysis of Capacity Fade in Lithium Ion Battery”. Journal of Power Sources, vol. 150, (2005). Pg. 229–239.
60. “Battery Test Manual for Plug-In Hybrid Electric Vehicles”. U.S. Department of Energy, Revision 2 (December 2010).
61. Yurkovich, B.J., and Guezennec, Y. “Dynamic Electro-thermal Battery Pack Modeling and Simulation of Pack Imbalance”.

62. Hu, Y., Yurkovich, S., Guezennec, Y., and Bornatico, R. “Model-Based Calibration for Battery Characterization in HEV Applications”. American Control Conference (2008).

63. Hu, Y., Yurkovich, S., Guezennec, Y., and Yurkovich, B. J. “A Technique for Dynamic Battery Model Identification in Automotive Applications Using Linear Parameter Varying Structures”. Control Engineering Practice 17 (2009). Pg. 1190–1201.

64. Hu, Y., Yurkovich, S., Guezennec, Y., and Yurkovich, B.J. “Electro-Thermal Battery Model Identification for Automotive Applications”. Journal of Power Sources, 196 (2011). Pg. 449–457.

65. Hu, Y., and Yurkovich, S. “Battery Cell State-of-Charge Estimation using Linear Parameter Varying System Techniques”. Journal of Power Sources, 198, (2012). Pg. 338–350.

66. Hu, Y., and Yurkovich, S. “Linear Parameter Varying Battery Model Identification using Subspace Methods”. Journal of Power Sources, 196, (2011). Pg. 2913–2923.

67. Guezennec, Y., and Canova, M. “ME-7383, Spring 2014, Course Notes”. The Ohio State University.